

Fluorometric approaches to analyze the structure-function relationship of Excitatory Amino Acid Transporters (EAATs)

Der Naturwissenschaftlichen Fakultät
der Gottfried Wilhelm Leibniz Universität Hannover
zur Erlangung des Grades

Doktorin der Naturwissenschaften

-Dr. rer. nat.-

genehmigte Dissertation

von

Dipl.-Biochem., Linda Sabrina Jasmin Hotzy
geboren am 2. April 1982 in Euskirchen

2013

Referent/Referentin: Prof. Dr. med. Christoph Fahlke

Korreferent/Korreferentin: Prof. Dr. Rita Gerardy-Schahn

Drittprüfer/Prüfungsvorsitzender: Prof. Dr. Anaclet Ngezahayo

Tag der Promotion: 22.08.2012

Schlagwörter:

Exzitatorische Aminosäuretransporter
(*Excitatory amino acid transporters*, EAATs)

Anionenkanal

Spannungsklemmfluorometrie
(*voltage clamp fluorometry*, VCF)

Keywords:

Excitatory amino acid transporters
(EAATs)

Anion channel

Voltage clamp fluorometry
(VCF)

Contents

1	Abstract	11
2	Zusammenfassung	13
3	Introduction	16
3.1	Membrane Transport	16
3.2	The solute-carrier 1 (SLC1) Family	18
3.2.1	Excitatory Amino Acid Transporters (EAATs)	19
3.2.1.1	L-Glutamate - A neurotoxic neurotransmitter	19
3.2.1.2	Localization and physiological function of EAATs in the CNS	22
3.2.1.3	EAAT structure and transport mechanism	23
3.2.1.3.1	A bacterial transporter homologue - Glt _{Ph} , a model for EAAT structure	23
3.2.1.3.2	EAATs - Dual functional proteins	26
3.2.1.3.3	EAAT transport mechanism	28
3.2.1.4	EAAT involvement in pathogenicity	29
3.2.1.4.1	The role of EAAT1 in episodic ataxia	30
4	Aims of this thesis	32
5	Discussion	33
5.1	Independent-acting subunits in heterotrimers of neuronal glutamate transporters EAAT3 and EAAT4	33
5.2	Interdependence of transport and anion channel function	35
5.3	Disturbed sodium association as underlying pathomechanism of EA6 - Another example for the intimate interdependence of glutamate uptake ability and anion channel function of EAATs	40
5.4	Observations made by an intermediate structure of Glt _{Ph}	47
5.5	Continuative questions and research	49
6	Conclusions	51
7	References	52

Contents

8	List of publications _____	63
9	Hetero-oligomerization of neuronal glutamate transporters* _____	64
9.1	Abstract _____	65
9.2	Introduction _____	65
9.3	Experimental Procedures _____	66
9.3.1	Heterologous Expression of EAATs _____	66
9.3.2	Purification and Gel Electrophoresis of EAAT Fusion Proteins _____	66
9.3.3	Electrophysiology _____	67
9.3.4	Laser Pulse Photolysis _____	67
9.3.5	Data Analysis _____	68
9.3.6	Confocal Microscopy _____	69
9.3.7	Surface Biotinylation and Western Blotting _____	69
9.4	Results _____	70
9.4.1	EAAT3 and EAAT4 Form Hetero-oligomeric Transporters _____	70
9.4.2	Co-expression of EAAT3 and EAAT4 in <i>Xenopus</i> Oocytes _____	73
9.4.3	Individual Subunits Transport Substrates Independently of Each Other _____	76
9.4.4	Targeting of Heterotrimeric Transporters in Polarized Epithelial Cells _____	80
9.5	Discussion _____	83
9.6	Acknowledgments _____	85
9.7	References _____	85
10	Neutralizing aspartate 83 modifies substrate translocation of Excitatory Amino Acid Transporter 3 (EAAT3) glutamate transporters ^{*s} _____	88
10.1	Abstract _____	89
10.2	Introduction _____	90
10.3	Experimental Procedures _____	91

Contents

10.3.1	Expression of WT and mutant <i>hEAAT3</i> transporters in <i>Xenopus laevis</i> oocytes	91
10.3.2	Electrophysiology	92
10.3.3	Voltage clamp fluorometry	92
10.3.4	Data analysis	92
10.3.5	Kinetic modeling	93
10.4	Results	93
10.4.1	Time, substrate and voltage dependence of EAAT-associated currents and fluorescence signals	93
10.4.2	Voltage clamp fluorometry reveals additional slow conformational changes	98
10.4.3	D83A modifies EAAT3 glutamate transport, anion currents and fluorescence amplitudes	100
10.4.4	Kinetic modeling reveals changes in the glutamate uptake cycle in D83A EAAT3	104
10.5	Discussion	111
10.6	Acknowledgments	115
10.7	Reference List	116
10.8	Supplemental Figures	119
11	A mutation causing Episodic Ataxia modifies sodium association to EAAT glutamate transporters	122
11.1	Abstract	123
11.2	Introduction	123
11.3	Results	124
11.4	P259R EAAT3 is a reliable model to study transport dysfunction of P290R EAAT1	124
11.4.1	P259R modifies conformational changes of M205C <i>hEAAT3</i>	127
11.4.2	P259R alters the sodium dependence of M205C <i>hEAAT3</i> conformational changes	129

Contents

11.4.3 Kinetic modeling reveals altered sodium-binding to P259R <i>hEAAT3</i> _____	132
11.5 Discussion _____	137
11.6 Methods _____	140
11.6.1 Expression of WT and mutant <i>hEAAT3</i> transporters in <i>Xenopus</i> <i>laevis</i> oocytes or mammalian cells _____	140
11.6.2 Voltage clamp fluorometry _____	141
11.6.3 Electrophysiology _____	142
11.6.4 Data analysis _____	142
11.6.5 Kinetic modeling _____	143
11.7 Acknowledgements _____	144
11.8 References _____	144
11.9 Supplemental Figures and Information _____	147
12 Abbreviations _____	151
13 Acknowledgments _____	153
14 Curriculum vitae _____	154
15 Erklärung _____	155

Figure List

Figure 3.1: Membrane Transport. _____	17
Figure 3.2: Glutamate transporter isoforms and glutamate recirculation at an excitatory synapse. _____	21
Figure 3.3: Membrane topology and crystal structures of a bacterial transporter homologue. _____	24

Contents

Figure 3.4:	Uptake cycle and transport scheme of glutamate transporters. _____	28
Figure 5.1:	Localization of S74 in Glt _{PH} , the homologue residue of D83 in EAAT3. _____	39
Figure 5.2:	C α -distances distances in the outward facing open conformation from P259 to the different sodium binding sites. _____	45
Figure 5.3:	C α -distances distances in the intermediate conformation from P259 to the sodium binding site D440. _____	48
Figure 9.1:	Co-assembly of EAAT3 and EAAT4. _____	72
Figure 9.2:	EAAT3 modifies membrane surface insertion and function of EAAT4. _____	75
Figure 9.3:	Substrates bind independently to individual subunits. _____	77
Figure 9.4:	Substrate translocation occurs independently by individual subunits. _____	78
Figure 9.5:	Epithelial sorting of homo- and heterotrimeric EAATs observed by confocal imaging. _____	81
Figure 9.6:	Epithelial sorting of homo- and heterotrimeric EAATs studied by cell surface biotinylation. _____	82
Figure 10.1:	Reporter mutations do not affect the function of EAAT3 associated currents. _____	95
Figure 10.2:	Voltage- and substrate-dependent conformational changes of EAAT3. _____	97
Figure 10.3:	Slow conformational changes in EAAT3. _____	99
Figure 10.4:	D83A changes substrate dependence of EAAT3 current amplitudes. _____	102
Figure 10.5:	Voltage- and substrate-dependent conformational changes of D83A EAAT3. _____	103

Figure 10.6:	Kinetic model and transport scheme of wildtype and mutant EAAT3. _____	105
Figure 10.7:	Simulated voltage- and substrate-dependent conformational changes, open probabilities and transport currents of cysteine-substituted and D83A EAAT3. _____	108
Suppl. Figure 10.8:	Time course of fluorescence labeling of cysteine-substituted EAAT3. _____	119
Suppl. Figure 10.9:	Voltage-dependent conformational changes are due to EAAT3 and are blocked by TBOA. _____	120
Suppl. Figure 10.10:	Anion independence of cysteine-substituted WT and D83A EAAT3. _____	121
Figure 11.1:	P259R changes EAAT1- and EAAT3-associated anion- and uptake currents. _____	126
Figure 11.2:	Voltage-, substrate- and time-dependent conformational changes of M205C and M205C-P259R EAAT3. _____	128
Figure 11.3:	Sodium dependence of M205C and M205C-P259R EAAT3 conformational changes. _____	130
Figure 11.4:	Kinetic model and simulated conformational changes and currents of M205C and M205C-P259R EAAT3. _____	134
Suppl. Figure 11.5:	P290R alters EAAT1 glutamate-activated anion currents and uptake currents in mammalian cells and oocytes similar to P259R in EAAT3. _____	147
Suppl. Figure 11.6:	Sodium dependence of WT, M205C and M205C-P259R EAAT3. _____	148
Suppl. Figure 11.7:	Residence probability of each state of EAAT3 transport cycle. _____	149
Suppl. Figure 11.8:	Simulated open probabilities of M205C and M205C-P259R EAAT3 anion channels. _____	150

Table List

Table 10.1: Parameters of the EAAT3 model. _____	110
Table 10.2: Fluorescence intensities used for simulations of cysteine-substituted wildtype and mutant EAAT3 fluorescence voltage relationships. _____	110
Table 10.3: State-specific open probabilities for channel opening from the respective state used in the kinetic modeling of cysteine-substituted wildtype and mutant EAAT3. _____	111
Table 11.1: Apparent dissociation constants and hill coefficients of M205C and M205C-P259R EAAT3 sodium dependence. _____	131
Table 11.2: Parameters of the EAAT3 model. _____	135
Table 11.3: Open probabilities used in the kinetic modeling of cysteine-substituted wildtype and mutant EAAT3. _____	136
Table 11.4: Fluorescence intensities used for simulations of cysteine-substituted wildtype and mutant EAAT3 fluorescence voltage relationships. _____	136
Table 11.5: Simulated dissociation constants and hill coefficients of M205C and M205C-P259R EAAT3 sodium dependence. _____	137

1 Abstract

L-Glutamate is the predominant excitatory neurotransmitter in the mammalian central nervous system (CNS) and involved in most physiological processes in the brain (106-109). Excitatory amino acid transporters (EAATs) remove glutamate from the synaptic cleft into neuronal and glial cells (58) and maintain low extracellular glutamate concentrations to prevent glutamate excitotoxicity (8, 182, 183). EAATs encompass eight transmembrane domains (TM) and assemble as functional trimers (50). Apart from functioning as secondary-active glutamate transporters, EAATs mediate a channel-like anion conductance (13-22, 138). Five different mammalian EAAT isoforms have been identified (13, 16, 136). Whereas EAAT1 and EAAT2 are mainly expressed in glia, EAAT3, EAAT4 and EAAT5 are neuronal glutamate transporters. Despite a different localization, EAAT isoforms vary in the ratio of transport to anion currents and are thus expected either to function primarily as glutamate transporters or as anion channels (16, 21, 158).

The aspect of trimerization and the EAAT-subtype specific variations pose the question if certain EAAT isoforms can form heterooligomers and if heteromultimerization has functional consequences. Hetero-oligomerization was examined by studying different EAAT isoforms by using biochemical, electrophysiological and confocal approaches. Solely the neuronal glutamate transporters EAAT3 and EAAT4, but neither the glial transporters EAAT1 and EAAT2, nor EAAT2 and EAAT3, or EAAT2 and EAAT4 co-assemble into stable heterotrimers. Hetero-oligomerization of EAAT3 and EAAT4 does not affect amino acid transport or EAAT-mediated anion conductance, but alters epithelial sorting. In EAAT3/EAAT4 heterotrimers EAAT4 guides EAAT3, which occupies a unique sorting signal for apical membranes, as well to basolateral membranes. Hetero-trimerization could alter the cellular distribution of transporter subtypes with a different affinity-capacitance ratio which might have a biological significance by tight regulation of the external glutamate concentration and neuronal excitability.

Whereas the EAAT transport function and its physiological importance are well understood, it is less known about the molecular basis of the pore-mediated anion conduction and the physiological impact. EAAT anion currents have been postulated to be involved in the regulation of cell excitability, and are thought to be conducted through an anion pathway that is opened and closed in response to conformational changes underlying glutamate transport. A point mutation neutralizing a conserved

aspartate at the intracellular loop of transmembrane domain 2 (TM2) was shown to exert effects on both transporter properties, glutamate transport and anion channel function, in EAAT1 and EAAT4 (158, 160). The interdependence of transporter and anion channel function was analyzed by studying the effects of the homologue point mutation D83A on EAAT3-associated conformational changes by the technique of voltage clamp fluorometry (VCF) in combination with kinetic simulations. Beside an enlargement of EAAT3 anion currents, a reduction of glutamate-activated anion currents, and coupled transport, D83A modifies the time, substrate, and voltage dependence of EAAT3 conformational changes by alterations of the substrate translocation. The direct effects of D83A on the EAAT3 transport cycle result in changed anion channel function which highlights the intimate interaction of the dual functions of EAAT glutamate transporters.

As glutamate by itself is involved in most normal and abnormal brain activities, EAAT dysfunctions and resulting high external glutamate concentrations are correlated with diverse neurological diseases and abnormal brain activity. It was shown that a rare human genetic disease characterized by paroxysmal cerebellar incoordination, episodic ataxia type six (EA6), is caused by mutations in *SLC1A3*. One mutation in *SLC1A3* - the gene encoding the glial glutamate transporter EAAT1 - predicts the substitution of the conserved proline 290 in the hinge of transmembrane domain 5 (TM5) by arginine (97). With the objective to clarify the pathomechanism underlying EA6, the homologue mutation P259R and the effects on EAAT3-associated currents and conformational changes were analyzed by using electrophysiological approaches, VCF and kinetic simulations. P259R EAAT3 exhibits increased anion currents, strongly reduced uptake currents and furthermore altered sodium-dependent conformational changes. Disturbed Na⁺-association represents the molecular basis of transporter dysfunction in episodic ataxia type 6.

2 Zusammenfassung

Die Aminosäure L-Glutamat ist der vorherrschende exzitatorische Neurotransmitter im Zentralen Nervensystem von Säugetieren (ZNS) und beeinflusst die meisten physiologischen Prozesse im Gehirn (106-109). Exzitatorische Aminosäuretransporter (*Excitatory amino acid transporters*, EAATs) sind für die Aufnahme von Glutamat aus dem synaptischen Spalt in Neuronen und Gliazellen zuständig (58) und verhindern die exzitotoxische Wirkung von Glutamat durch die Aufrechterhaltung niedriger extrazellulärer Glutamatkonzentrationen (8, 182, 183). EAATs umfassen acht Transmembrandomänen (TM) und setzen sich zu funktionellen Trimeren zusammen (50). Neben der sekundär-aktiven Glutamattransportfunktion vermitteln EAATs eine kanalähnliche Anionenleitfähigkeit (13-22, 138). Es wurden fünf unterschiedliche Säugetier-EAATs identifiziert (13, 16, 136). Während EAAT1 und EAAT2 hauptsächlich in Gliazellen exprimiert sind, sind EAAT3, EAAT4 und EAAT5 neuronale Glutamattransporter. Neben der unterschiedlichen Lokalisierung, variieren verschiedene EAAT-Isoformen in dem Verhältnis von Transport- zu Anionenstrom (16, 21, 158). Daher wird angenommen, dass EAATs entweder hauptsächlich als Glutamattransporter oder als Anionenkanäle wirken.

Durch den Aspekt der Trimerisierung und der Variation der subtypspezifischen Eigenschaften entsteht die Frage, ob verschiedene EAAT-Isoformen Heterooligomere bilden können und ob eine Heterooligomerisierung funktionelle Auswirkungen hat. Die Heterooligomerisierung wurde an verschiedenen EAAT-Isoformen mit Hilfe von biochemischen, elektrophysiologischen Techniken und Konfokalmikroskopie untersucht. Lediglich die neuronalen Glutamattransporter EAAT3 und EAAT4 bilden stabile funktionelle Heterotrimere, jedoch nicht die Glutamattransporter der Gliazellen, EAAT1 und EAAT2, noch EAAT2 und EAAT3 oder EAAT2 und EAAT4. Die Heterooligomerisierung hat keinen Einfluss auf den Aminosäuretransport oder die EAAT-vermittelte Anionenleitfähigkeit, verändert allerdings die Anreicherung der Transporter in apikale oder basolaterale Membranen. In EAAT3/EAAT4-Heterotrimeren leitet EAAT4 den Glutamattransporter EAAT3, der ein einzigartiges Signal für die Anreicherung in apikale Membranen besitzt, auch in basolaterale Membranen. Die Heterotrimerisierung kann die zelluläre Verteilung von Transportersubtypen mit unterschiedlichen Affinitäts-Leitfähigkeits-Verhältnissen

ändern und damit eventuell eine stärkere Regulation der externen Glutamatkonzentration und der Zellerregbarkeit ermöglichen.

Während die Transportfunktion der Exzitatorischen Aminosäuretransporter und deren physiologische Bedeutung gut verstanden sind, ist weniger über die molekulare Grundlage der porenvermittelten Anionenleitfähigkeit und deren physiologischer Bedeutung bekannt. Es wurde postuliert, dass EAAT-Anionenströme durch einen Anionenweg, der sich in Erwidern auf Konformationsänderungen während des Glutamattransportes öffnet und schliesst, vermittelt werden. Diese Anionenleitfähigkeit ist eventuell in die Regulierung der zellulären Erregbarkeit involviert. Es wurde gezeigt, dass eine Punktmutation in EAAT1 und EAAT4, die einen konservierten Aspartatrest im intrazellulären Bereich der Transmembrandomäne 2 (TM2) neutralisiert, Auswirkungen auf beide Transportereigenschaften hat, den Glutamattransport sowie die Anionenleitfähigkeit (158, 160). Anhand der Auswirkungen der homologen Mutation D83A auf EAAT3-assoziierte Konformationsänderungen, wurde das Zusammenwirken der Transport- und Anionkanal-Eigenschaft mit Hilfe der Technik der Spannungsklemmfluorometrie (*voltage clamp fluorometry*, VCF) in Kombination mit kinetischen Simulationen untersucht. Neben der Vergrößerung der EAAT3-Anionenströme, einer Reduktion der glutamataktivierten Anionenströme und des gekoppelten Transportes, verändert die Mutation D83A die Zeit-, Substrat- und Spannungsabhängigkeit der Konformationsänderungen in EAAT3 durch Änderungen der Substrat-Translokation. Der direkte Effekt der Punktmutation D83A auf den Transportzyklus führt zu einer veränderten Anionkanal-Funktion, was die enge Interaktion der dualen Funktionen der EAAT Glutamattransporter aufzeigt.

Da Glutamat in die meisten normalen und abnormalen Gehirnaktivitäten involviert ist, stehen Fehlfunktionen Exzitatorischer Aminosäuretransporter und daraus resultierende hohe extrazelluläre Glutamatkonzentrationen mit einer Reihe neurologischer Erkrankungen und abnormer Gehirnaktivität in Zusammenhang. Episodische Ataxie Typ 6 (EA6) ist eine seltene genetische Erkrankung, charakterisiert durch paroxysmale cerebrale Koordinationsstörungen. Es wurde gezeigt, dass EA6 durch Mutationen in *SLC1A3*, dem Gen das den Glutamattransporter EAAT1 der Gliazellen kodiert, verursacht wird. Eine dieser Mutationen in *SLC1A3* sagt einen Aminosäureaustausch eines konservierten Prolins an Position 290 im Knick der Transmembrandomäne 5 (TM5) gegen Arginin voraus

(97). Mit dem Ziel den der EA6 zugrundeliegenden Pathomechanismus aufzuklären, wurde die homologe Mutation P259R und deren Auswirkungen auf EAAT3-assoziierte Ströme und Konformationsänderungen mittels elektrophysiologischer Methoden, VCF und kinetischen Simulationen untersucht. Die Mutation P259R in EAAT3, zeigt erhöhte Anionenströme, stark reduzierte Glutamataufnahmeströme und darüber hinaus veränderte natriumabhängige Konformationsänderungen. Eine veränderte Natriumassoziation stellt die molekulare Grundlage der Transporterfehlfunktion in der Erkrankung der Episodischen Ataxie Typ 6 dar.

3 Introduction

3.1 Membrane Transport

Biomembranes delimit the cytoplasm of every living cell from the extracellular surrounding or define enclosed compartments within a cell. Mainly, biomembranes consist of a lipid bilayer with embedded proteins. Biomembranes inherit several important functions like, cellular organization, cell-cell recognition, they have mechanical and elastic properties, but probably the most important feature is the selective permeability. Depending on the size and charge of ions and molecules the exchange across biomembranes is accomplished by different transport mechanisms. Small lipophilic molecules, e.g. CO₂, O₂, alcohol and urea pass the lipid bilayer via simple diffusion (Figure 3.1). In contrast, the transport of macromolecules, like proteins or polysaccharides and even other smaller cells is mediated by membrane transferring processes like endo-, exo- and transcytosis. The transport of ions and small hydrophilic molecules, like sugars, nucleotides and amino acids is enabled by membrane embedded proteins via passive or active transport mechanisms.

The passive transport of solute molecules along their electrochemical gradient can be conducted by carriers or channels (Figure 3.1). During the passive transport by carriers molecules binding from the intra- or extracellular side, induce a conformational change which enables the passage across the membrane. Equally to carriers, channels are accessible from both sides of the plasma membrane and alleviate the movement of ions along their electrochemical gradient when the channel is open. Some channels possess a “gate” which opens and closes upon external stimuli, like chemical or electrical signals, temperature and mechanical forces. Transport by ion channels exhibits no fixed stoichiometry. The number of transported ions depends on the channel open time (1).

Active transport mechanisms across membranes can be divided into primary- and secondary-active transport (Figure 3.1). In contrast to the passive transport, active transport necessitates diverse energy-coupling mechanisms to carry substrates against an electrochemical gradient. During primary-active transport energy provided by the hydrolysis of high-energy compounds, redox reactions or light absorption is directly used to pump protons and anorganic ions against their concentration gradient and by this generating and maintaining electrochemical ion gradients. Most common primary-active mechanisms are directly coupled to the binding and hydrolysis of

adenosine triphosphate (ATP). Secondary-active transport involves using energy to establish a gradient across the cell membrane, and then utilizing that gradient to transport a second molecule of interest up its concentration gradient, either in the same direction (symport) or in the opposite direction (antiport or exchange).

Figure 3.1
Membrane Transport

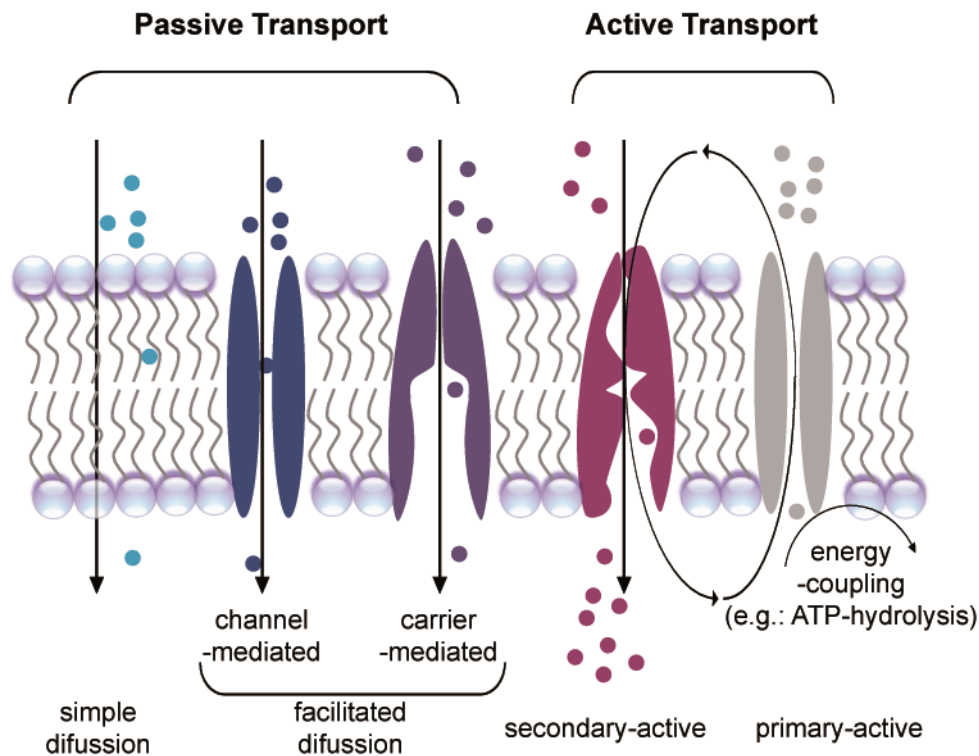


Figure 3.1: Membrane Transport.

Different passive and active transport mechanisms across biomembranes, as depicted in the figure.

In summary, transporters facilitate the movement of a specific substrate, either with or against its concentration gradient. It is generally believed that a conformational change of the transporter protein is important in this transfer process. Many of these transporters belong to the solute-carrier (SLC) gene superfamily, including passive transporters, symporters and antiporters, as well as mitochondrial and vesicular transporters.

3.2 The solute-carrier 1 (SLC1) Family

The solute-carrier (SLC) gene superfamily includes currently 362 putative functional protein-coding genes and is organized into 55 different families (2). Members of the same SLC gene family share at least 20-25 % amino acid sequence identity.

The SLC1 family includes seven eukaryotic members, five high-affinity excitatory amino acid transporters (EAAT: EAAT3 (EAAC1), EAAT2 (GLT1), EAAT1 (GLAST), EAAT4 and EAAT5 (*SLC1A1*, *SLC1A2*, *SLC1A3*, *SLC1A6*, and *SLC1A7*,)) and two neutral amino acid transporters (ASCT1, 2 (*SLC1A4*, *SLC1A5*)) and a large number of bacterial amino acid and dicarboxylic acid transporters (3, 4, 5).

The five high-affinity glutamate transporter subtypes share 50-60% amino acid sequence identity with each other, 30-40% identity with the neutral amino acid transporters (6), and around 20-30% identity with bacterial glutamate transporters (7). Between mammalian members of the glutamate transporters, the five isoforms are about 90% identical to the equivalent proteins of another species (8).

All excitatory amino acid transporters use L-glutamate and L-aspartate as high-affinity substrates. The high-affinity substrates for neutral amino acid transporters are mainly alanine, serine, cysteine and threonine, to a minor extent glutamine and asparagine and with a lower affinity several other amino acids (6, 9-12). Both the eukaryotic excitatory amino acid transporters and the neutral amino acid transporters, exhibit thermodynamically uncoupled ion fluxes, as substrate-independent cation leaks and substrate-dependent chloride currents (13-22). As described for other neurotransmitter transporters of the SLC6 family, which encompasses the Na⁺/Cl⁻-dependent transporters for dopamine, 5-hydroxytryptamine (serotonin), noradrenaline, GABA and glycine (139-147), these transporters are dual functional proteins which invalidates the strict distinction of channels and transporters.

3.2.1 Excitatory Amino Acid Transporters (EAATs)

Excitatory amino acid transporters (EAATs) execute diverse cellular functions in the central nervous system, in sensory organs as well as in the kidney (8). EAATs are trimeric integral membrane proteins (50) which remove synaptically released glutamate from the extracellular space to ensure low resting glutamate levels and to prevent glutamate excitotoxicity and cell death (8, 182, 183) in the CNS. Five different mammalian EAAT isoforms have been identified (13, 16, 136). Glutamate transport by *human* excitatory amino acid transporters (*hEAATs*) is a secondary-active transport mechanism, in which glutamate transport is coupled to the co-transport of three sodium ions, one proton and to the counter-transport of one potassium ion (137). Apart from functioning as secondary-active glutamate transporters, EAATs mediate a less understood channel-like anion conductance (13-22, 138).

3.2.1.1 L-Glutamate - A neurotoxic neurotransmitter

The amino acid L-glutamate is the predominant excitatory neurotransmitter in the mammalian CNS. It is involved in almost all normal brain activities, like cognition, memory and learning (106-109). Glutamate participates also in several aspects of the CNS development, e.g. in regulation of development by glutamatergic signaling (110-114), in neuronal migration (115), in synapse elimination (116), in long-term potentiation and in synapse induction (117-119). Over- (112) as well as the understimulation (120, 121) of glutamate receptors is harmful to the developing brain. Glutamate acts via glutamate receptors, and most neurons and glial cells express glutamate receptors in their plasma membranes (127-132), but glutamate plays as well a signalling role in peripheral organs and tissues, like the heart (122), intestine (123,124), liver, kidney (123) and in endocrine cells (125, 126). For example, in pancreatic islets of Langerhans, glutamate is proposed to act as an intracellular messenger, regulating insulin secretion from β -cells (186). In pinealocytes glutamate was suggested to participate as chemical transmitter in a receptor mediated manner in melatonin synthesis (125).

In contrast to other excitatory neurotransmitters, glutamate concentrations in the CNS are quite high, reaching 5-10 mmol/kg (133), whereas the concentration in the

extracellular solution is about 3-4 μM (134), thus creating a concentration gradient across the membrane of several thousands. Glutamate receptor activation requires just 1-10 μM glutamate; higher levels (10-100 μM) are neurotoxic (135) by glutamate receptor overstimulation and subsequent increased Na^+ - and especially Ca^{2+} -influx which leads to Ca^{2+} -dependent toxicity. Ca^{2+} is one of the most important secondary messengers and its intracellular concentration has to be tightly regulated. Calcium is involved in several cellular processes, e.g.: cell proliferation, gene expression, energy metabolism and apoptosis. Calcium-influx results in increased concentrations of intracellular free radicals, cytoskeletal breakdown and DNA degradation via activation of phospholipases, Ca^{2+} -binding proteins, proteases and endonucleases. High intracellular calcium concentrations furthermore lead to mitochondrial damage, ATP-downregulation and to a low intracellular pH.

Maintaining a low extracellular glutamate concentration is not just important to prevent the effect of excitotoxicity. It is obligatory for an effective and tight regulated synaptic communication on glutamatergic synapses. Furthermore, re-uptake provides glutamate for metabolic processes or neurotransmitter re-use.

Synaptic release of glutamate activates ionotropic glutamate receptors as AMPA- , NMDA receptors and metabotropic glutamate receptors (mGluR) (Figure 3.2). Excess glutamate in the synaptic cleft is taken up into postsynaptic nerve terminals by the excitatory amino acid transporters EAAT3 and EAAT4 and into glial cells by the EAAT1 and EAAT2. In glial cells glutamate can be converted to glutamine by the glutamine synthetase (Gln). In presynaptic nerve terminals glutamine can be reconverted into glutamate which is transported into synaptic vesicles by a vesicular glutamate transporter (VGLUT) and subsequently released by exocytosis. Glutamine may not solely serve as a neurotransmitter precursor in the glutamine-glutamate cycle, but may also serve as a nutrient for neurons. Furthermore, glutamate is used by system X_c^- exchanging it against cystine, providing cysteine as precursor for glutathione. Beside excitotoxicity by glutamate receptor overstimulation, high external glutamate can cause cell death by blocking system X_c^- which subsequently leads to depletion of the antioxidant glutathione.

Figure 3.2
Glutamate transporter isoforms and glutamate recirculation at an excitatory synapse

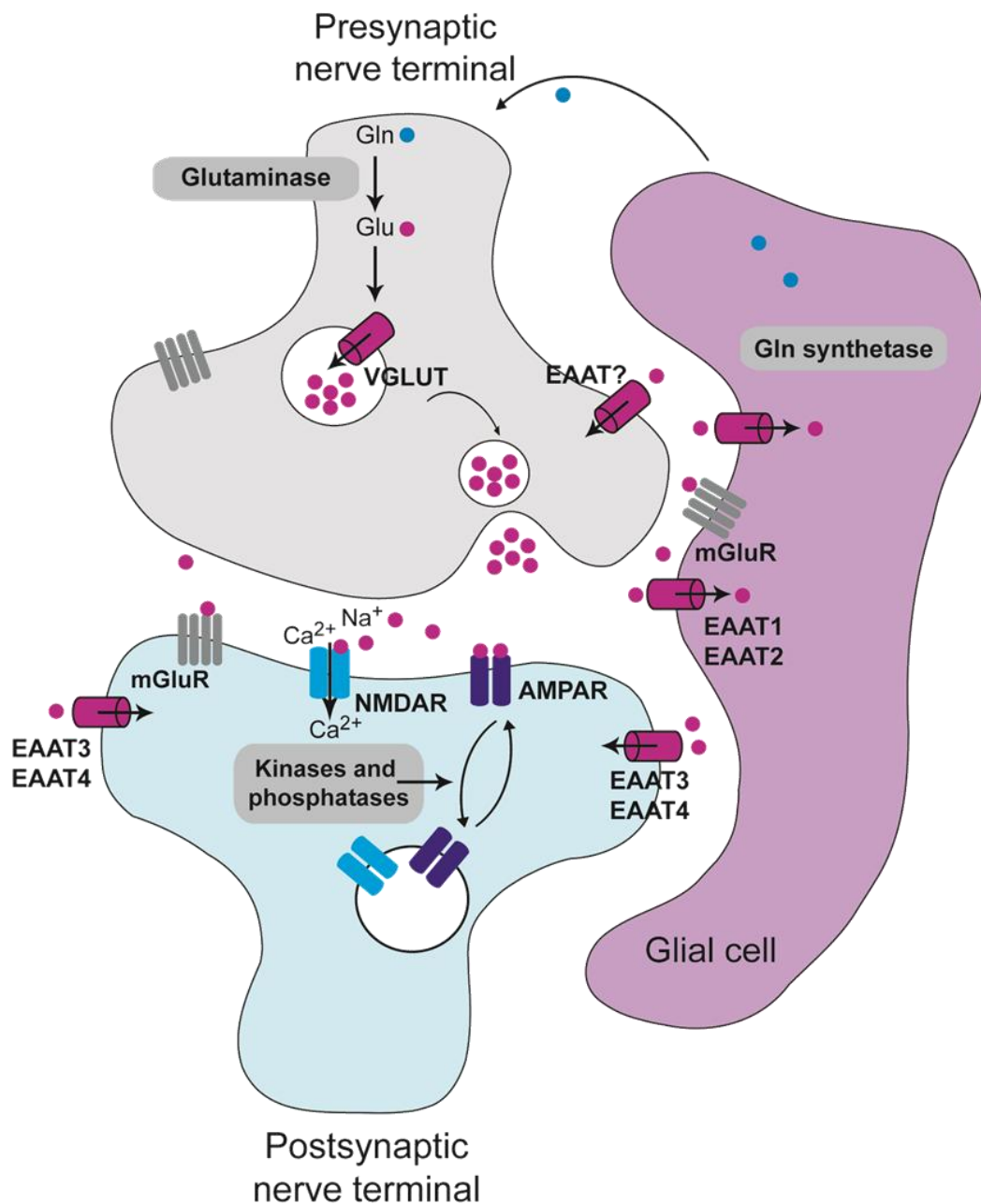


Figure 3.2: Glutamate transporter isoforms and glutamate recirculation at an excitatory synapse.

Synaptic release of glutamate activates ionotropic (AMPA, NMDAR) and metabotropic glutamate receptors (mGluR). Glutamate in the synaptic cleft is taken up into postsynaptic nerve terminals and into glial cells by the excitatory amino acid transporters, EAAT3, EAAT4 and EAAT1 and EAAT2, respectively. In glial cells glutamate can be converted to glutamine by the glutamine (Gln) synthetase. In presynaptic nerve terminals glutamine is reconverted into glutamate by Glutaminase, transported into synaptic vesicles by a vesicular glutamate transporter (VGLUT) and released by exocytosis.

3.2.1.2 Localization and physiological function of EAATs in the CNS

Five major EAAT subtypes (EAAT1-5) have been identified. EAAT subtypes differ in their functional characteristics and possess distinct localizations on a cellular and regional level. They can be roughly divided by their localization into glial and neuronal glutamate transporters.

EAAT1 (GLAST) and EAAT2 (GLT-1) are primarily expressed in glial cells and therefore considered to be glial glutamate transporters, although EAAT2 has been found as well in neurons and oligodendrocytes (23-25) and on presynaptic nerve terminals (26-27). Most synapses in the central nervous system are in close proximity to glial cells and glial glutamate transporters are predominantly responsible for glutamate clearance from the synaptic cleft. EAAT1 displays highest expression levels in cerebellum and lower levels in cortex and spinal cord (28-31). EAAT2 is highly expressed throughout the brain and spinal cord, and is responsible for > 90% of the total glutamate uptake (28-30).

Besides preventing glutamate excitotoxicity, glutamate re-uptake by glial transporters returns glutamate to metabolic processes as the glutamate-glutamine cycle. Via activation of the Na⁺ /K⁺-ATPase and glucose transporters, and changes in the levels of ATP and lactate they also signal the energy needs of nearby neurons (32).

Neuronal glutamate transporters, EAAT3 (EAAC1), EAAT4 (SLC1A6) (16, 33) and EAAT5 (SLC1A7) appear to have more specialized roles. EAAT3 is expressed at postsynaptic nerve terminals throughout the brain, particularly in cortex, hippocampus, cerebellum and basal ganglia (28, 29, 30, 33), but has like EAAT4 also been detected in astrocytes (34-36). EAAT4 is almost exclusively localized in soma and dendrites of GABAergic Purkinje cells of the cerebellum and with much lower expression levels in hippocampus, neocortex and other CNS regions (16, 30, 33, 37). EAAT5 (SLC1A7) is mainly present in rod photoreceptor and bipolar cells of the retina (13, 38). Weak expression levels of EAAT5 were detected furthermore in the liver, the heart, in muscles, and in brain tissue (13).

Neuronal glutamate transporters assume greater significance in the selective modulation of glutamate signalling at particular glutamate receptors at synapses, especially in the cerebellum, where many peri- or extrasynaptic glutamate receptors are present (39). For example, signalling at metabotropic glutamate receptors (mGluR) on cerebellar Purkinje neurons is limited by glutamate uptake (40). At parallel fibre and climbing fibre synapses on Purkinje neurons, EAATs limit mGluR

responses under resting conditions (41). Inhibition of neuronal EAATs in the cerebellum facilitates mGluR-mediated long-term depression (42). Since EAAT4 anion conductance exceeds its glutamate uptake capability, this transporter isoform may constitute an important regulator of neuronal excitability of neurons, counteracting the depolarization of neurons brought on by the postsynaptic glutamate receptor activation (16).

3.2.1.3 EAAT structure and transport mechanism

Beside biochemical and electrophysiological studies on glutamate transporters several crystallographic studies on a bacterial glutamate transporter homologue, Glt_{Ph} from *Pyrococcus horikoshii*, deliver insights into the structure and structure-function relationship of these transporters. Glt_{Ph} shares as much as 36% amino acid sequence identity with the eukaryotic EAATs and exhibits even more identity in functional important regions (43-49) and is thus a good model for the eukaryotic glutamate transporter structure.

3.2.1.3.1 A bacterial transporter homologue - Glt_{Ph}, a model for EAAT structure

Glutamate transporters are trimeric integral membrane proteins (Figure 3.3B). The trimer forms a bowl-shaped structure with a concave solvent-filled basin accessible from the extracellular solution and a peaked base directed towards the cytoplasm (50). The basin is 50 Å broad in diameter and 30 Å deep. The aqueous basin with its hydrophilic surface extends halfway across the membrane bilayer and by this allows aqueous, bulk solution and solutes to reach the middle of the membrane.

Each protomer consists of eight primarily α -helical transmembrane domains (TMs 1-8) and two helical hairpins (HPs 1-2) (Figure 3.3A) (50). One protomer possesses a cylinder-like structure (Figure 3.3C-E). The open ends of three cylinders of a trimer define the outer border of the basin, whereas the cylinder tips form the bottom of the bowl-shaped structure, reaching the intracellular solution.

The N-terminal part of the protein consists of the transmembrane domains TM1-6. The C-terminal part of the protein is buried within the N-terminal cylinder-shape and encompasses TM7, TM8, HP1 and HP2.

Figure 3.3
Membrane topology and crystal structures of a bacterial transporter
homologue

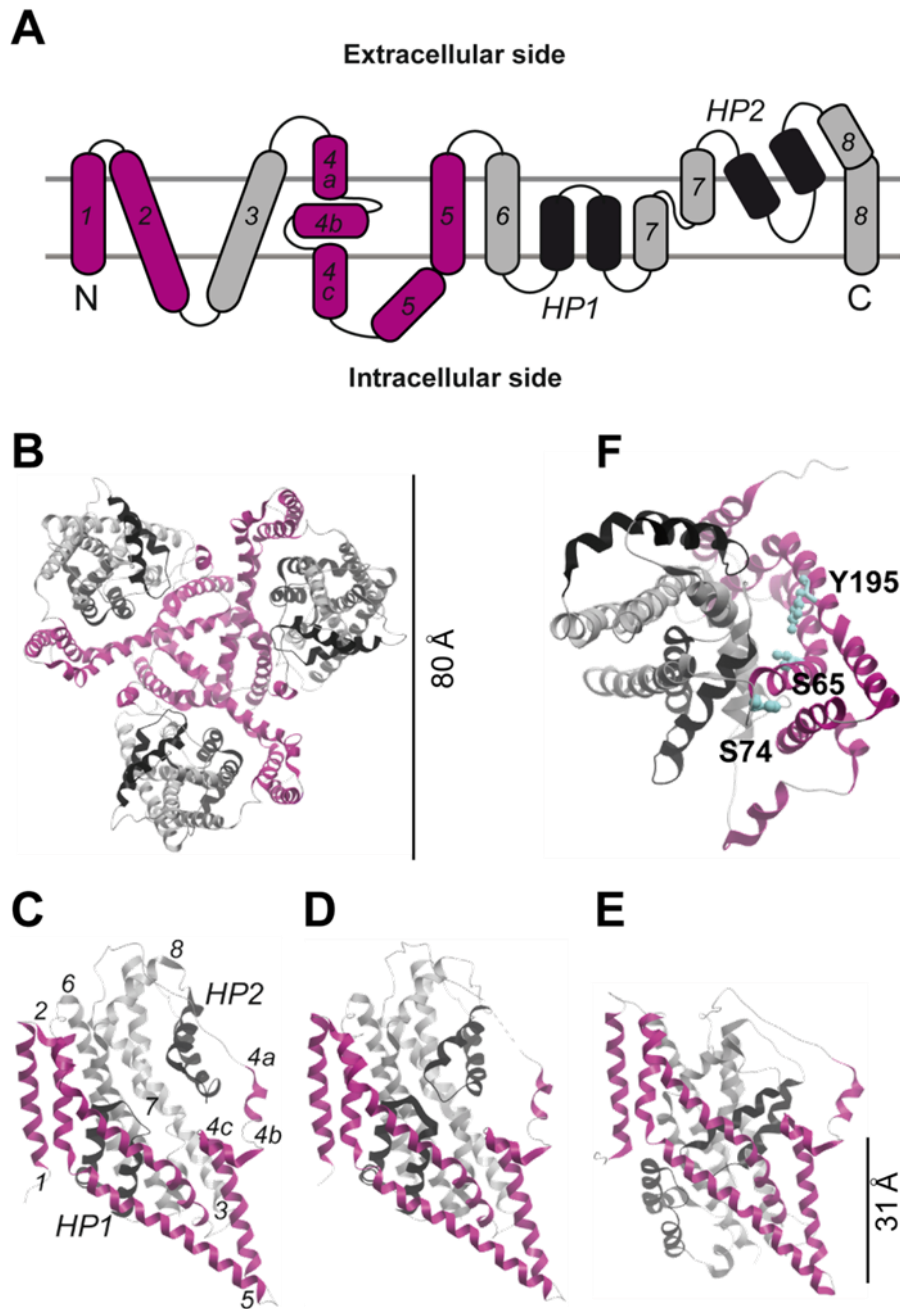


Figure 3.3: Membrane topology and crystal structures of a bacterial transporter homologue.

A, Membrane topology model of EAATs, deduced from crystallographic data of a bacterial transporter homologue from *Pyrococcus horikoshii*, Glt_{PH}. B-F, Ribbon representation of the trimer viewed from the extracellular side (B) or of the protomer viewed in the plane of the membrane in the outward facing open (C) (pdb-file: 2NWW), in the outward facing occluded (D) (pdb-file: 2NWX), in the inward facing occluded (E) (pdb-file: 3KBC) and in an intermediate state (F) (pdb-file: 3V8G) shown from the intracellular side with the residues S65, S74 and Y195 (light blue) flanking a proposed anion channel. The trimerization domain is shown in fuchsia, the transport domain in grey and the hairpins in black.

Early studies roughly subdivided glutamate transporters into two functional compartments - the N-terminal and C-terminal part - as to be responsible for intersubunit interactions and for substrate transport, respectively. The helical HP1 and HP2 are composed of helix-turn-helix motifs and represent structural key elements of glutamate transporters (50). Whereas HP1 is buried within the N-terminal cylinder, beginning on the cytoplasmic surface and reaching up to the bottom of the extracellular basin, HP2 is mostly solvent-exposed and faces the extracellular basin. Following crystallographic studies revealed that the aspartate binding site (substrate homologue transported by Glt_{Ph} instead of glutamate in eukaryotic glutamate transporters) is formed by the tips of HP1 and HP2, the unwound region of TM7 and polar residues of the amphipathic TM8 (51). The substrate binding site is thus buried within a polar pocket located halfway across the membrane. Glt_{Ph} 's sodium binding sites could be identified to be close to the aspartate binding pocket. Site 1 is coordinated by three carbonyl oxygens in TM7 and TM8, a carboxyl group of D405 in TM8 and possibly by hydroxyl oxygen of S278 in HP1 (51). The sodium site 2 is coordinated by carbonyl oxygens of TM7 and HP2.

Potassium binding sites of the eukaryotic glutamate transporters are still controversial discussed. It was shown that the residues Y403 and E404 in rat EAAT2 and R447 in EAAC1 are involved (52, 53, 150). The residue E404 is conserved in all eukaryotic glutamate transporters, but not in the bacterial or neutral-amino-acid transporters, which correlates with the fact that those are K^+ -independent.

Furthermore, it could be shown, that HP2 acts as the extracellular gate, either in the open state exposing the binding sites to the extracellular solution (outward facing open conformation, Figure 3.3C) or in the closed state occluding the binding sites (outward facing occluded conformation, Figure 3.3D). HP1 was hypothesized to act as the corresponding intracellular gate, which - in a similar manner - by opening and closure allows occlusion and exposure of the substrates to the intracellular solution (54). A third crystal structure of Glt_{Ph} , in which the transporter is fixed by cross-linking, establishes the inward facing occluded conformation (Figure 3.3E) (54).

The inward facing open conformation has to be proven by crystallographic studies and is still hypothetical. Further results suggest that Glt_{Ph} can be divided into two functional compartments, the trimerization domain, consisting of TM1, 2, 4 and TM5 and the transport domain, consisting of TM3, 6, 7, 8 and the two HPs (54).

A recent study reports on an intermediate conformation between the outward and inward facing states generated during substrate translocation (Figure 3.3F) (55). This intermediate state shows a transient cavity which is bordered by residues of TM2 and TM5, flanked by the polar residues S65, S74 and Y195 and supposed to be the pathway for the uncoupled anion conductance. Residues of TM2 were shown to modulate anion fluxes (158). This last crystallization study might be a starting point to understand the channel property of glutamate transporters.

3.2.1.3.2 EAATs - Dual functional proteins

Transporters and ion channels originally have been thought to function distinct and to have structurally different determinants. As it has been described for several other neurotransmitter transporters, e.g. the Na⁺/Cl⁻-dependent transporters for dopamine, 5-hydroxytryptamine (serotonin), noradrenaline, GABA and glycine (139-147), EAATs are dual functional proteins, melting the boundary between channels and transporters.

Beside the glutamate uptake function, EAATs mediate a less understood channel-like anion conductance (13-22, 138). This uncoupled anion conductance requires sodium and glutamate binding to the transporter, but is thermodynamically independent of the glutamate transport (14, 16, 20, 21, 138, 149) and is distinct from a glutamate independent chloride leak-current (138, 151, 152). The physiological importance of the glutamate-dependent anion conductance is less clear than that of glutamate uptake. It was suggested that the anion conductance acts as voltage-clamp by counteracting the neuronal depolarization upon postsynaptic glutamate receptor activation and that it might play an important role in regulation of neuronal excitability (16). Neither the exact mechanism nor the structural determinants of this uncoupled channel-like anion conductance are defined. Up to date, several models accounting for the dual functions of EAATs have been proposed. Mainly, they vary in the assumption of a single or a dual pore for glutamate transport and anion flux (19, 21, 153, 154). There are some mutagenesis studies which indicate rather independent structural determinants for both functions than a single glutamate and anion pathway (155-157). Recently, TM2 was suggested to form at least a part of the anion pathway (158). Since TM2 has a lot of polar residues and positive charges at extra- and

intracellular edges and is furthermore accessible for the aqueous solution it is a good candidate for an anion pore adjacent transmembrane domain. Mutations in TM2 were shown to alter anion conductance without affecting glutamate transport. Furthermore, a residue at the edge of TM2 - D112 in EAAT1 (S74 in Glt_{Ph}, D83 in EAAT3, D117 in EAAT4) - can influence glutamate transport as well as anion conduction and may form the gate of the chloride channel. That study proposes a single pore with a chloride permeation pathway in close proximity to a domain that influences glutamate transport and that glutamate binding and/or translocation modifies the anion permeation properties of the transporter (158), which is in agreement with several other studies (159-162). In EAAT4 the homologue residue D117A changes unitary anion current amplitudes and relative anion selectivities (160). The exact role of this region (TM2) and of flanking residues still has to be clarified and was analyzed in detail on the basis of D83 by voltage clamp fluorometry (VCF) (see section 10).

Currently, a crystallization study reports on an intermediate conformation of Glt_{Ph} between the outward and inward facing states (55) (see section 3.2.1.3.1, Figure 3.3F). This intermediate state shows a cavity which is proposed to be the pathway for the uncoupled anion conductance and is bordered by residues of TM2 and TM5 and flanked by the two polar residues S65 and Y195. Residues of TM2 were shown to modulate anion fluxes (158) and S65 was formerly proposed to be involved in anion conduction and to be part of the selectivity filter in EAATs (148,158). The residue, S74 in Glt_{Ph} (D83 in EAAT3, D112 in EAAT1 and D117 in EAAT4), earlier studied in EAAT1 and EAAT4 and analyzed within this work, exactly resides at the edge of the proposed anion cavity (158, 160, 161).

This structural model could explain the substrate dependence of anion conduction, by transient formation of the anion pathway during substrate translocation. Furthermore, they hypothesized that intermediate anion states could be reached even if translocation to the inward facing states is prevented and by this they explain mutations which show abrogation of transport, whereas anion conductance is maintained.

The structural characterization of Glt_{Ph} gave more and more insights into the structure-function relationship and enables to establish a transport scheme for glutamate transporters.

3.2.1.3.3 EAAT transport mechanism

Currently, it is believed that the glutamate transport cycle is composed of 17 reactions (56, 57) (Figure 3.4A) and structural fulfilled by isomerization between four major conformations (54) (Figure 3.4B).

Figure 3.4
Uptake cycle and transport scheme of glutamate transporters

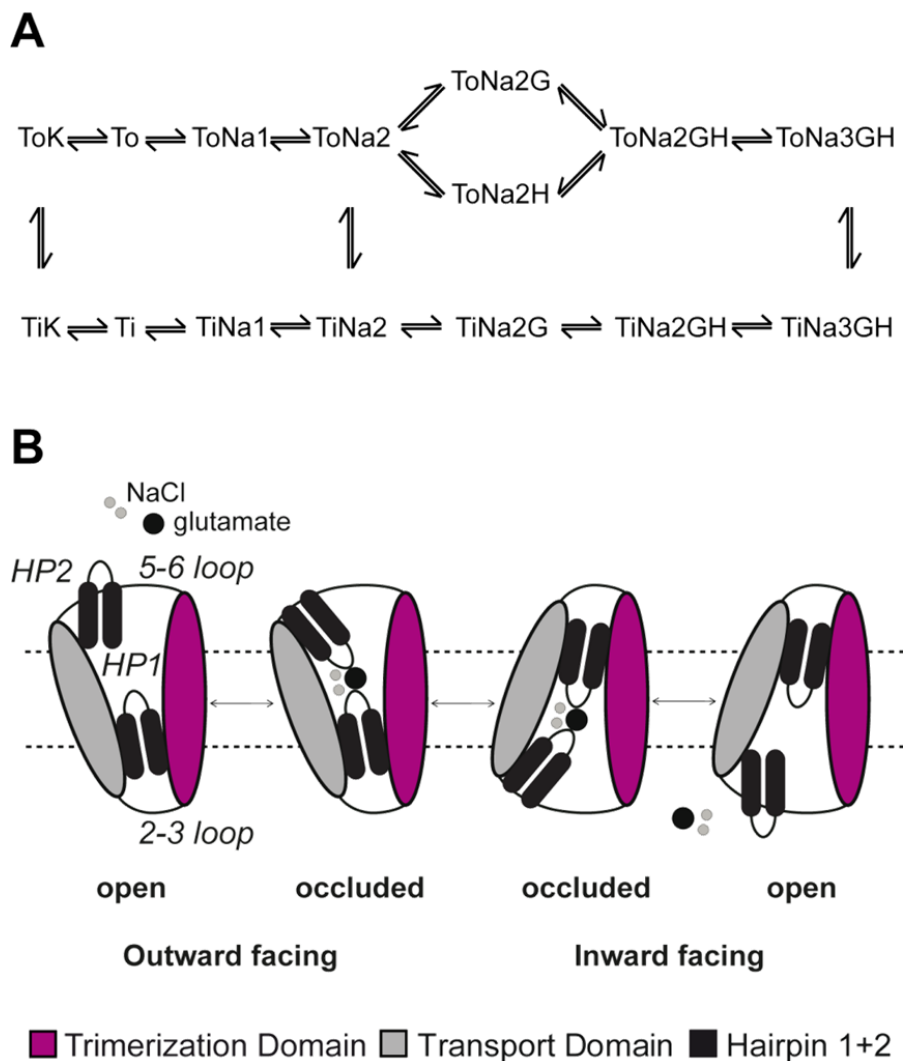


Figure 3.4: Uptake cycle and transport scheme of glutamate transporters.

A, shows a 15-state model of the uptake cycle of eukaryotic glutamate transporters consisting of 17 reactions (adapted from (57)). B, illustrates a schematic transport mechanism (modified from (54)). Shown is a single protomer. The isomerization between the outward and inward facing occluded states occurs upon movement of the whole transport domain (grey), relative to the trimerization domain (fuchsia). The inward facing open state has not been structurally characterized and is hypothetical.

The empty transporter resides in an outward facing state, the extracellular gate - HP2 - is open and the substrate binding sites are exposed to the extracellular space (ToK, To). Eukaryotic glutamate uptake is initiated by association of three sodium ions, one proton and one glutamate. Association of these substrate causes closure of HP2 (ToNa1, ToNa2, ToNa2G, ToNa2H, ToNa2GH, ToNa3GH), and the isomerization between outward and inward facing conformations which involves a rotation and a large piston-like movement of the whole transport domain results in the inward-facing occluded conformation (TiNa3GH, TiNa2GH, TiNa2G, TiNa2, TiNa1). Opening of the intracellular gate - HP1 - is followed by substrate release and exposure of the binding sites to the intracellular solution (Ti, TiK) (54), the inward facing open conformation is reached.

The trimerization domain is fixed in the membrane and acts by this as a counterbalance to the movements of the transport domain. The 2-3 loop and the 5-6 loop connect the corresponding transmembrane domains to the trimerization domain and enable the large inward movement. Retranslocation after association of internal K^+ completes the uptake cycle.

3.2.1.4 EAAT involvement in pathogenicity

A low extracellular glutamate concentration is important to ensure an appropriate signal-to-noise ratio and to prevent over-excitation of glutamate receptors and resulting cell death, which is known as glutamate excitotoxicity. The neurotoxic effect of glutamate was first shown 1957 by Lucas and Newhouse by systemic glutamate application which caused retina-degeneration in mice.

EAATs remove glutamate from the synaptic cleft into neuronal and glial cells (58) and by this they exhibit a neuroprotective role. EAAT dysfunctions and resulting high external glutamate concentrations are correlated with diverse neurological diseases and abnormal brain activity. An increased extracellular glutamate concentration has been associated with a wide range of chronic neurodegenerative disorders, e.g. amyotrophic lateral sclerosis, Huntington's and Alzheimer's disease, multiple sclerosis (59-64) and with neuropsychiatric disorders like schizophrenia (65). Additionally, glutamate provokes severe damages in acute insults as stroke or traumatic injury, ischemia, anoxia and epilepsy (66-72). Glutamate excitotoxicity and

oxidative stress have furthermore impact on retinal diseases, e.g. retinal ischemia, glaucoma, diabetic retinopathy and age-related macular degeneration (73-75).

This wide variety of involvement of EAAT dysfunctions in diverse diseases made them an attractive target from a therapeutic perspective. Surprisingly, the medicinal chemistry attempt in the glutamate field focused almost only on glutamate receptors (76-78) while EAATs attract minor attention. A better understanding of glutamate transporters, their regulation, expression and structure-function relationship might be beneficial in creating new therapies and pharmaceutical products against e.g. neurodegenerative diseases. In this work, attention is in particular turned to one neurological disorder - episodic ataxia (EA) - which has its seeds in mutations in *SLC1A3*, the gene encoding EAAT1.

3.2.1.4.1 The role of EAAT1 in episodic ataxia

Episodic ataxias (EAs) are rare autosomal dominant channelopathies that manifest as imbalance and paroxysmal cerebellar incoordination associated with additional other neurological symptoms, which are mainly cerebellar in origin.

So far, six episodic ataxia syndromes have been identified, differing in the genetic origin and clinical features (79). The genetic origin of EA3 and EA4 is unknown. Whereas EA1 (mutated gene: *KCNA1*, mutant protein: Kv1.1) (80-90), EA2 (mutated gene: *CACNA1A*, mutant protein: Cav2.1) (91-95) and EA5 (mutated gene: *CACNB4*, mutant protein: Cav2.1) (96) are caused by mutations in genes encoding voltage-gated cation channels, episodic ataxia type 6 is caused by mutations in *SLC1A3*, the gene encoding EAAT1 the major glutamate transporter in cerebellar Bergmann glia (97, 98).

In contrast to the other types of episodic ataxia, EA6 is characterized by long duration of attacks, epilepsy and absent myokymia, nystagm, and tinnitus (79). So far, EA6 has been reported in two families with two distinct disease-causing *SLC1A3* mutations. One mutation predicts a substitution of cysteine in TM4 by serine (C186S EAAT1) (98). File studies of a ten-year-old boy suffering from episodic ataxia type 6 determined another mutation, on which this work partly focused on, and which predicts a substitution of a highly conserved proline by arginine at position 290 in EAAT1 (97). Both mutations have been reported to reduce glutamate uptake (97-99). Ongoing studies showed that P290R reduces EAAT1 expression levels and surface

membrane insertion, diminishes individual glutamate transport rates and increases EAAT1-associated anion currents (99). As antisense knockdown of EAAT1 was shown to cause excitotoxicity in *in-vivo* and *in-vitro* models (100) and EAAT1 deletion results in increased susceptibility to seizures and cerebellar injury after traumata (101), EAAT1 plays a crucial role in glutamate clearance and reduced glutamate uptake by the disease-causing mutation was suggested to contribute to neuronal hyperexcitability and seizures, hemiplegia, and episodic ataxia (97).

The role of the anion conductance in the pathomechanism of EA6 is controversial, since *hEAAT1* is almost exclusively expressed in Bergmann glia cells in the cerebellum which exhibit a negligible anion conductance (102). GABA_A-mediated excitation is caused by high internal chloride concentrations (103-105). And it was suggested that an activated channel property of EAAT1 by P290R and resulting low intracellular chloride concentrations might impair GABAergic astrocyte excitation (99). EAAT1 anion currents may attenuate GABA_A- and GABA_B-mediated synaptic transmission by stimulating GABA re-uptake by GABA transporters which are coupled to Cl⁻ movement (99) and expressed in Bergmann glia.

The exact mechanism and physiological impact still has to be clarified. To get further insights into the molecular pathophysiology of EA6 and to define particular steps on the transport cycle affected by this disease-associated mutation, voltage clamp fluorometry (VCF) was employed (see section 11).

4 Aims of this thesis

Although several biochemical, electrophysiological and crystallographic studies expand the knowledge of glutamate transporters, their localization, physiological importance, pathogenicity, structure and their transport mechanism, the details of structure-function relationship are still covered.

Among a minor project dealing with hetero-oligomerization studied by biochemical and electrophysiological and confocal approaches, the principal objective was to employ the technique of voltage clamp fluorometry (VCF) to analyze EAAT-associated conformational changes and by this gaining detailed insights into the structure-function relationship of human glutamate transporters. The technique of VCF enables simultaneous measurements of whole-cell currents and detection of fluorescence changes of fluorescently labeled proteins. Thereby fluorophores are attached to moving parts of the protein. Since the emission of a fluorophore is sensitive to the local environment, a conformational change in response to a stimulus, (e.g., a change in membrane potential or changing substrate concentrations), resulting in an environmental change of the fluorophore, could be either reported as an increase or decrease of the fluorescence signal. Prior VCF-studies on EAAT3 already revealed several positions for fluorophore attachment and demonstrated that the technique is applicable to detect EAAT-associated conformational changes during glutamate uptake (163, 164).

Beside biomolecular, biochemical and electrophysiological approaches, voltage-dependent conformational changes of *h*EAATs and altered conformational changes of mutant *h*EAATs heterologously expressed in *Xenopus laevis* oocytes should be analyzed via VCF. Thereby the focus was set primary on two mutations. One mutation, D83A in EAAT3, was shown to exert effects on both transporter functions and was therefore a good target to investigate the interdependence of transporter and anion channel function. Analyzing the conformational changes of P259R EAAT3, the homologue mutation shown to cause episodic ataxia type 6 in EAAT1, should clarify the disease underlying pathomechanism.

5 Discussion

5.1 Independent-acting subunits in heterotrimers of neuronal glutamate transporters EAAT3 and EAAT4

Different EAAT isoforms can be roughly subdivided by their localization as being either glial (EAAT1, EAAT2) or neuronal (EAAT3, EAAT4, EAAT5) glutamate transporters. Furthermore, EAAT isoforms vary in the ratio of transport to anion currents and are thus expected either to function primarily as glutamate transporter or as anion channels (16, 21, 158). As it is already known, functional EAATs assemble as trimers and it is interesting if certain EAAT isoforms can form heterooligomers and if hetero-multimerization has functional consequences on the heterotrimeric assembly.

To study whether EAAT isoforms assemble into heterotrimeric complexes, different EAAT isoforms were co-expressed in mammalian cells, either as YFP fusion protein or as a His fusion protein and analyzed by SDS- or BN-PAGE by their different molecular masses added by the distinct tags. The glial transporters EAAT1 and EAAT2, or EAAT2 and EAAT3, or EAAT2 and EAAT4, do not co-assemble. Solely the two neuronal transporters EAAT3 and EAAT4 form heterotrimers (see section 9.4.1, Figure 9.1).

As EAAT3 and EAAT4 exhibit different unitary glutamate transport rates (165) and display isoform-specific time and voltage dependences of macroscopic anion currents (168), heterotrimers of these isoforms provide an excellent possibility to study intersubunit interactions. By introducing a mutation which changes the substrate sensitivity from glutamate to serine (150, 167), EAAT3- and EAAT4-currents can be distinguished. Co-expression of EAAT3 and EAAT4 in *Xenopus laevis* oocytes revealed no changes of the apparent dissociation constants for glutamate, serine or sodium. Employing expression in mammalian cells and rapid application of glutamate with subsequent analysis of the time constants of the transport- and anion-associated currents showed no effect by co-expression. Individual subunits within heterotrimeric complexes act independently of each other (see section 9.4.2 and 9.4.3, Figure 9.2-4).

EAAT3 is polarized to the apical surface in epithelial cells and localized to hippocampal neuronal dendrites by a unique sorting signal (166). Epithelial sorting was analyzed by co-expression of fluorescent protein-tagged EAAT3 and EAAT4 in

Madin-Darby canine kidney (MDCK) cells, confocal imaging and surface biotinylation. Confocal imaging and surface biotinylation revealed an altered epithelial sorting of EAAT3/EAAT4-heterotrimers (see section 9.4.4, Figure 9.5 and Figure 9.6).

Summarizing this, it could be shown that the neuronal glutamate transporters EAAT3 and EAAT4 co-assemble into stable heterotrimers (see section 9). Hetero-oligomerization of EAAT3 and EAAT4 has no effects on amino acid transport or on EAAT-mediated anion conductance, but alters epithelial sorting.

The observation of fully independent-acting subunits in terms of substrate transport and anion conduction is in agreement with other studies of co-expressed WT and mutant EAATs (167, 169, 170). The physiological importance of the glutamate-dependent anion conductance is less clear than that of glutamate uptake, but it was suggested that it acts as voltage-clamp and that it has an important role in regulation of neuronal excitability (16). The result that the anion conductance is as well rather mediated independently than cooperatively, may play a role for its physiological impact. At low glutamate concentrations, the anion conductance will be effectively activated in independently working subunits. In contrast, cooperative intersubunit interactions would require higher glutamate concentrations for a same effective activation. Furthermore, the advantage of the trimeric nature of the transporter with fully independently acting subunits might be founded in the large aqueous bowl-shaped basin in a multimeric structure, which plays a functional role by facilitation of the transport of charged substrates across the membrane dielectric. An additional function of the central basin in a trimeric structure in modifying ligand diffusion was suggested by the kinetics of β -2-fluorenyl-aspartylamide (2-FAA) interactions with EAAT3 (185). By steric effects of the aqueous cavity itself, it might present a significant diffusion barrier which would not slow the microscopic subunit unbinding rate but would result in a kinetic advantage by slowing the effective loss of substrate to the bulk space. This could provide a mechanism to modulate the buffering kinetics at low substrate concentrations.

Hetero-trimerization, as reported here, is not a common feature of different EAAT isoforms. It is special for EAAT3 and EAAT4, which were selectively enriched in Purkinje cell bodies, dendrites, and spines (29, 33). Heterotrimeric assemblies of EAAT3 and EAAT4 might be a native appearance in these regions. The presence of both, EAAT3 and EAAT4, facilitates rapid glutamate binding, and may have a role in shaping the amplitude of postsynaptic responses in Purkinje cells (171,172) and

could modulate the metabolism of GABA (173). Different targeting signals in native heterotrimers might result in a changed insertion of heterotrimers on a cellular level than that of homotrimers. Hetero-trimerization of a low affinity/high capacity (EAAT3) and a high affinity/low capacity (EAAT4) transporter (165), may serve as tight regulation of the external glutamate concentration and as fine modulation of neuronal excitability by EAAT-associated anion channels (174, 175).

5.2 Interdependence of transport and anion channel function

EAATs act as dual functional proteins. Beside the secondary-active glutamate transport, they exhibit a pore-mediated anion conduction. EAATs occupy a neuroprotective role by their glutamate uptake ability and might be involved in the regulation of cell excitability by their anion channel property. Gating of EAAT anion channels is tightly coupled to transitions within the glutamate uptake cycle, resulting in Na^+ - and glutamate-dependent anion currents. These anion currents are thought to be conducted through an anion pathway that is opened and closed in response to conformational changes underlying glutamate transport. The exact molecular determinants of the anion conduction or of the interconnection of both functions are poorly understood. In a systematic screen of TM2 for mutations affecting EAAT1 anion channel function, a highly conserved aspartate (D112) at the intracellular loop of TM2 was found to have serious effects on both transporter functions. Neutralizing D112 in EAAT1 abolishes the glutamate dependence of anion currents and reduces glutamate uptake rates by about 40% (158). Continuing studies revealed that the corresponding mutation D117A changes unitary anion current amplitudes and relative anion selectivities of EAAT4 anion channels (160). By these effects, aspartate 112, respectively 117, was suggested to be localized in close proximity to a domain influencing substrate transport, and furthermore to flank the anion channel of EAATs and to possess gating properties.

Investigating the effects of the homologue point mutation D83A on EAAT3 conformational changes by VCF promised insights into the interaction of transporter and anion channel function of EAAT glutamate transporters. To permit site-directed fluorescence labeling of EAAT3, different single cysteines for fluorophore attachment localized in different parts of the transporter, V120C (3-4 loop), M205C (TM4c) and

A430C (7-8 loop) were introduced into *hEAAT3* (see section 10.4.1, Figure 10.1). To study conformational changes, WT, cysteine-substituted or D83A EAAT3 was expressed in *Xenopus laevis* oocytes. It could be ensured by two-electrode voltage clamp measurements that cysteine insertions do not modify basic features of EAAT3, since voltage-dependent currents, composed of a mixture of anion and uptake currents, as well as pure uptake currents resemble those of WT EAAT3 (see section 10.4.1, Figure 10.1). Uninjected oocytes or oocytes expressing EAAT3 lacking cysteines for fluorophore attachment do not exceed background fluorescence, in contrast to each of the reporter mutants (see section 10.8, Suppl. Figure 10.9), indicating an EAAT3-specific fluorescence labeling.

V120C, M205C and A430C EAAT3 display pronounced voltage-dependent fluorescence changes which mirror conformational changes during transport or anion conduction. Fluorescence amplitudes can be modified by transporter substrates, such as Na⁺ and glutamate. The EAAT-specific blocker, threo- β -benzyloxyaspartate (TBOA) is known to prevent substrate-binding by locking EAATs into an outward facing conformation with HP2 open (51). TBOA blocks the observed fluorescence changes by about 90 % (see section 10.4.1, Figure 10.2 and section 10.8, Suppl. Figure 10.9), supporting the notion that fluorescence changes are strictly associated with conformational changes of EAAT3. Further experiments revealed that conformational changes are not affected by total substitution of external anions (see section 10.8, Suppl. Figure 10.10). Moreover, observed fluorescence changes are time-dependent and time courses differ for different fluorophore attachment sites and are therefore thought to depend not only on global conformational changes of the EAAT proteins, but also reflect additional distinct micro-environmental changes.

A special observation was made for M205C EAAT3 fluorescence time courses. M205C EAAT3 discovers an ultra slow voltage- and glutamate-dependent process (single time constants ~ 4 s and ~ 7 s) (see section 10.4.2, Figure 10.3). There are several possibilities what kind of process might be reflected by this slow conformational change: a) a process occurring within the uptake cycle, b) a branching process outside the uptake cycle to another conformational state with reciprocal dependence and c) a branching process outside the uptake cycle to another conformational state with partial dependence. As EAAT3 turnover rates are determined to be above 10/s (165), and glutamate transport currents do not change with the same time constants as the fluorescence, possibility a) and b) are excluded.

This conformational change might reflect a process that occurs from certain states of EAAT3 and does not interfere with the uptake cycle, but depends on substrates as sodium and glutamate. A possible explanation of these slow processes might be a large collective motion, recently reported by Jiang and colleagues (176). These large collective motions are described as processes which are functionally important for substrate transport, but not for the substrate-gated anion conductance and which are coupled to the inward movement of the transport domain. This might explain why the slow conformational changes observed in this study are anion-independent, but altered by glutamate. Alternatively, the slow fluorescence changes correspond to a slow gating process within the EAAT anion channel, initially described in EAAT4, but also observed in EAAT3 (unpublished observation). This gating process slowly changes the anion to cation selectivity upon membrane depolarization with resembling time and voltage dependences (175). Further studies have to uncover the exact underlying process of this ultra slow conformational change.

Recapitulatory, fluorescence changes of fluorophores added to V120C, M205C and A430C report on conformational changes that require external Na^+ , are changed by glutamate, are blocked by TBOA, but are independent of the anion composition. These results indicate that the reported fluorescence changes rather reflect conformational changes during the transport cycle than conformational changes initiated by anion flux.

Expression of cysteine-substituted D83A EAAT3 revealed strongly reduced glutamate uptake, reduced glutamate-activated and increased anion currents (see section 10.4.3, Figure 10.4) resembling earlier results on this mutation (158, 160). Furthermore, D83A changes the voltage and substrate sensitivity of conformational changes for each fluorophore attachment site (see section 10.4.3, Figure 10.5). The observed fluorescence changes are still sodium- and glutamate-dependent and anion-independent (see section 10.8, Suppl. Figure 10.10).

Employing kinetic simulation of observed current and fluorescence data enables to determine the concrete steps/reactions and or transitions within the EAAT uptake cycle disturbed by neutralizing aspartate 83. The voltage and substrate dependence of EAAT3 fluorescence signals can be well described by a kinetic model that is based on the glutamate transport cycle, composed of 17 reactions (56, 57) and structurally fulfilled by isomerization between four major conformations (54) assigned to different fluorescence amplitudes. To account for the anion channel ability, branching open

channel states from certain states of the uptake cycle were added (see section 10.4.4, Figure 10.6). In this scheme the empty transporter resides in an outward facing state, with HP2 being open and the substrate binding sites exposed to the extracellular space ($F_{O_{open}}$: ToK, To). Glutamate uptake is initiated by association of three Na^+ , one H^+ and one glutamate. Association of these substrate causes closure of HP2 ($F_{O_{occluded}}$: ToNa1, ToNa2, ToNa2G, ToNa2H, ToNa2GH, ToNa3GH), and a large piston-like movement of the transport domain results in the inward-facing conformation ($F_{i_{occluded}}$: TiNa3GH, TiNa2GH, TiNa2G, TiNa2, TiNa1). Opening of HP1 is followed by substrate release and exposure of the binding sites to the intracellular solution ($F_{i_{open}}$: Ti, TiK). Association of internal K^+ and subsequent retranslocation completes the uptake cycle. WT EAAT3 rate constants within the uptake were adopted from a previous VCF study on EAAT3 (163). The anion channel open probabilities were determined by fitting the model to the experimentally observed fluorescence and current data of V120C, M205C and A430C EAAT3. The resulting simulation demonstrates a good agreement of the simulated and observed fluorescence-voltage relationship under different substrate conditions and could reproduce current characteristics of EAAT3 (see section 10.4.4, Figure 10.7), but it fails to reproduce as high transport rates of EAAT3 for reverse transport at high external K^+ as published (177). As all experimentally data were obtained by measurements in the absence of external K^+ this limitation of the kinetic simulation was accepted.

By unrestricted distinct reactions, groups of reactions and or transitions within the EAAT uptake cycle or anion channel open probabilities, kinetic simulation revealed that D83A modifies translocation rates between outward and inward facing states (reaction 8, 15, 17). Modifying these transitions enables to accurately describe all existing data, glutamate transport, anion currents and fluorescence data (see section 10.4.4, Figure 10.7). This result is in partial disagreement with a recently performed analysis of the effects of D117A on EAAT4 anion currents (160). There it was suggested that D117 is in close proximity to the anion conduction pathway and that neutralizing this residue alters anion channel open probabilities by direct and exclusive modification of the anion channel. EAAT3 and EAAT4 anion channel properties are very well conserved (168) in contrast to glutamate transport rates (165). EAAT4 is a high-affinity/low capacity transporter, contrariwise EAAT3. The glutamate uptake as serious effect of D117 was disregarded in that study, although

first reports on D112 in EAAT1 report on about 40% reduced glutamate uptake (158). D83A reduced EAAT3 uptake current amplitudes to values between 30% - 50% in full agreement with Ryan *et. al.*. Especially this parameter seems to be crucial for a correct determination of the disruption underlying the effects of neutralizing aspartate 83, 112 and 117, respectively.

The large movement of the transport domain is enabled by the membrane-fixed trimerization domain acting as counterbalance (see section 3.2.1.3.3). During the movement of the transport domain TM3 is shifted relative to TM2, resulting in an altered orientation of the 2-3 loop. Crystal structures of Glt_{Ph} place the homologous residue of D83/D112/D117 to the 2-3 loop between the trimerization and the transport domain (Figure 5.1). Homology models of EAAT to Glt_{Ph} structures predict a rotational movement of the residue upon transition from the outward to the inward-facing conformation (160). Altered translocation by D83A might occur by changing the hinge function of the 2-3 loop connecting the trimerization and the transport domain and by this D83A might affect the isomerisation between inward and outward facing conformations.

Figure 5.1
Localization of S74 in Glt_{Ph}, the homologue residue of D83 in EAAT3

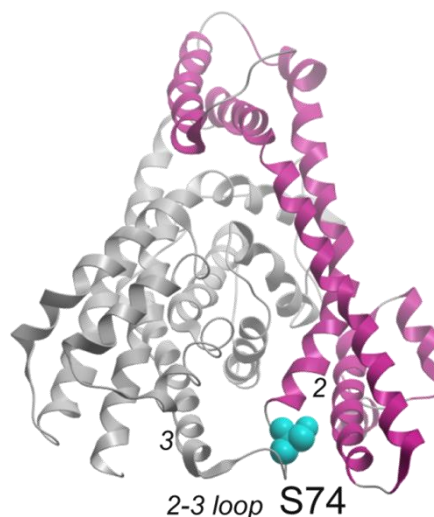


Figure 5.1: Localization of S74 in Glt_{Ph}, the homologue residue of D83 in EAAT3.

Ribbon representation of a Glt_{Ph} monomer viewed from the intracellular side (pdb-file: 3KBC) with the residue S74 (*light blue*), the homologue residue of D83 in EAAT3, localized in the 2-3 loop connecting the trimerization domain (*fuchsia*) with the transport domain (*grey*).

This study primarily shows that conformational changes in EAAT3 are anion-independent. It seems rather unlikely that anion-dependent conformational changes were just invisible, since the anion independence of conformational changes was observed for different fluorophore attachment sites, localized in the 3-4 loop, in TM4c and in the 7-8 loop. Moreover, a mutation previously suggested to exert its effects on transport and anion channel-mediated currents by solely affecting the anion pathway by itself, was here shown to modify the transition between inward and outward facing states. By a changed translocation, D83A directly impairs glutamate uptake which leads to changed anion channel properties of EAATs, providing further evidence for the intimate interaction of both transporter functions.

5.3 Disturbed sodium association as underlying pathomechanism of EA6 - Another example for the intimate interdependence of glutamate uptake ability and anion channel function of EAATs

EAAT dysfunctions and resulting high external glutamate concentrations are correlated with diverse neurological diseases and abnormal brain activity (see section 3.2.1.4). Investigating EAAT-associated diseases might assist to gain insights into the pathomechanisms of certain rare human diseases and might be beneficial in creating new strategies against them. Further, it will help to understand the physiological impact of the impaired transporters and to permit additional knowledge of the structure-function relationship of EAATs.

In terms of defining EAAT-associated pathomechanisms, this work focuses on one neurological disorder - episodic ataxia type 6 (EA6) - which has its seeds in mutations in *SLC1A3*, the gene encoding the glial glutamate transporter EAAT1. Episodic ataxias (EAs) are rare autosomal dominant channelopathies that manifest as imbalance and paroxysmal cerebellar incoordination associated with additional other neurological symptoms, which are mainly cerebellar in origin. In contrast to other types of EAs, EA6 is characterized by long duration of attacks, epilepsy and absent myokymia, nystagm, and tinnitus (79). In a systematic genetic screen for polymorphisms in *SLC1A3* two mutations were found in patients suffering from EA6.

One of these mutations predicts the substitution of a highly conserved proline 290 in the hinge of transmembrane domain 5 (TM5) by arginine (97). Former studies showed that P290R reduces EAAT1 expression levels and surface membrane insertion, diminishes glutamate uptake and increases EAAT1-associated anion currents (97, 99). EAAT1 plays a crucial role in glutamate clearance and in one of the studies reduced glutamate uptake by P290R was suggested to be the major cause of EA6-symptoms (97). The other study paid more attention on the disturbed anion channel function and proposed it to be the EA6-underlying pathomechanism (99).

The exact mechanism and physiological impact is controversial and still has to be clarified. To get further insights into the molecular pathophysiology of EA6 and to define particular steps on the transport cycle affected by this disease-associated mutation, voltage clamp fluorometry (VCF) was employed (see section 11). Since P290R affects both transporter functions, as D83A (see section 10), the technique of VCF may expose another example for the intimate interdependence of glutamate uptake ability and anion channel function of EAATs.

To enable cysteine-specific fluorophore attachment for subsequent VCF analysis, a cysteine was introduced at position 238 in P290R EAAT1. This mutation is localized in TM4c and the homologue mutation in EAAT3 was shown to report on pronounced EAAT3-specific conformational changes, without affecting basic features of the transporter (161, 164).

As V238C P290R *hEAAT1* did not express at levels sufficiently high to allow current and fluorescence measurements in *Xenopus laevis* oocytes, a related isoform, *hEAAT3* was chosen to study the effects of the homologue mutation P259R. To ensure that mutation of the conserved proline exerts similar effects in both EAAT isoforms, P259R was expressed in mammalian cells, electrophysiologically analyzed and compared to P290R EAAT1 measurements. P259R alters *hEAAT3* current characteristics similar as P290R *hEAAT1*, i.e. increases anion currents and displays similar voltage-dependent time courses (see section 11, Figure 11.1 and Suppl. Figure 11.5) (99). Two-electrode voltage clamp measurements furthermore showed similar effects in oocytes expressing P259R EAAT3 or P290R EAAT1 and could confirm drastically reduced glutamate uptake currents (see section 11, Figure 11.1 and Suppl. Figure 11.5). As exchanging the conserved proline by arginine exerts similar effects in both EAAT isoforms after expression in oocytes as well as in

mammalian cells, EAAT3 is an appropriate model-isoform to study the disease-causing mutation.

To permit site-directed fluorescence labeling of EAAT3, an established cysteine mutation for fluorophore attachment localized in TM4c (M205C) was introduced into *h*EAAT3 (see Figure 11.1) and combined with P259R. Earlier work on M205C EAAT3 revealed that this mutation reports on pronounced fluorescence changes specific for EAAT3 and furthermore does not change basic features of WT EAAT3 (161, 164). EAAT3 carrying the fluorescence attachment site M205C displays voltage-, substrate- and time-dependent conformational changes (see Figure 11.2, *left column*). These conformational changes are altered by substrates such as sodium and glutamate. P259R profoundly changes the voltage, substrate and time dependences of M205C EAAT3 conformational changes. P259R inverts the voltage dependence, alters the glutamate-induced fluorescence change and decelerates the time dependence of these signals (see Figure 11.2, *right column*).

Extensive studies and kinetic simulations on M205C (161) demonstrated that fluorescence changes mirror conformational changes during the EAAT uptake cycle. The EAAT uptake cycle is elaborately composed of 17 different reactions and structural accomplished by isomerization between four major conformational states (see section 3.2.1.3.3), i.e.: the outward facing open and occluded and the inward facing open and occluded states. Calculations of the steady-state distribution identify fluorescence changes upon hyperpolarization in the absence of glutamate to reflect primary sodium-binding events to the empty transporter (T_0) (see Suppl. Figure 11.7). P259R shows most severe alterations on M205C *h*EAAT3 fluorescence under the conditions causing the transitions from T_0 to T_0Na_2H , indicating a disturbed sodium association. Sodium dependence VCF measurements adduce evidence of a modified Na^+ -association, represented in a decreased sodium affinity and extremely decelerated time constants of sodium-binding and unbinding induced conformational changes. Furthermore, P259R fluorescence signals upon sodium binding occupy a changed voltage dependence. An additional effect on the third sodium-binding which occurs under saturating glutamate concentrations could be excluded as P259R resembles WT and M205C EAAT3 K_D 's as well as published data on EAAT3 (see Suppl. Figure 11.6) (181).

Employing kinetic simulation of observed current and fluorescence data enables to discover individual reactions or transitions within the EAAT uptake cycle which are

disturbed by P529R. An earlier developed kinetic scheme to describe fluorescence signals as well as transport and anion currents of M205C *h*EAAT3 was used to confirm or to invalidate a disturbed sodium association (see section 10, 11) (161). In fact, random alterations revealed that modifying reactions 1, 2, 12 and 13 that report on Na⁺-association/-dissociation to the transporter in the outward or in the inward facing state and the additional increase of the voltage dependence of reaction 1 and the adjustment of the voltage dependence of reaction 2, could simulate almost all functional alterations by P259R (see Figure 11.4). The simulation predicts the voltage, substrate and [Na⁺] dependence of fluorescence signals of mutant transporters correctly. The decreased glutamate uptake currents and increased anion currents in the absence of glutamate were as well calculated in agreement with the measurements (see Figure 11.4). Furthermore, the kinetic model for P259R could support the extremely decelerated time dependence as binding and unbinding of the first and second sodium is calculated to be around 100 times slower (Table 11.2). Time-dependent simulations of current and fluorescence responses qualitatively resemble the deceleration by P259R. Calculations of the steady-state distribution show that P259R is mostly trapped in the outward facing open states (T₀ and T₀Na₂H) (see Suppl. Figure 11.7) in the absence of glutamate. Application of glutamate just slightly changes the residence probability of P259R EAAT3 by increasing the probability to reside in glutamate-bound outward facing states and in T₁Na₁. Appropriate glutamate uptake and fulfilling the complete transport cycle necessarily requires binding of the first and second sodium prior to glutamate. The shift of the steady-state distribution by P259R illustrative demonstrates the consequence of an enervated sodium binding.

The disease-causing mutation, either in EAAT1 or EAAT3, leads to an extremely reduced glutamate uptake capability and increased anion currents on a slow time course by a slowed Na⁺-association to the mutant transporters. Recently, a study on EAAT5 (186) identified slow Na⁺-association as basis for a slow activation time course of anion currents and very low glutamate transport. The result that the high capacity glutamate transporters EAAT1 or EAAT3 carrying a disease-causing mutation functionally resemble the low capacity glutamate transporter EAAT5 further support the results presented in this work and illustrates the importance of the evolutionary optimization of EAAT isoform with distinct functional properties.

However, the predictions by the established kinetic model fail to correctly describe the increased anion currents calculated by the prediction of open probabilities of P259R EAAT3 in the presence of glutamate (Figure 11.4). P290R EAAT1 was shown to increase anion currents while surface membrane insertion was reduced (99). Noise analysis measurements revealed an incompatible high absolute open probability for WT EAAT1. Under saturating glutamate concentrations EAAT3 absolute anion channel open probabilities were defined to be around 0.9. Assuming that these values are correctly determined, a fourfold increase of EAAT3 glutamate-induced anion currents by P259R has to result in open probabilities larger than 1. Therefore, noise analysis might underestimate the number of active WT EAAT anion channels. A similar disagreement was found analyzing CIC-4 (184). CIC-4 acts like EAATs as dual functional channel and transporter. Noise analysis revealed that changing the external chloride concentration, changes the apparent number of CIC-4 proteins without affecting the surface membrane density. It was suggested that CIC-4 can switch in an anion-dependent manner between its two functional states. As anion binding and unbinding is rapid compared to the transition to the channel mode, CIC-4 equilibrates into a semi-equilibrium distribution between the two transport modes. Noise analysis will only report on opening and closing transitions of the anion channels and in such a mechanism underestimate the number of active anion channels and overestimate the open probability. Na⁺-association is likewise fast for WT *hEAAT3* and noise analysis might provide as well incorrect high absolute open probabilities of *hEAAT3* anion channels via a similar mechanism.

Nevertheless, kinetic simulation could correctly describe all other functional alterations by P259R by a disturbed sodium association to EAAT3. This raises the question how exchanging proline by arginine can cause the described effects on sodium binding and unbinding. Is there a direct effect on the binding site causing enfeebled sodium coordination by a sterical barrier or does P259R disturb a conformational change associated with sodium binding or might there be global structural change?

On the first view crystal structures of the bacterial transporter homologue Glt_{Ph} show no indication for a direct influence on the sodium binding sites by P259R (Figure 5.2). Sodium binding sites of EAAT3 have been identified as the aspartate residues at position D368 (TM7), D440 and D455 (TM8) (51, 178-180). The episodic ataxia causing mutation P259R is not in close proximity to these residues (C α -distances in

the outward facing open conformation from P259 to: D368 = 26.3, D440 = 21.2, D455 = 24.4 Å) (Figure 5.2).

Figure 5.2

C α -distances distances in the outward facing open conformation from P259 to the different sodium binding sites

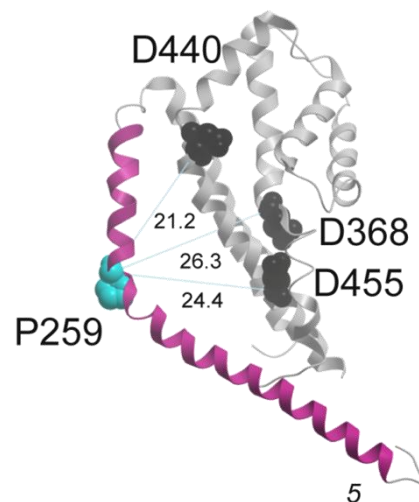


Figure 5.2: C α -distances distances in the outward facing open conformation from P259 to the different sodium binding sites.

Ribbon representation of a Glt_{P_H} monomer viewed from the side of the membrane (pdb-file: 2NWW) with the residue P259 (*light blue*), localized in TM5 (*fuchsia*), the three sodium binding sites (*black*) and parts of the transport domain (*grey*). Given are C α -distances in the outward facing open conformation from P259 to: D368 = 26.3, D440 = 21.2, D455 = 24.4 Å. For simplification parts of the protein were removed from the crystal structure and residue numbers of EAAT3 are used.

Furthermore, cation association is assumed to be a fast diffusion-controlled process and a dramatic effect of a 100-fold reduction of reaction rates seems rather unlikely. The structural basis for altered sodium binding to P259R *h*EAAT3 seems to be rather an effect on sodium associated conformational changes or a global structural change than a direct effect of P259R on the sodium binding sites.

The influence on a process associated with sodium binding, possibly a conformational change, is supported by the sodium-dependent saturating time constants of M205C or M205C-P259R EAAT3 fluorescence changes (Figure 11.3). Inverse time constants saturates at high sodium concentrations, implicating that rapid sodium binding is followed by a slower step, that becomes independent of sodium concentration once all binding sites are occupied. Since sodium site 2 is coupled to

opening and closure of HP2, P259R might affect these particular movements. Proline by itself functions as structural disruptor of α -helices and β -sheets and might be the structural determinant of the kinked shape of TM5 and exchanging proline by arginine might result in an overall structural change. Such an overall structural change could impair sodium-binding and subsequent induced conformational changes including translocation to the inward facing conformation of EAAT. It might be that P259 comes in close proximity to the sodium binding sites by such a global change. A possible scenario of a global structural change might be an altered orientation of the transport domain to the trimerization domain by a loss of the kinked shape of TM5 in P259R. A resulting changed coordination of the transport domain in the membrane dielectric might result in a changed electric field in the environment of moving protein parts upon sodium binding. Moreover, the position of Na^+ binding sites within the electric field could be altered. This interpretation could explain the inversed voltage dependence of conformational changes (Figure 11.2) and the increased electrical distances simulated for sodium binding (Table 11.2). Furthermore, a global structural change might as well explain the increased anion conduction by structural induced alterations of anion-conducting states and/or of the anion pathway by itself.

Recapitulatory, the effects of the EA6-causing mutation on the transport capability and anion channel function of EAATs are molecular founded in an impaired sodium-binding which might be triggered by a structural change influencing sodium associated conformational changes or by a global structural change induced by a disruption of the kinked shape of TM5. By direct intervention in the uptake cycle P259R exerts dual effects and sets another example for the intimate interaction of transporter and anion channel function.

The physiological relevance of the EAAT1 mutation found in patients suffering from EA6 might have its seeds in both EAAT functions: the impaired uptake ability and resulting high extracellular glutamate concentrations contributing to neuronal hyperexcitability and the increased anion channel function might impair GABAergic astrocyte excitation.

5.4 Observations made by an intermediate structure of Glt_{PH}

Finally, the results presented in this work, the independence of individual subunits in heterotrimers, the tight interaction of substrate transport and anion channel function discovered by two different mutations are in full agreement with a recently proposed structural model (55).

In this study a crystal structure of an asymmetric trimer of Glt_{PH} with two protomers in inward facing states and the third in an intermediate conformation between the outward and inward facing states is presented. In the asymmetric structure, single protomers show similar state-independent transport activities, supporting the observation of individual-acting subunits in EAAT-trimers.

The intermediate conformation furthermore shows a transient cavity which is proposed to be the pathway for the uncoupled anion conductance and is bordered by residues of TM2 and TM5. This intermediate conformation could be reached even if translocation to the inward facing states is prevented and by this the structural model can explain abrogation of transport, whereas anion conductance is maintained. The mutation D83A, localized at the edge of TM2 and the disease-causing mutation P259R, localized in the kink of TM5, reside exactly in the region described as transient cavity and the flank of it. Both mutations were shown to nearly abolish substrate transport, whereas anion conduction was maintained or even increased.

D83A exerts its effects on both transporter functions by modulation of the three translocation reactions (reaction 8, 15, 17). Theoretically, this altered translocation by D83A might occur by changing the hinge function of 2-3 loop and by this D83A might affect the isomerisation between inward and outward facing conformations, as discussed above (see section 5.2). It is also possible that D83A earlier intervenes in the uptake cycle by disturbing the isomerization to one of the intermediate states. By changing the translocation trajectory, D83A could not only affect substrate translocation and anion channel opening/closing, but also the anion conduction pathway itself.

Interestingly, the crystal structure of this intermediate state discovers a reduction of one of the C α -distances from P259 (P206 in Glt_{PH}) to one of the sodium binding sites. The C α -distance between P259 to D440 is reduced from 21.2 to 12.9 Å (Figure 5.3) which is possibly close enough to exert effects on the sodium binding site in a direct way. Although isomerization from the outward facing to the intermediate state requires sodium and glutamate binding in the proposed structural model (55), one

might speculate about a possible stepwise isomerization from and to several conducting states so that first a conformation is captured which develops a reduced distance between P259 and D440. In the currently accepted glutamate uptake cycle, isomerization is as well possible prior to glutamate binding (reaction 17), even if the reaction rates for this translocation are low compared to the translocation rates after glutamate binding. One might speculate about a further translocation possibility between ToNa1 and TiNa1.

Figure 5.3
C α -distances distances in the intermediate conformation from P259 to the sodium binding site D440

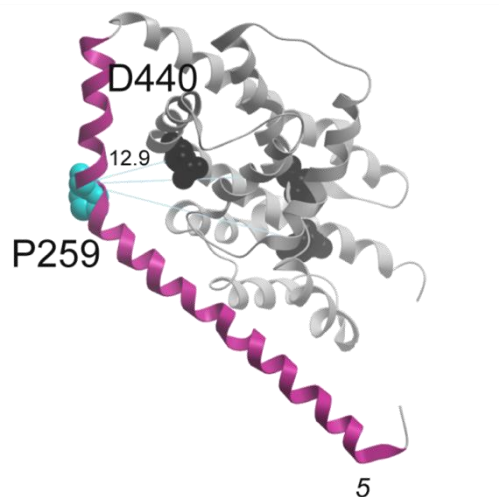


Figure 5.3: C α -distances distances in the intermediate conformation from P259 to the sodium binding site D440.

Ribbon representation of a Glt_{Ph} monomer viewed from the side of the membrane (pdb-file: 3V8G) with the residue P259 (*light blue*), localized in TM5 (*fuchsia*), the three sodium binding sites (*black*) and parts of the transport domain (*grey*). For simplification parts of the protein were removed from the crystal structure, residue numbers of EAAT3 are used and solely one C α -distance in the intermediate conformation from P259 to D440 = 12.9 Å is given in the picture.

5.5 Continuative questions and research

Although this work provides novel insights in terms of cooperativity between individual subunits in heterotrimeric EAAT complexes, the effects of two mutations residing in the region of the proposed anion cavity and the interconnection of transport and anion conduction by itself, there are still a lot of open questions, e.g.:

“Is heterotrimerization of the neuronal glutamate transporters EAAT3 and EAAT4 a native state?” and “What are the regulation mechanisms and physiological consequences of heterotrimerization and the changed epithelial sorting?”

“What is the structural background of the ultra slow conformational changes observed in EAAT3?” - As discussed above, these conformational changes might represent large collective motions, which are coupled to the inward movement of the transport domain. It is planned in a future project to test for such large collective motions by VCF experiments of co-expressed fluorescently stainable (M205C EAAT3) and serine-sensitive mutants of EAAT3 (R447E EAAT3). Application of serine should result in an inward movement of the serine-sensitive monomer, but not in a fluorescence change by itself. In case of fluorescence changes which reflect same time constants as the ultra-slow fluorescence changes, but do not exactly mimic the fluorescence changes induced in homotrimeric M205C EAAT3 by glutamate, one could support the suggestion of somehow cooperative large collective movements without inconsistency with non-cooperatively acting subunits.

Further posed questions are:

“What is the exact localization of the anion pathway?”, “Which residues are important for the correct development of the pathway and mandatory for the gating mechanism?” and “What is the definite physiological role of the anion conductance mediated by glutamate transporters?” Answering and investigating these questions necessitates more crystallographic evidence of the localization of the anion channel and might be adduced by a systematic screen of residues flanking the proposed anion channel and by combining molecular dynamics simulations and electrophysiological experiments on mutations of those residues. It is suggested that the anion channel is transiently formed by isomerization between inward and outward facing states. Mutations which avoid this movement and in consequence abrogate anion conduction, but do not directly interfere with substrate-binding (to exclude the possibility that the inward movement is avoided by a disturbed substrate-binding)

would expand the chance to understand anion conduction in EAATs. Studies in this direction have already started.

Furthermore, such a mutation on an EAAT isoform, which rather mediates anion flux than glutamate uptake (EAAT4) and which has less influence on the total glutamate uptake ability, could be studied in a mouse model and probably discover the physiological impact of the anion channel activity.

Concerning the project analyzing the episodic ataxia causing mutation, there are as well some unsettled questions:

“Is the impaired Na^+ -association to P259R the result of an overall structural change of the transporter caused by a modification of the kinked shape of TM5?” or “Might there exist another conformation in which a direct modulation of sodium binding by P259R is possible?” Ongoing work in our institute targets crystallization of the homologous mutation P206R in the bacterial glutamate transporter Glt_{Ph} and hopefully will provide structural access to the P206R-mediated alterations. One could as well use Photo-induced electron transfer (PET) between tryptophane and bimane fluorescence, a short distance-dependent quenching method, introduced in Glt_{Ph} to prove whether this residue gets into close contact with the suggested sodium binding sites and therefore could influence them directly. To improve the understanding of what exactly happens in patients suffering from episodic ataxias, a P290R EAAT1 knock-in mouse model will be studied in detail in a future project.

6 Conclusions

This work essentially deals with detailed investigations of the structure-function relationship in human excitatory amino acid transporters. It could be shown that individual subunits within EAAT heterotrimers act independently of each other. Furthermore, analyzing the interdependence of glutamate transport and the feature of anion conductance on the basis of two different mutations, shown to exert effects on both transporter functions, permits deeper insights concerning this particular question. The project analyzing aspartate 83 demonstrates that sole modification of the isomerization between outward and inward facing transporter states is effectual enough not only to constrict the transport function but also to modify anion channel conduction. Analyzing an episodic ataxia causing mutation could clarify the constitutive steps within the glutamate uptake cycle underlying the EA6 pathomechanism and furthermore revealed that both effects on EAAT function, i.e. on glutamate uptake and anion conduction could be triggered by a modified sodium-binding. The results on hetero-multimerization, on D83 and on P259 are in full agreement with a recently proposed model on the basis of a crystal-structure, in which the anion cavity is transiently established during the movement of the transport domain.

Primary, this structure-function analysis was achieved by investigations of conformational changes via voltage clamp fluorometry and kinetic simulations. By this means, this work demonstrates an alternative experimental access to determine particular details of structure-function relationship.

7 References

1. Hille B., (1970), *Prog. Biophys. Mol. Biol.*, **21**, 1-32
2. He L., Vasiliou K., and Nebert DW., (2009), *Hum. Genomics*, **3**, 195–206
3. Bergeron MJ., Simonin A., Burzle M., Hediger MA. (2008), *J. Inherit. Metab. Dis.*, **31**,178–187
4. Torres GE., Amara SG., (2007), *Curr. Opin. Neurobiol.*,**17**, 304–312
5. Kanai Y., Hediger MA., (2004), *Pflugers Arch.*, **447**, 469-79
6. Arriza JL., Kavanaugh MP., Fairman WA., Wu YN., Murdoch GH., North RA., Amara SG., (1993), *J. Biol. Chem.*, **268**, 15329-32
7. Tolner B., Poolman B., Wallace B., Konings WN., (1992), *J. Bacteriol.*, **174**, 2391-3
8. Danbolt NC., (2001), *Prog. Neurobiol.*, **65**, 1-105
9. Kekuda R., Prasad PD., Fei YJ., Torres-Zamorano V., Sinha S., Yang-Feng TL., Leibach FH., and Ganapathy V., (1996), *J. Biol. Chem.*, **271**, 18657-18661
10. Kekuda R., Torres-Zamorano V., Fei YJ., Prasad PD., Li HW., Mader LD., Leibach FH., and Ganapathy V., (1997), *Am. J. Physiol.*, **272**, G1463-G1472
11. Tamarappoo BK., McDonald KK., and Kilberg MS., (1996), *Biochim. Biophys. Acta.*, **1279**, 131-136
12. Utsunomiya-Tate N., Endou H., and Kanai Y., (1996), *J. Biol. Chem.*, **271**, 14883-14890
13. Arriza JL., Eliasof S., Kavanaugh MP., and Amara SG., (1997), *Proc. Natl. Acad. Sci. USA*, **94**, 4155-4160
14. Billups B., Rossi D., and Attwell D., (1996), *J. Neurosci.*,**16**, 6722-6731
15. Eliasof S., Arriza JL., Leighton BH., Kavanaugh MP., and Amara SG., (1998), *J. Neurosci.*, **18**, 698-712
16. Fairman WA., Vandenberg RJ., Arriza JL., Kavanaugh MP., and Amara SG., (1995), *Nature*, **375**, 599-603

References

17. Kanai Y., Nussberger S., Romero MF., Boron WF., Hebert SC., and Hediger MA., (1995), *J. Biol. Chem.*, **270**, 16561-16568
18. Picaud S., Larsson HP., Wellis DP., Lecar H., and Werblin F., (1995), *Proc. Natl. Acad. Sci. USA*, **92**, 9417-9421
19. Sonders MS., and Amara SG., (1996), *Curr. Opin. Neurobiol.*, **6**, 294-302
20. Vandenberg RJ., Arriza JL., Amara SG., and Kavanaugh MP., (1995), *J. Biol. Chem.*, **270**, 17668-17671
21. Wadiche JI., Amara SG., and Kavanaugh MP., (1995), *Neuron*, **15**, 721-728
22. Zerangue N., and Kavanaugh MP., (1996), *J. Biol. Chem.*, **271**, 27991-27994
23. Sheldon AL., Robinson MB., (2007), *Neurochem. Int.*, **51**, 333-355
24. Lauriat TL., McInnes LA., (2007), *Mol. Psychiatry.*, **12**, 1065-1078
25. Domercq M., Sánchez-Gómez MV., Areso P., Matute C., (1999), *Eur. J. Neurosci.*, **11**, 2226-2236
26. Schmitt A., Asan E., Lesch KP., Kugler P., (2002), *Neuroscience.*, **109**, 45-61
27. Chen W., Mahadomrongkul V., Berger UV., Bassan M., DeSilva T., Tanaka K., Irwin N., Aoki C., Rosenberg PA., (2004), *J. Neurosci.*, **24**, 1136-1148
28. Maragakis NJ., Rothstein JD., (2004), *Neurobiol. Dis.*, **15**, 461-473
29. Furuta A., Rothstein JD., Martin LJ., (1997), *J. Neurosci.*, **17**, 8363-8375
30. Bar-Peled O., Ben-Hur H., Biegon A., Groner Y., Dewhurst S., Furuta A., Rothstein JD., (1997), *J. Neurochem.*, **69**, 2571-2580
31. Storck T., Schulte S., Hofmann K., Stoffel W., (1992), *Proc. Natl. Acad. Sci. USA.*, **89**, 10955-10959
32. Voutsinos-Porche B., Bonvento G., Tanaka K., Steiner P., Welker E., Chatton JY., Magistretti PJ., Pellerin L., (2003), *Neuron.*, **37**, 275-286
33. Furuta A., Martin LJ., Lin CL., Dykes-Hoberg M., Rothstein JD., (1997), *Neuroscience*, **81**, 1031-1042
34. Conti F., DeBiasi S., Minelli A., Rothstein JD., Melone M., (1998), *Cereb.*

References

- Cortex.*, **8**, 108-116
35. Schlag BD., Vondrasek JR., Munir M., Kalandadze A., Zeleniaia OA., Rothstein JD., Robinson MB., (1998), *Mol. Pharmacol.*, **53**,355-369
 36. Hu WH, Walters WM, Xia XM, Karmally SA., Bethea JR., (2003), *Glia*, **44**, 13-25
 37. Massie A., Cnops L., Smolders I., McCullumsmith R., Kooijman R., Kwak S., Arckens L., Michotte Y., (2008), *J. Comp. Neurol.*, **511**, 155-172
 38. Pow DV., Barnett NL., (2000), *Neurosci. Lett.*, **280**, 21-24
 39. Huang YH., Bergles DE., (2004), *Curr. Opin Neurobiol.*, **14**, 346-352
 40. Wadiche JI., Jahr CE., (2005), *Nat. Neurosci.*, **8**, 1329-1334
 41. Otis TS., Brasnjo G., Dzubay JA., Pratap M., (2004), *Neurochem. Int.*, **45**, 537-544
 42. Brasnjo G., Otis TS., (2001), *Neuron.*, **31**, 607-16
 43. Grunewald M., Bendahan A. & Kanner BI., (1998), *Neuron*, **21**, 623–632
 44. Slotboom DJ., Lolkema JS. & Konings WN., (1996), *J. Biol. Chem.*, **271**, 31317–31321
 45. Seal RP. & Amara SG., (1998), *Neuron*, **21**, 1487–1498
 46. Slotboom DJ., Sobczak I., Konings WN. & Lolkema JS., (1999), *Proc. Natl. Acad. Sci. USA*, **96**, 14282–14287
 47. Grunewald M. & Kanner BI., (2000), *J. Biol. Chem.*, **275**, 9684–9689
 48. Slotboom DJ., Konings WN. & Lolkema JS., (2001), *J. Biol. Chem.*, **276**, 10775–10781
 49. Grunewald M., Menaker D. & Kanner, BI., (2002), *J. Biol. Chem.*, **277**, 26074–26080
 50. Yernool D., Boudker O., Jin Y., Gouaux E., (2004), *Nature*, **431**, 811-818
 51. Boudker O., Ryan RM., Yernool D., Shimamoto K., Gouaux E., (2007), *Nature*, **445**, 387-393

References

52. Kavanaugh MP., Bendahan A., Zerangue N., Zhang Y., and Kanner BI., (1997), *J. Biol. Chem.*, **272**, 1703-1708
53. Zhang Y., Bendahan A., Zerbiv R., Kavanaugh MP., and Kanner BI., (1998), *Proc. Natl. Acad. Sci. USA*, **95**, 751-755
54. Reyes N., Ginter C., Boudker O., (2009), *Nature*, **462**, 880-885
55. Verdon G., Boudker O., (2012), *Nat. Struct. Mol. Biol.*, **19**, 355-357
56. Tzingounis AV., Larsson HP. & Kavanaugh MP., (2002), in *Transmembrane Transporters*, ed. Quick, M. (Wiley-Liss, New York), pp. 203–215
57. Bergles DE., Tzingounis AV., and Jahr CE., (2002), *J. Neurosci.*, **22**, 10153-10162
58. Lehre KP., Danbolt NC., (1998), *J. Neurosci.*, **18**, 8751-8757
59. Appel SH., (1993), *Trends. Neurosci.*, **16**, 3-5
60. Portera-Cailliau C., Hedreen JC., Price DL., Koliatsos VE., (1995), *J. Neurosci.*, **15**, 3775-3787
61. Lesch KP., Heils A., Riederer PJ., (1996), *Mol. Med.*, **74**, 365-378
62. Kanai Y., (1997), *Curr. Opin. Cell. Biol.*, **9**, 565-572
63. Pitt D., Werner P., Raine CS., (2000), *Nat. Med.*, **6**, 67-70
64. Smith T., Groom A., Zhu B., Turski L., (2000), *Nat. Med.*, **6**, 62-66
65. Laruelle M., Kegeles LS., Abi-Dargham A., (2003), *Ann. N. Y. Acad. Sci.*, **1003**, 138-158
66. Benveniste H., Drejer J., Schousboe A., Diemer NH., (1984), *J. Neurochem.*, **43**, 1369-1374
67. Sandberg M., Butcher SP., Hagberg H., (1986), *J. Neurochem.*, **47**, 178-184
68. Sherwin A., Robitaille Y., Quesney F., Olivier A., Villemure J., Leblanc R., Feindel W., Andermann E., Gotman J., Andermann F., *et al.*, (1988), *Neurology.*, **38**, 920-323
69. Storm-Mathisen J., Danbolt NC., Rothe F., Torp R., Zhang N., Aas JE., Kanner

References

- Bl., Langmoen I., Ottersen OP., (1992), *Prog. Brain. Res.*, **94**, 225-241
70. During MJ., Spencer DD., (1993), *Lancet.*, **341**, 1607-1610
71. Szatkowski M, Attwell D., (1994), *Trends. Neurosci.*, **17**, 359-365
72. Kanai Y., Bhide PG., DiFiglia M., Hediger MA., (1995), *Neuroreport.*, **6**, 2357-2362
73. Li Q., Puro DG., (2002), *Invest. Ophthalmol. Vis. Sci.*, **43**, 3109-3116
74. Ohia SE., Opere CA., Leday AM., (2005), *Mutat. Res.*, **579**, 22-36
75. Lipton SA., (2001), *Prog. Brain. Res.*, **131**, 712-718
76. Bräuner-Osborne H., Egebjerg J., Nielsen EO., Madsen U., Krogsgaard-Larsen P., (2000), *J. Med. Chem.*, **43**, 2609-2645
77. Bunch L., Krogsgaard-Larsen P., (2009), *Med. Res. Rev.*, **29**, 3-28
78. Jensen AA., (2004), *Humana Press*, 47-82
79. Jen JC., Graves TD., Hess EJ., Hanna MG., Griggs RC., Baloh RW., and the CINCH investigators, (2007), *Brain.*, **130**, 2484-2493
80. Litt M., Kramer P., Browne D., Gancher S., Brunt ER., Root D., Phromchotikul T., Dubay CJ., Nutt J., (1994), *Am. J. Hum. Genet.*, **55**, 702-709
81. Browne DL., Gancher ST., Nutt JG., Brunt ER., Smith EA., Kramer P., Litt M., (1994), *Nat. Genet.*, **8**, 136-140
82. Browne DL., Brunt ER., Griggs RC., Nutt JG., Gancher ST., Smith EA., Litt M., (1995), *Hum. Mol. Genet.*, **4**, 1671-1672
83. Scheffer H., Brunt ER., Mol GJ., van der Vlies P., Stulp RP., Verlind E., Mantel G., Averyanov YN., Hofstra RM., Buys CH., (1998), *Hum. Genet.*, **102**, 464-466
84. Zuberi SM., Eunson LH., Spauschus A., De Silva R., Tolmie J., Wood NW., McWilliam RC., Stephenson JB., Kullmann DM., Hanna MG., (1998), *Brain.*, **122**, 817-25
85. Knight MA., Storey E., McKinlay, Gardner RJ., Hand P., Forrest SM., (2000), *Hum. Mutat.*, **16**, 374

References

86. Klein A., Boltshauser E., Jen J., Baloh RW., (2004), *Neuropediatrics.*, **35**, 147–149
87. Chen H., von Hehn C., Kaczmarek LK., Ment LR., Pober BR., Hisama FM., (2007), *Neurogenetics.*, **8**, 131–135
89. Eunson LH., Rea R., Zuberi SM., Youroukos S., Panayiotopoulos CP., Liguori R., Avoni P., McWilliam RC., Stephenson JB., Hanna MG., Kullmann DM., Spauschus A., (2000), *Ann. Neurol.*, **48**, 647-656
90. Poujois A., Antoine JC., Combes A., Touraine RL., (2006), *J. Neurol.*, **253**, 957-959
91. Kramer PL., Yue Q., Gancher ST., Nutt JG., Baloh R., Smith E., *et al.*, (1995), *Am. J. Hum. Genet.*, **57**, 182-185
92. Vahedi K., Joutel A., Van Bogaert P., Ducros A., Maciaseck J., Bach JF., Bousser MG., Tournier-Lasserre E., (1995), *Ann. Neurol.*, **37**, 289-293
93. Ophoff RA., Terwindt GM., Vergouwe MN., van Eijk R., Oefner PJ., Hoffman SM., Lamerdin JE., Mohrenweiser HW., Bulman DE., Ferrari M., Haan J., Lindhout D., van Ommen GJ., Hofker MH., Ferrari MD., Frants RR., (1996), *Cell.*, **87**, 543-552
94. Joutel A., Bousser MG., Biousse V., Labauge P., Chabriat H., Nibbio A., *et al.*, (1993), *Nat. Genet.*, **5**, 40
95. Zhuchenko O., Bailey J., Bonnen P., Ashizawa T., Stockton DW., Amos C., Dobyns WB., Subramony SH., Zoghbi HY., Lee CC., (1997), *Nat. Genet.*, **15**, 62-69
96. Escayg A., De Waard M., Lee DD., Bichet D., Wolf P., Mayer T., Johnston J., Baloh R., Sander T., Meisler MH., (2000), *Am. J. Hum. Genet.*, **66**, 1531-1539
97. Jen JC., Wan J., Palos TP., Howard BD. & Baloh RW., (2005), *Neurology*, **65**, 529-534
98. de Vries B., Mamsa H., Stam AH., Wan J., Bakker SL., Vanmolkot KR., Haan J., Terwindt GM., Boon EM., Howard BD. *et al.*, (2009), *Arch. Neurol.*, **66**, 97-101
99. Winter N., Kovermann P., & Fahlke C., (2010), *Brain.*, in revision
100. Rothstein JD., Dykes-Hoberg M., Pardo CA., *et al.* (1996), *Neuron.*, **16**, 675-

References

- 686
101. Watase K., Hashimoto K., Kano M., et al. (1998), *Eur. J. Neurosci.*, **10**, 976-988
 102. Walz W., (2002), *Glia*, **40**, 1-10
 103. Kettenmann H., Backus KH. & Schachner M., (1984), *Neurosci. Lett.*, **52**, 25-29
 104. MacVicar BA., Tse FW., Crichton SA. & Kettenmann H., (1989), *J. Neurosci.*, **9**, 3577-3583
 105. Meier SD., Kafitz KW. & Rose CR., (2008), *Glia*, **56**, 1127-1137
 106. Fonnum F., (1984), *J. Neurochem.*, **42**, 1-11
 107. Ottersen OP., Storm-Mathisen J., (1984), *J. Comp. Neurol.*, **229**, 374-392
 108. Collingridge GL., Lester RA., (1989), *Pharmacol. Rev.*, **41**, 143-210
 109. Headley PM, Grillner S., (1990), *Trends. Pharmacol. Sci.*, **11**, 205-211
 110. McDonald JW., Johnston MV., (1990), *Brain. Res. Brain. Res. Rev.*, **15**, 41-70
 111. Komuro H., Rakic P., (1993), *Science*, **260**, 95-97
 112. Johnston MV., (1995), *Brain. Dev.*, **17**, 301-306
 113. LaMantia AS., (1995) , *Neuron.*, **15**, 1223-1225
 114. Vallano ML., (1998), *Crit. Rev. Neurobiol.*, **12**, 177-204
 115. Rossi DJ., Slater NT., (1993), *Neuropharmacology.* , **32**, 1239-1248
 116. Rabacchi S., Bailly Y., Delhay-Bouchaud N., Mariani J., (1992), *Science*, **256**, 1823-1825
 117. Durand GM., Kovalchuk Y., Konnerth A., (1996), *Nature*, **38**, 171-175
 118. Kurihara H., Hashimoto K., Kano M., Takayama C., Sakimura K., Mishina M., Inoue Y., Watanabe M., (1997), *J. Neurosci.*, **17**, 9613-9623
 119. Quinlan EM, Olstein DH, Bear MF., (1999), *Proc. Natl. Acad. Sci. USA*, **96**,

References

- 12876-12880
120. Deutsch SI., Mastropaolo J., Rosse RB., (1998), *Clin. Neuropharmacol.*, **21**, 320-332
121. Ikonomidou C., Stefovskaja V., Turski L., (2000), *Proc. Natl. Acad. Sci. USA*, **97**, 12885-12890
122. Nakayama T., Kawakami H., Tanaka K., Nakamura S., (1996), *Brain. Res. Mol. Brain. Res.*, **36**, 189-192
123. Kanai Y. and Hediger MA., (1992), *Nature*, **360**, 467-471
124. Erickson RH., Gum JR., Lindstrom MM., McKean D., Kim YS., (1995), *Biochem. Biophys. Res. Commun.*, **216**, 249-257
125. Rimaniol AC., Haïk S., Martin M., Le Grand R., Boussin FD., Dereuddre-Bosquet N., Gras G., Dormont D., (2000), *J. Immunol.*, **164**, 5430-5438
126. Moriyama Y., Hayashi M., Yamada H., Yatsushiro S., Ishio S., Yamamoto A., (2000), *J. Exp. Biol.*, **203**, 117-125
127. Hösl E., Hösl L., (1993), *Prog. Neurobiol.*, **40**, 477-506
128. Steinhäuser C., Gallo V., (1996), *Trends. Neurosci.*, **19**, 339-345
129. Vernadakis A., (1996), *Prog. Neurobiol.*, **49**, 185-214
130. Conti F., Barbaresi P., Melone M., Ducati A., (1999), *Cereb. Cortex.*, **9**, 110-120
131. Shelton MK., McCarthy KD., (1999), *Glia.*, **26**, 1-11
132. Bergles DE., Roberts JD., Somogyi P., Jahr CE., (2000), *Nature*, **405**, 187-191
133. Butcher SP., Hamberger A., (1987), *J. Neurochem.*, **48**, 713-721
134. Lehmann A., Isacson H., Hamberger A., (1983), *J. Neurochem.*, **40**, 1314-1320
135. Choi DW., (1987), *J. Neurosci.*, **7**, 369-79
136. Arriza JL., Fairman WA., Wadiche JI., Murdoch GH., Kavanaugh MP., Amara SG., (1994), *J. Neurosci.*, **14**, 5559-5569

References

137. Zerangue N., and Kavanaugh MP., (1996), *Nature*, **383**, 634-637
138. Wadiche JI., Kavanaugh MP., (1998), *J. Neurosci.*, **18**, 7650-7661
139. Mager S., Naeve J., Quick M., Labarca C., Davidson N., Lester HA., (1993), *Neuron.*, **10**, 177-188
140. Mager S., Min C., Henry DJ., Chavkin C., Hoffman BJ., Davidson N., Lester HA., (1994), *Neuron.*, **12**, 845-859
141. Galli A., Blakely RD., DeFelice LJ., (1996), *Proc. Natl. Acad. Sci. USA.*, **93**, 8671-8676
142. Galli A., Petersen CI., deBlaquiere M., Blakely RD., DeFelice LJ., (1997), *J. Neurosci.*, **17**, 3401-3411
143. Galli A., Jayanthi LD., Ramsey IS., Miller JW., Fremeau Jr. RT., DeFelice LJ., (1999), *J. Neurosci.*, **19**, 6290-6297
144. Ingram SL., Amara SG. , (2000), *J. Neurosci.*, **20**, 550-557
145. Ingram SL., Prasad BM., Amara SG., (2002), *Nat. Neurosci.*, **5**, 971-978
146. Quick MW., (2003), *Neuron.*, **40**, 537-549
147. Risso S., DeFelice LJ., Blakely RD., (1996), *J. Physiol.*, **490**, 691-702
148. Ryan RM., Mindell JA., (2007), *Nat. Struct. Mol. Biol.*, **14**, 365-371
149. Wadiche JI., Arriza JL., Amara SG., Kavanaugh MP., (1995), *Neuron.*, **14**, 1019-1027
150. Bendahan A., Armon A., Madani N., Kavanaugh MP., and Kanner BI., (2000) *J. Biol. Chem.*, **275**, 37436-37442
151. Otis TS., Jahr CE., (1998), *J. Neurosci.*, **18**, 7099-7110
152. Grewer C., Watzke N., Wiessner M., Rauen T., (2000), *Proc. Natl. Acad. Sci. USA.*, **97**, 9706–9711
153. Franciolini F. , Nonner W. , (1987), *J. Gen. Physiol.*, **90**, 453-478
154. Larsson HP., Picaud SA., Werblin FS., Lecar H., (1996), *Biophys. J.*, **70**, 733-742

References

155. Borre L., Kavanaugh MP., Kanner Bl., (2002), *J. Biol. Chem.*, **277**, 501-507
156. Ryan RM., Vandenberg RJ., (2002), *J. Biol. Chem.*, **277**, 494-500
157. Seal RP., Shigeri Y., Eliasof S., Leighton BH., Amara SG., (2001), *Proc. Natl. Acad. Sci. USA.*, **98**, 324-329
158. Ryan RM., Mitrovic AD., Vandenberg RJ., (2004), *J. Biol. Chem.*, **279**, 742-751
159. Melzer N., Biela A., Fahlke C., (2003), *J. Biol. Chem.*, **278**, 112-119
160. Kovermann P., Machtens JP., Ewers D., Fahlke C., (2010), *J. Biol. Chem.*, **285**, 23676-23686
161. Hotzy J., Machtens JP., Fahlke C., (2012), *J. Biol. Chem.*, **287**, 20016-20026
162. Machtens JP., Kovermann P., Fahlke C., (2011), *J. Biol. Chem.*, **286**, 23780-23788
163. Larsson HP., Tzingounis AV., Koch HP., and Kavanaugh MP. (2004) *Proc. Natl. Acad. Sci. USA*, **101**, 3951-3956
164. Koch HP., Hubbard JM., Larsson HP., (2007), *J. Biol. Chem.*, **282**, 24547-24553
165. Mim C., Balani P., Rauen T., and Grewer C., (2005), *J. Gen. Physiol.*, **126**, 571-589
166. Cheng C., Glover G., Banker G., and Amara SG., (2002), *J. Neurosci.*, **22**, 10643-10652
167. Grewer C., Balani P., Weidenfeller C., Bartusel T., Tao Z., and Rauen T., (2005), *Biochemistry*, **44**, 11913-11923
168. Torres-Salazar D., and Fahlke C., (2007), *J. Biol. Chem.*, **282**, 34719-34726
169. Leary GP., Stone EF., Holley DC., and Kavanaugh MP., (2007), *J. Neurosci.* **27**, 2938-2942
170. Koch HP., Brown RL., and Larsson HP. (2007) *J. Neurosci.* **27**, 2943-2947
171. Barbour B., Keller BU., Llano I., Marty A., (1994), *Neuron*, **12**, 1331-1343

References

172. Takahashi M., Kovalchuk Y., Attwell D., (1995), *J. Neurosci.*, **15**, 5693-5702
173. Eccles CU., Dykes-Hoberg M., Rothstein JD., (1996), *Soc. Neurosci. Abstr.*, **22**, 1570
174. Amara SG., and Fontana AC., (2002), *Neurochem. Int.*, **41**, 313-318
175. Melzer N., Torres-Salazar D., and Fahlke Ch., (2005), *Proc. Natl. Acad. Sci. USA*, **102**, 19214-19218
176. Jiang J., Shrivastava IH., Watts SD., Bahar I., and Amara SG., (2011), *Proc. Natl. Acad. Sci. USA*, **108**, 15141-15146
177. Zhang Z., Tao Z., Gameiro A., Barcelona S., Braams S., Rauen T., and Grewer C., (2007), *Proc. Natl. Acad. Sci. USA*, **104**, 18025-18030
178. Larsson HP., Wang X., Lev B., Bacongus I., Caplan DA., Vyleta NP., Koch HP., ez-Sampedro A., and Noskov SY., (2010), *Proc. Natl. Acad. Sci. USA*, **107**, 13912-13917
179. Tao Z., Grewer C.,(2007), *J. Gen. Physiol.*, **129**, 331-344
180. Tao Z., Rosental N., Kanner Bl., Gameiro A., Mwaura J., Grewer C., (2010), *J. Biol. Chem.*, **285**, 17725-17733
181. Rosental N., Kanner Bl., (2010), *J. Biol. Chem.*, **285**, 21241-21248
182. Kanner Bl., (2006) , *J. Membr. Biol.*, **213**, 89-100
183. Grewer C., Gameiro A., Zhang Z., Tao Z., Braams S., and Rauen T., (2008), *IUBMB. Life*, **60**, 609-619
184. Alekov A., Fahlke C., (2009), *J. Gen. Physiol.*, **133**, 485-496
185. Leary GP., Holley DC., Stone EF., Lyda BR., Kalachev LV., Kavanaugh MP., (2011), *Proc. Natl. Acad. Sci. USA.*, **108**, 14980-14985
186. Gammelsaeter R., Coppola T., Marcaggi P., Storm-Mathisen J., Chaudhry A., Attwell D., Regazzi R., Gundersen V., (2011)., *Plos One*, **6**, 22960
187. Gameiro A., Braams S., Rauen T., Grewer C, (2011), *Biophys. J.*, **100**, 2623-2632

8 List of publications

Hetero-oligomerization of neuronal glutamate transporters

Nothmann D., Leinenweber A., Torres-Salazar D., Kovermann P., **Hotzy J.**, Gameiro A., Grewer C., Fahlke C.

J. Biol. Chem., 2011, 286, 3935-3943

Neutralizing aspartate 83 modifies substrate translocation of Excitatory Amino Acid Transporter 3 (EAAT3) glutamate transporters

Hotzy J., Machtens JP, Fahlke C.

J. Biol. Chem., 2012, 287, 20016-20026

A mutation causing Episodic Ataxia modifies sodium association to EAAT glutamate transporters

Hotzy J., Schneider N., Kovermann P., Fahlke C.

Nat. Struct. Mol. Biol., 2012 [to be submitted]

9 Hetero-oligomerization of neuronal glutamate transporters*

Doreen Nothmann^{‡§1}, Ariane Leinenweber^{‡§1}, Delany Torres-Salazar^{‡§1, 2}, Peter Kovermann^{‡§}, Jasmin Hotzy^{‡§}, Armanda Gameiro[¶], Christof Grewer[¶], and Christoph Fahlke^{‡§3}

From the [‡]Institut für Neurophysiologie, Medizinische Hochschule Hannover, D-30625 Hannover, Germany, the [§]Zentrum für Systemische Neurowissenschaften, D-30559 Hannover, Germany, and the [¶]Department of Chemistry, Binghamton University, State University of New York, Binghamton, New York 13902

* This work was supported, in whole or in part, by National Institutes of Health Grant R01-NS049335-05 (to C. G.). This work was also supported by Deutsche Forschungsgemeinschaft Grants FA301/6 and 9 (to Ch. F.).

¹ These authors contributed equally to this work.

² Present address: Dept. of Neurobiology, University of Pittsburgh, Pittsburgh, PA 15260.

³ To whom correspondence should be addressed: Institut für Neurophysiologie, Medizinische Hochschule Hannover, Carl-Neuberg-Str. 1, D-30625 Hannover, Germany. Tel.: 49 511 532 2777; Fax: 49 511 532 2776; E-mail: fahlke.christoph@mh-hannover.de.

⁴ The abbreviations used are: EAAT, excitatory amino acid transporter; BN, blue native; CFP, cyan fluorescent protein; MDCK, Madin-Darby canine kidney.

This research was originally published in *J. Biol. Chem.*. Doreen Nothmann^{‡§1}, Ariane Leinenweber^{‡§1}, Delany Torres-Salazar^{‡§1, 2}, Peter Kovermann^{‡§}, Jasmin Hotzy^{‡§}, Armanda Gameiro[¶], Christof Grewer[¶], and Christoph Fahlke^{‡§3}.

Hetero-oligomerization of neuronal glutamate transporters*. *J. Biol. Chem.*, 2011, 286: 3935-3943 © the American Society for Biochemistry and Molecular Biology.

9.1 Abstract

Excitatory amino acid transporters (EAATs) mediate the uptake of glutamate into neuronal and glial cells of the mammalian central nervous system. Two transporters expressed primarily in glia, EAAT1 and EAAT2, are crucial for glutamate homeostasis in the adult mammalian brain. Three neuronal transporters (EAAT3, EAAT4, and EAAT5) appear to have additional functions in regulating and processing cellular excitability. EAATs are assembled as trimers, and the existence of multiple isoforms raises the question of whether certain isoforms can form heterooligomers. Co-expression and pull-down experiments of various glutamate transporters showed that EAAT3 and EAAT4, but neither EAAT1 and EAAT2, nor EAAT2 and EAAT3 are capable of co-assembling into heterotrimers. To study the functional consequences of hetero-oligomerization, we co-expressed EAAT3 and the serine-dependent mutant R501C EAAT4 in HEK293 cells and *Xenopus laevis* oocytes and studied glutamate/serine transport and anion conduction using electrophysiological methods. Individual subunits transport glutamate independently of each other. Apparent substrate affinities are not affected by hetero-oligomerization. However, polarized localization in Madin-Darby canine kidney cells was different for homo- and heterooligomers. EAAT3 inserts exclusively into apical membranes of Madin-Darby canine kidney cells when expressed alone. Co-expression with EAAT4 results in additional appearance of basolateral EAAT3. Our results demonstrate the existence of heterotrimeric glutamate transporters and provide novel information about the physiological impact of EAAT oligomerization.

9.2 Introduction

Glutamate is the major excitatory neurotransmitter in the mammalian central nervous system. After its release from glutamatergic nerve terminals, glutamate is quickly taken up into glial and neuronal cells by glutamate transporters belonging to the “excitatory amino acid transporter” (EAAT)⁴ family (1, 2). Five different mammalian EAAT isoforms have been identified. Two of those, EAAT1 and EAAT2, are expressed mainly in glia, whereas EAAT3, EAAT4, and EAAT5 are considered to be neuronal transporters. All EAAT glutamate transporters sustain two fundamentally distinct transport mechanisms. They function as stoichiometrically coupled co-

transporters of one glutamate, three sodium ions, and one proton, while one potassium ion is countertransported (3, 4). In addition, all EAATs are capable of functioning as anion channels (5). Different EAAT isoforms differ in the relative contribution of anion currents to the total transporter-mediated current (5–8). These differences have been interpreted as an indication that some EAATs play a physiological role as glutamate transporters (9, 10) and others as glutamate-gated anion channels involved in the regulation of cellular excitability (2, 11, 12).

EAAT glutamate transporters are assembled as trimers (13–16). At present, it is not clear whether distinct isoforms can form heterotrimers, and moreover, whether subunits might acquire new functions within heterotrimeric assemblies. We here use biochemical and electrophysiological approaches to study co-assembly of different EAATs and possible functional consequences of hetero-multimerization.

9.3 Experimental Procedures

9.3.1 Heterologous Expression of EAATs

Coding regions of rat EAAT1, human EAAT2, rat and human EAAT3, rat EAAT4, and human SLC26A9 were subcloned into pcDNA3.1 or pRcCMV using PCR-based strategies. YFP, GFP, CFP, and His fusion proteins were generated by PCR-based techniques. All constructs were verified by restriction analysis and DNA sequencing. For each construct, two independent recombinants from the same transformation were examined and shown to exhibit indistinguishable functional properties. Transient transfection of tsA201 and MDCKII cells using the $\text{Ca}_3(\text{PO}_4)_2$ technique or Lipofectamine (Invitrogen) was performed as described previously (8).

9.3.2 Purification and Gel Electrophoresis of EAAT Fusion Proteins

EAAT fusion proteins were purified from tsA201 cells as described (22). For PAGE under denaturing conditions, proteins were denatured for 15 min at 56 °C with SDS sample buffer containing 20 mM dithiothreitol (DTT) and electrophoresed on linear SDS-polyacrylamide gels. Blue native (BN)-PAGE was performed immediately after protein purification as described (22, 23). YFP-tagged proteins were visualized by

scanning the wet polyacrylamide gels with a fluorescence scanner (Typhoon 9400; GE Healthcare). Each experiment was at least performed three times and illustrated as representative result.

9.3.3 Electrophysiology

For expression in oocytes, cRNA was synthesized from MluI-linearized pTLN2-*hEAAT3* (24) or from NheI-linearized pGEMHE-R501C *rEAAT4* (20) templates through use of MESSAGE machine kits (Ambion, Austin, TX). Injection and handling of oocytes were performed as described elsewhere (25). Current recordings from oocytes expressing *hEAAT3* were usually performed 1 day after injection. To account for differences in expression levels, this period was increased to 4-5 days for R501C *rEAAT4*. For coexpression experiments in oocytes, *hEAAT3* and R501C *rEAAT4* RNAs were injected at a 1:5 ratio unless otherwise stated.

EAAT-associated currents were recorded by two-electrode voltage clamp using a CA1 amplifier (Dagan, Minneapolis, MN). Oocytes were held at 0 mV, and currents elicited by 200-ms voltage steps between -120 mV and +80 mV were filtered at 2 kHz (-3d B) and digitized with a sampling rate of 10 kHz, using either a Digidata AD/DA converter (Molecular Devices, Sunnyvale, CA) or an ITC-18 Computer Interface (Instrutech Corporation). The external solution contained 96 mM NaNO₃, 4 mM KCl, 0.3 mM CaCl₂, 1 mM MgCl₂, 5 mM HEPES, pH 7.4, either with or without 500 μM L-glutamate or L-serine.

After each experiment with substrate application, the substrate was washed out by perfusion with substrate-free solution and consequently at least once applied again. Cells were only incorporated into the analysis if current amplitudes measured at different times with the same substrate concentration perfectly superimpose. For the experiment shown in Figure 9.2E-G, the application order was changed from experiment to experiment.

9.3.4 Laser Pulse Photolysis

Transient transfection of subconfluent human embryonic kidney cell cultures with the calcium phosphate-mediated transfection method and laser pulse photolysis

experiments were performed as described previously (26). Electrophysiological recordings were performed 24 h after the transfection for 3 days.

In these experiments, the extracellular solution contained 140 mM NaMES, 2 mM CaMES₂, 2 mM MgMES₂, and 30 mM HEPES (pH 7.4/NaOH). The pipette solution contained 140 mM NaMES (exchange transport current)/NaSCN (exchange anion current), 2 mM MgMES₂, 10 mM EGTA, 10 mM glutamate and serine, and 10 mM HEPES (pH 7.4/NaOH).

Briefly, glutamate or 4-methoxy-7-nitroindoliny-caged glutamate (Tocris Bioscience, Ellisville, MO) was applied to cells by means of a small quartz tube (350- μ m diameter) with a mean velocity of 5 cm/s and a time resolution of 20-30 ms (10–90% rise time with whole cells). Photolysis of caged glutamate was initiated with a light flash (355 nm, 5 ns, frequency-tripled NdYag laser; Continuum, Santa Clara, CA), which was delivered to the cell with an optical fiber (350- μ m diameter). Laser energies were varied in the range of 50–450 mJ/cm² with neutral density filters. To estimate the concentration of photolytically released glutamate, a standard glutamate concentration of 100 μ M was applied to the cells by rapid perfusion before and after photolysis experiments, and the steady-state current amplitude was used to calculate the free glutamate concentration from the dose-response curve (26). Current responses to the laser pulse were low pass-filtered at 3 kHz (100- μ s time resolution) and recorded with a 100-kHz sampling rate.

9.3.5 Data Analysis

Data were analyzed with a combination of pClamp9 (Molecular Devices) and SigmaPlot (Jandel Scientific, San Rafael, CA) programs. Current amplitudes were used without applying a subtraction procedure. Current-voltage relationships at various substrate concentrations were constructed by plotting isochronal current amplitudes determined 1 ms after the voltage step versus the membrane potential. To obtain the concentration dependence of anion channel activation by Na⁺ and glutamate, isochronal anion current amplitudes were measured at various concentrations at a given test potential. The so-obtained substrate dependences were normalized to the maximum current amplitude, fit with Hill equations,

$$\left(I = \frac{I_{max}[substrate]^n}{[substrate]^n + K_D^n} + I_0 \right) \quad (\text{Eq. 1})$$

and averaged after normalization to the maximum current amplitude ($I_{max} + I_0$). All data are given as means \pm S.E.. For statistic evaluation the Student's t test was used.

9.3.6 Confocal Microscopy

MDCKII cells were transiently transfected with mCFP-*hEAAT3*, mYFP-*rEAAT4*, barttin-YFP, or hSLC26A9-mYFP and grown on Ibidi glass-bottom dishes. Additionally, co-transfections of CFP-*hEAAT3*/YFP-*rEAAT4* and GFP-*hEAAT3*/mCherry-*hEAAT2* were performed (see Figure 9.5). Confocal imaging was carried out on living cells with a TCS SP2 AOBS scan head and an inverted Leica DM IRB. CFP was excited at 405 nm, and the emission was detected after filtering with a 450-505 nm bandpass filter. YFP/GFP/mCherry were excited at 514 nm/488 nm/514 nm, and the emission was detected after filtering with 520–580 nm/500-535 nm/555-700 nm bandpass filters, respectively.

9.3.7 Surface Biotinylation and Western Blotting

Cell surface expression of *hEAAT3* was assayed with a modification of cell surface biotinylation methods described previously (27, 28). In these experiments, *hEAAT3* was expressed as a GFP fusion protein because the fluorescence scanner (Typhoon) had preferable imaging capabilities for GFP. GFP-*hEAAT3* alone or GFP-tagged *hEAAT3* together with untagged *rEAAT4* or *hEAAT2* was expressed in MDCKII cells, grown until 70% confluence on filters (see Figure 9.6), and incubated with 2 mg/ml biotin (sulfo-NHS-SS-biotin; Pierce) in triethanolamine buffer (2 mM CaCl_2 , 150 mM NaCl, 10 mM $\text{C}_6\text{H}_{15}\text{NO}_3$, pH 7.5) for 1-2 h, either added to the apical or to the basolateral side. The membrane domain that was not treated with biotin was incubated with biotinylation buffer only. The reaction was quenched by repeated washing with quenching buffer (100 mM glycine in PBS). After washing with PBS, the cells were scraped in lysis buffer (150 mM NaCl, 1% Triton X-100, and 5 mM EDTA with 50 mM Tris, pH 7.5) and transferred to a tube. After 15 min on ice, they were

centrifuged at 14,000 × g for 10 min at 4 °C, and the cell lysate was collected. Cell lysates were incubated with Ultralink immobilized NeutrAvidin beads (Pierce) for 2 h. After washing with either lysis buffer or high salt wash buffer (0.1% Triton, 500 mM NaCl, 5 mM EDTA, 50 mM Tris, pH 7.5), proteins on the beads were released by incubation with SDS loading buffer containing 200 mM DTT and 4.1% SDS. The proteins were separated on 10% polyacrylamide gradient gels. Fluorescence intensities of apical/basolateral channels were determined by fluorescence scanning and given as fraction of the total surface transporter fluorescence, obtained by adding apical and basolateral fluorescence intensities. Gels were blotted onto polyvinylidene (Bio-Rad), and actin was visualized with rabbit anti-actin antibody (Sigma-Aldrich) and anti-rabbit Cy5 antibody (GE Healthcare). Results were used only from experiments in which no actin was detected in purified membrane fractions. We used heterologously expressed hSLC26A9-YFP as apical (29) and endogenous Na⁺,K⁺-ATPase as basolateral markers (27). Biotinylated hSLC26A9-YFP was quantified using fluorescent scanning, but we used antibodies (Abcam) and Western blotting for endogenous Na⁺,K⁺-ATPases.

9.4 Results

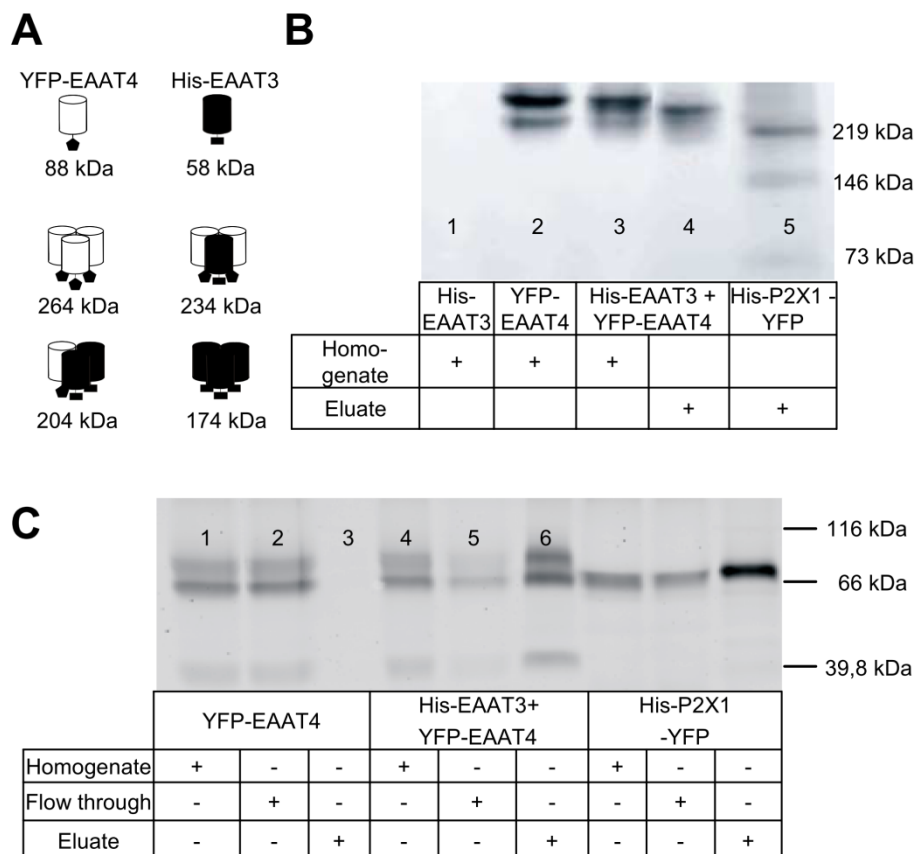
9.4.1 EAAT3 and EAAT4 Form Hetero-oligomeric Transporters

To study whether different EAAT isoforms assemble into heterotrimeric complexes, we co-expressed two different EAAT isoforms in mammalian cells, one as a YFP fusion protein and the other as a His fusion protein. The tested mammalian EAATs acquire different molecular masses by the distinct added tags and can, thus, be distinguished by gel electrophoresis (Figure 9.1A). Transporters were either purified in their native multimeric state by Ni²⁺-nitrilotriacetic acid-based affinity chromatography before gel electrophoresis (eluate fractions) or resolved as full lysates by denaturing SDS- or BN-PAGE (homogenate fractions). YFP-tagged proteins were then visualized by scanning the wet polyacrylamide gels with a fluorescence scanner.

Figure 9.1B shows a BN-PAGE from cells co-expressing His-*h*EAAT3 and YFP-*r*EAAT4 (*lanes 3 and 4*) and from cells expressing each transporter alone (*lanes 1 and 2*). Because His-*h*EAAT3 homotrimers are not fluorescent, we verified

expression of His-*h*EAAT3 by Western blotting. BN-PAGE of full lysates from cells expressing YFP-*r*EAAT4 resulted in two different fluorescent bands that correlate to non- or core-glycosylated and complex-glycosylated forms of homotrimers (Figure 9.1B, lane 2) (14). The full homogenate of cells co-transfected with both transporters also contains homotrimeric YFP-*r*EAAT4 (Figure 9.1B, lane 3). After Ni²⁺-nitrilotriacetic acid-based affinity chromatography, homotrimeric YFP-*r*EAAT4, which lacks an affinity tag, is absent from the retained fraction. The protein fraction with the highest molecular mass must represent heterotrimers because it contains the His tag, which is only present in His-*h*EAAT3, exhibits fluorescence from YFP-*r*EAAT4, and is of a smaller molecular mass than the YFP-*r*EAAT4 homotrimer (Figure 9.1B, lane 4, Eluate).

Figure 9.1
Co-assembly of EAAT3 and EAAT4



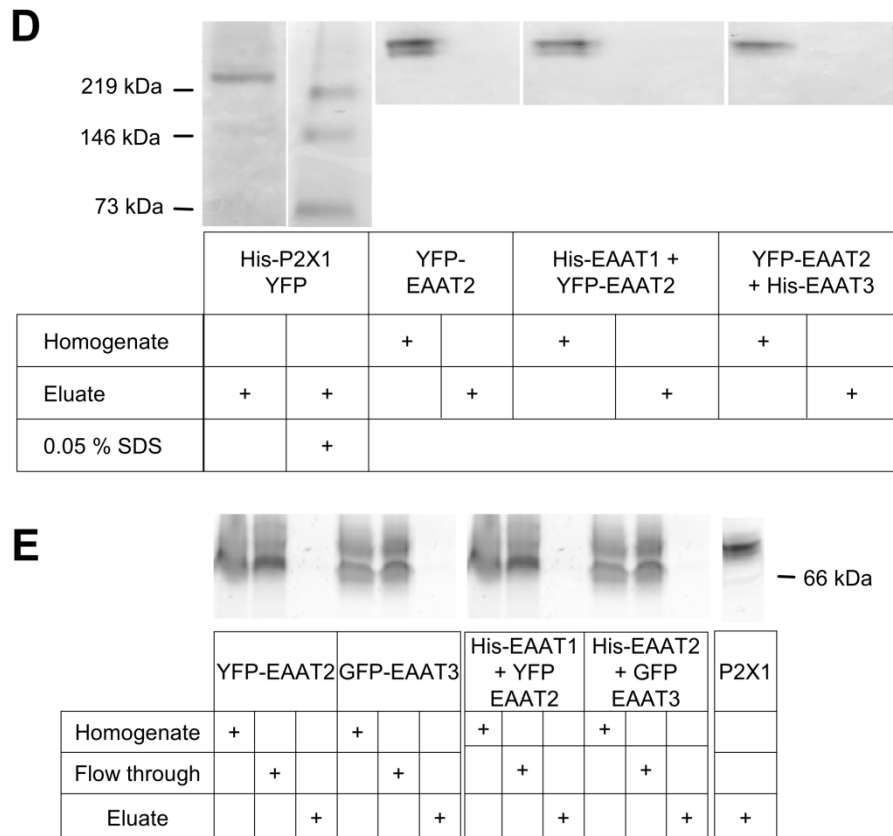


Figure 9.1: Co-assembly of EAAT3 and EAAT4.

A, YFP and His fusion proteins differ in size, allowing distinction of homo- and heterotrimeric proteins by gel electrophoresis. B, BN-PAGE of homogenates and eluates from Ni²⁺-affinity chromatography from cells co-expressing His-EAAT3 and YFP-EAAT4 (lane 3 and 4). The trimeric membrane protein P2X1 was used as size standard (lane 5). C, SDS-PAGE from various fractions obtained by a pull-down assay using Ni²⁺-affinity chromatography. D, BN-PAGE of lysates and eluted proteins after Ni²⁺-affinity chromatography from cells expressing YFP-*h*EAAT2 (third and fourth lanes) or cells co-expressing His-*r*EAAT1 and YFP-*h*EAAT2 (fifth and sixth lanes) as well as His-*h*EAAT3 and YFP-*h*EAAT2 (seventh and eighth lanes). Eluates were concentrated 8-fold. E, SDS-PAGE from various fractions obtained by Ni²⁺-affinity chromatography from cells co-expressing His-*r*EAAT1 and YFP-*h*EAAT2, His-*h*EAAT2 and GFP-*h*EAAT3.

Figure 9.1C shows a SDS-PAGE of various fractions isolated from affinity chromatography. Homotrimeric YFP-*r*EAAT4 does not bind the Ni²⁺ resin and appears completely in the flow-through (lanes 1-3). In contrast, hetero-trimerization of *h*EAAT3 and *r*EAAT4 allows pulldown of YFP-*r*EAAT4 together with His-*h*EAAT3 by metal affinity chromatography (Figure 9.1C, lanes 4-6). We used human EAAT3 and rat EAAT4 for these experiments because functional properties of these isoforms were recently studied and compared by our group (25). Although human and rat EAAT3 are highly conserved, they do not exhibit complete sequence identity. To

demonstrate that EAAT3/EAAT4 hetero-oligomerization also occurs with isoforms from the same species, we repeated coexpression and pulldown experiments with His-*r*EAAT3 and YFP-*r*EAAT4. The outcome of these experiments closely resembled those with *h*EAAT3 and *r*EAAT4 (data not shown). YFP-*r*EAAT4 and His-*r*EAAT3 form heterotrimers.

We conclude that EAAT3 and EAAT4 can co-assemble into heteromultimers. Other isoforms fail to co-assemble (Figure 9.1D and E). Neither BN-PAGE analysis (Figure 9.1D) nor pull-down assays (Figure 9.1E) revealed any indication for hetero-oligomerization for three other EAAT isoform combinations, the two glial transporters EAAT1 and EAAT2 as well as for EAAT2 and EAAT3.

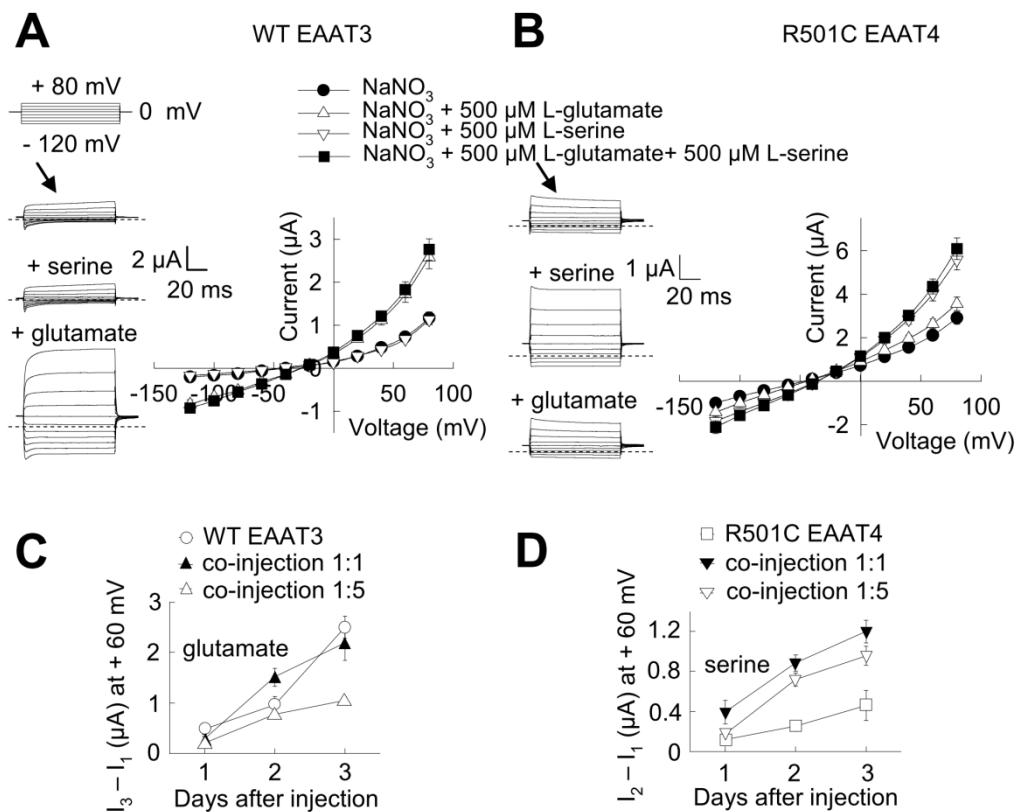
9.4.2 Co-expression of EAAT3 and EAAT4 in *Xenopus* Oocytes

*h*EAAT3 and *r*EAAT4 differ in the unitary glutamate transport rate (30) but not in the unitary anion current (25). Moreover, macroscopic anion currents display isoform-specific time and voltage dependences (25). *h*EAAT3/*r*EAAT4 heterotrimers therefore provide an excellent possibility to study potential intersubunit interactions. To separate currents conducted by *h*EAAT3 or *r*EAAT4 subunits, we mutated *r*EAAT4 at position 501 (R501C) to modify the substrate binding pocket in a way that glutamate cannot bind anymore, but serine or cysteine can bind instead (17, 20, 31). Figure 9.2 shows current recordings from *Xenopus* oocytes expressing either WT *h*EAAT3 or R501C *r*EAAT4 alone, or co-expressing both isoforms. In the presence of extracellular NO_3^- these currents are dominated at positive membrane potentials by the anion component (8, 32, 33). When the membrane potential is stepped to more positive values, WT *h*EAAT3 currents display time- and voltage-dependent increases (Figure 9.2A, *arrow*), likely due to channel activation (25).

In contrast R501C *r*EAAT4, like WT *r*EAAT4, is inactivated by positive voltages (Figure 9.2B) (8, 20, 25), resulting in decreased channel open probabilities and time-dependent current amplitude reductions (*arrow*) (8, 25, 34). WT *h*EAAT3 currents are greatly increased in the presence of extracellular glutamate, but are not responsive to serine (Figure 9.2A). In contrast, R501C *r*EAAT4 currents are not significantly affected by glutamate, but they are augmented by application of extracellular serine (Fig. 9.2B).

Figure 9.2C and D, shows the time course of the development of glutamate- and serine-dependent currents with time after mRNA injection. Serine-dependent anion currents are larger in oocytes co-expressing WT *hEAAT3* and R501C *rEAAT4* than in those expressing R501C *rEAAT4* alone (Figure 9.2D), indicating that *hEAAT3* stimulates the insertion of *rEAAT4* subunits into the surface membrane. Confocal images from oocytes expressing YFP-*rEAAT4* alone or co-expressing YFP-*rEAAT4* and untagged *hEAAT3* revealed increased surface insertion of YFP-*rEAAT4* in the presence of *hEAAT3* (data not shown). In contrast, expression of R501C *rEAAT4* did not increase glutamate-dependent *hEAAT3* anion currents, but rather decrease this current amplitude at certain time intervals (Figure 9.2C).

Figure 9.2
EAAT3 modifies membrane surface insertion and function of EAAT4



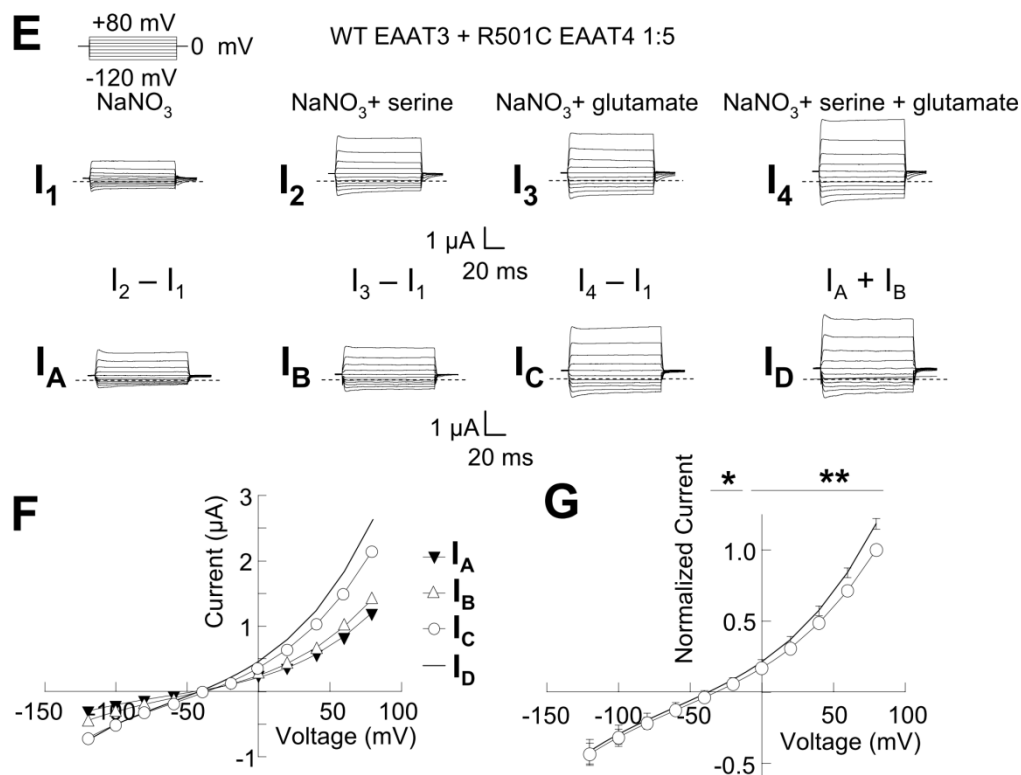


Figure 9.2: EAAT3 modifies membrane surface insertion and function of EAAT4.

A and *B*, representative recordings and current-voltage relationships from oocytes expressing WT EAAT3 (*A*) or R501C EAAT4 (*B*) in the following conditions, 96 mM NaNO₃ (filled circles), 96 mM NaNO₃ + 500 μ M L-glutamate (upward triangles), and 96 mM NaNO₃ + 500 μ M L-serine (downward triangles). Mean \pm S.E. from 6-7 experiments is shown. *C* and *D*, dependences of the glutamate-induced (*C*) and serine-induced (*D*) currents on the time after mRNA injection for oocytes expressing WT EAAT3 ($n = 8$ for each time point), R501C EAAT4 ($5 < n > 10$), and oocytes co-expressing WT EAAT3 and R501C EAAT4 ($5 < n > 10$) at different ratios. *E*, representative recordings from an oocyte co-expressing *h*EAAT3 and R501C *r*EAAT4 without substrate (I_1) in the presence of 96 mM NaNO₃ + 500 μ M L-serine (I_2) or 500 μ M L-glutamate (I_3), or after application of both (I_4). *F*, current-voltage relationship for serine-activated ($I_A = I_2 - I_1$) and glutamate-activated ($I_B = I_3 - I_1$) currents as well as of currents activated in the simultaneous presence of serine and glutamate ($I_C = I_4 - I_1$) from the example shown in *E*. The solid line gives the sum of serine- and glutamate-activated current amplitudes. *G*, averaged normalized current-voltage relationship for different substrate-sensitive current components ($n = 6$, *, $p < 0.05$; **, $p < 0.01$).

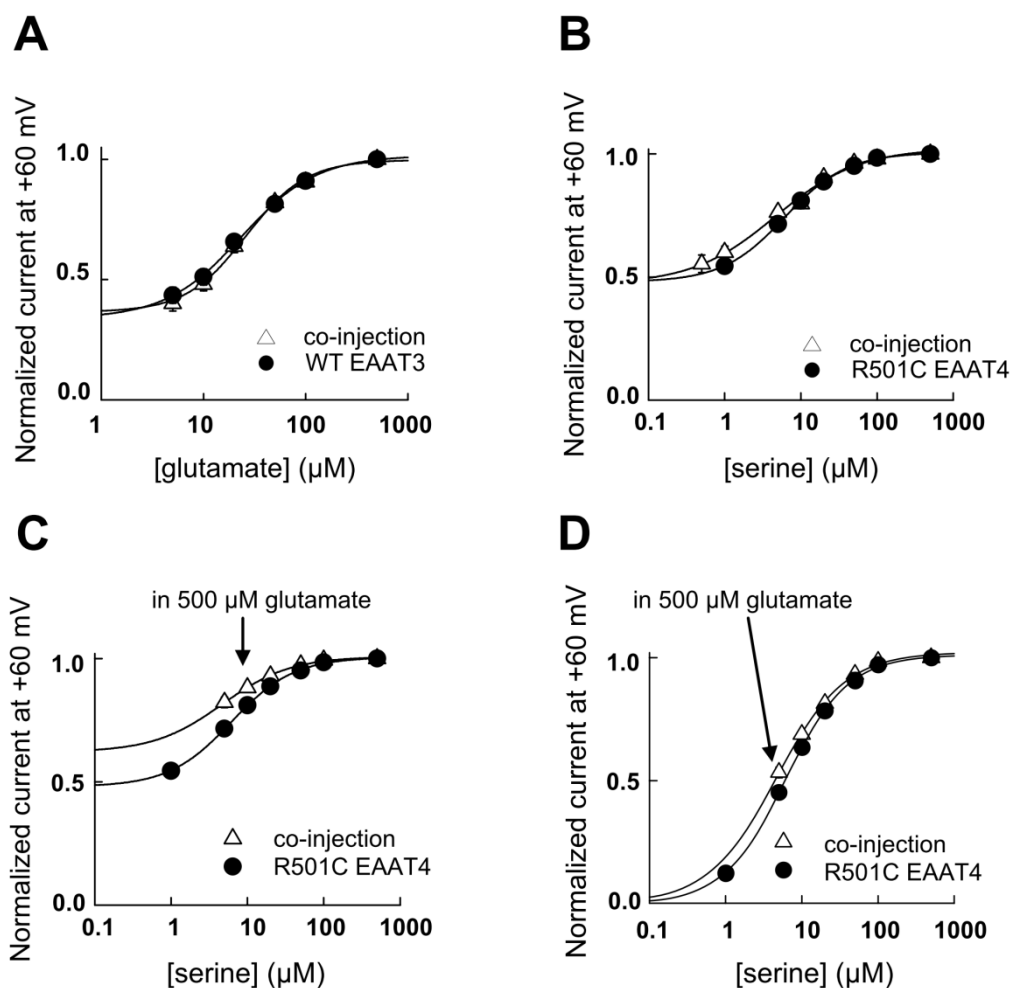
Figure 9.2E shows representative recordings from a single co-injected oocyte and the corresponding analysis. Currents were measured in the absence as well as in the presence of glutamate and serine. For the application of each substrate alone as well as for the simultaneous application of both, we determined substrate-dependent current amplitudes for various voltages and constructed current-voltage relationships from these data (Figure 9.2F). Current increases elicited by the simultaneous presence of glutamate and serine were slightly smaller than the sums of the current

amplitudes induced by only one substrate at positive potentials (Figure 9.2G). At negative potentials, where current amplitudes are dominated by coupled transport currents, no difference between the two amplitudes could be observed (Figure 9.2G).

9.4.3 Individual Subunits Transport Substrates Independently of Each Other

WT *hEAAT3* and R501C *rEAAT4* differ in the apparent dissociation constants for glutamate/serine and sodium (25, 30). To test whether binding of an amino acid substrate/cation to one subunit is affected by the neighboring subunit, we determined glutamate concentration dependences of *hEAAT3* anion currents when expressed alone or co-expressed together with R501C *rEAAT4* in oocytes (Figure 9.3A), or serine concentration dependences of R501C *rEAAT4* currents either expressed alone or co-expressed with WT *hEAAT3* (Figure 9.3B).

Figure 9.3
Substrates bind independently to individual subunits



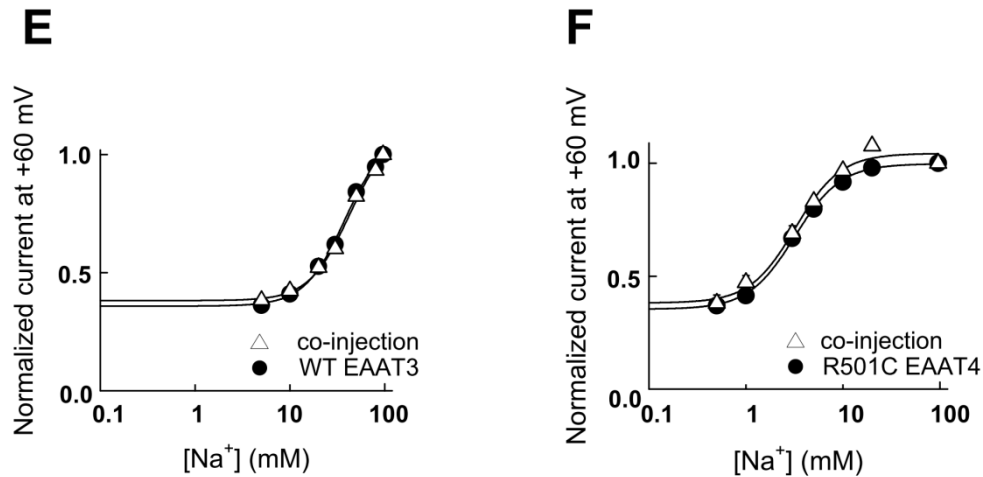


Figure 9.3: Substrates bind independently to individual subunits.

A, glutamate dependence of isochronal current amplitudes measured at +60 mV from oocytes expressing WT EAAT3 (filled circles, $n = 3$, $K_D = 23.4 \pm 1.2 \mu\text{M}$) and oocytes co-expressing WT EAAT3 and R501C EAAT4 (*open triangles*, $n = 6$, $K_D = 26.0 \pm 2.4 \mu\text{M}$) in the absence of serine. B, serine dependence of isochronal current amplitudes from oocytes expressing R501C EAAT4 (*filled circles*, $n = 3$, $K_D = 6.1 \pm 0.1 \mu\text{M}$) or co-expressing WT EAAT3 and R501C EAAT4 (*open triangles*, $n = 6$, $K_D = 4.6 \pm 0.7 \mu\text{M}$) in the absence of glutamate. C, comparison of the serine dependence of isochronal current amplitudes from oocytes expressing R501C EAAT4 (shown in B) with the serine dependence from oocytes co-expressing WT EAAT3 and R501C EAAT4 in the presence of 500 μM glutamate (*open triangles*, $n = 5$, $K_D = 4.6 \pm 0.2 \mu\text{M}$). D, serine dependence of substrate-dependent anion current amplitudes. Data from C were scaled by setting the minimum values to 0 and the maximum values to 1. E, sodium dependence of isochronal current amplitudes from oocytes expressing WT EAAT3 (*filled circles*, $n = 5$, $K_D = 38.2 \pm 0.8 \text{mM}$) and oocytes co-expressing WT EAAT3 and R501C EAAT4 (*open triangles*, $n = 8$, $K_D = 42.5 \pm 0.5 \text{mM}$) in the presence of 500 μM L-glutamate. F, sodium dependence of the isochronal current amplitude from oocytes expressing R501C EAAT4 (*closed circles*, $n = 6$, $K_D = 6.4 \pm 1.4 \text{mM}$) or co-expressing WT EAAT3 and R501C EAAT4 (*open triangles*, $n = 4$, $K_D = 5.5 \pm 0.5 \text{mM}$) in the presence of 500 μM L-serine.

No differences in the apparent dissociation constants were observed. Moreover, the serine concentration dependence was not affected when co-applied with a saturating concentration of glutamate (Figure 9.3C and D), a condition in which the *hEAAT3* is expected to be predominantly in the inward-facing, but not in the outward-facing configuration. At saturating glutamate (Figure 9.3E) or serine concentrations (Figure 9.3F), WT *hEAAT3* and R501C *rEAAT4* differ significantly in the apparent dissociation constants for sodium, with R501C *rEAAT4* showing significantly higher apparent affinity. However, co-expression of the two transporters does not modify sodium binding (Figure 9.3E and F).

Figure 9.4
Substrate translocation occurs independently by individual subunits

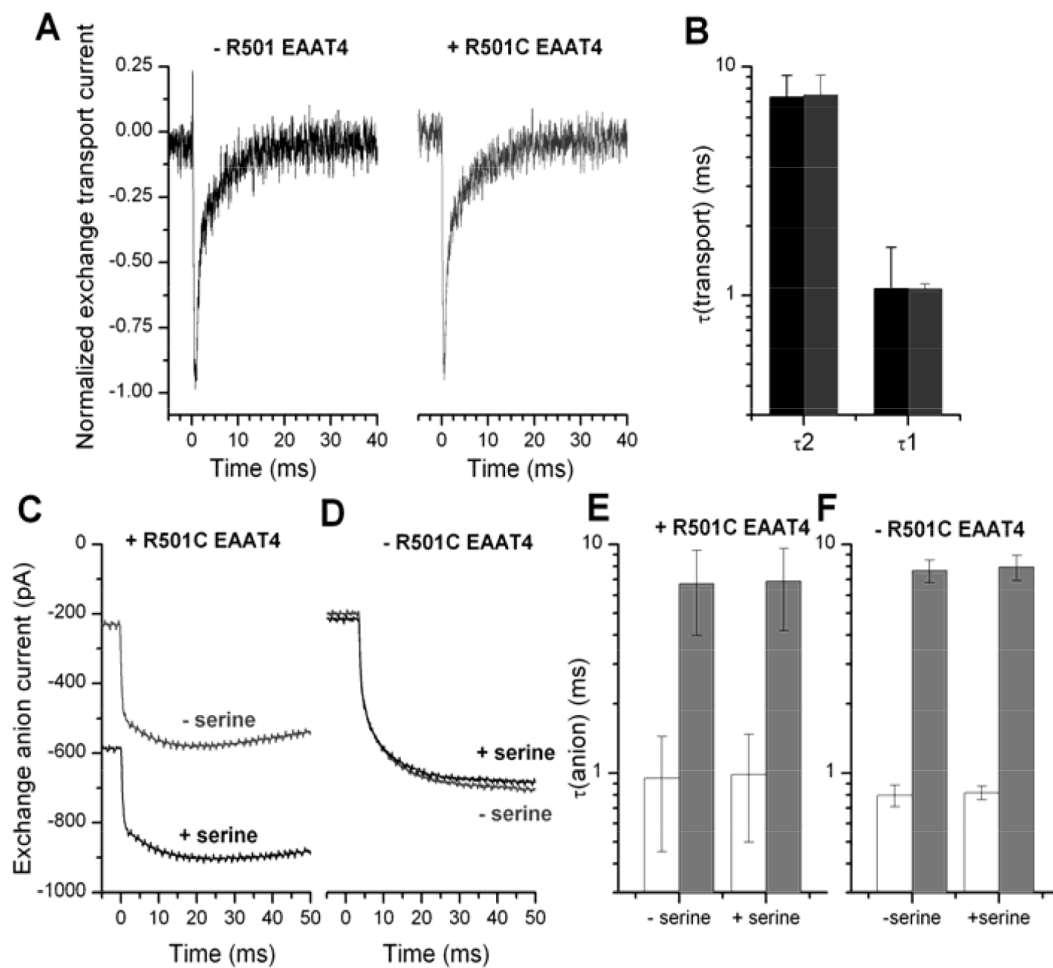


Figure 9.4: Substrate translocation occurs independently by individual subunits.

A, typical exchange transport current recordings (in the absence of permeating anions) after laser pulse photolytic release of glutamate at $t = 0$ with cells expressing WT EAAT3 alone or co-expressing WT EAAT3 and R501C EAAT4 (internal solution contained 140 mM NaMES and 10 mM glutamate and serine, exchange mode). The presence of R501C EAAT4 was tested by applying a saturating serine concentration in the anion-conducting mode. The decay of the transport current is biphasic in both cases and could be fit with a sum of two exponentials, yielding two time constants. B, quantification of the time constants associated with the rapidly and slowly decaying phases of the exchange transport current for WT EAAT3-expressing cells (*black*, $n = 3$) and R501C EAAT4 + WT EAAT3-expressing cells (*grey*, $n = 3$). C and D, typical anion current recordings (inward current caused predominantly by outflow of the highly permeant anion SCN^-) after laser pulse photolytic release of glutamate at $t = 0$ with cells expressing WT EAAT3 alone or co-expressing WT EAAT3 and R501C EAAT4 in the absence (*grey traces*) and presence (*black traces*) of serine (internal solution contained 140 mM NaSCN and 10 mM glutamate and serine, exchange mode). In C, the baseline current of the black trace is increased due to the continuous presence of serine, preactivating R501C EAAT4. In the absence of R501C EAAT4, serine had no effect. The rise of the current was fit with a sum of two exponentials, yielding two time constants. E and F, quantification of the time constants associated with the rapidly (*open bars*) and slowly (*gray bars*) rising phases of the exchange anion current for R501C EAAT4 + WT EAAT3-expressing cells (E, $n = 3$) and WT EAAT3-expressing cells (F, $n = 3$) in the presence and absence of extracellular serine. Error bars, S.D.

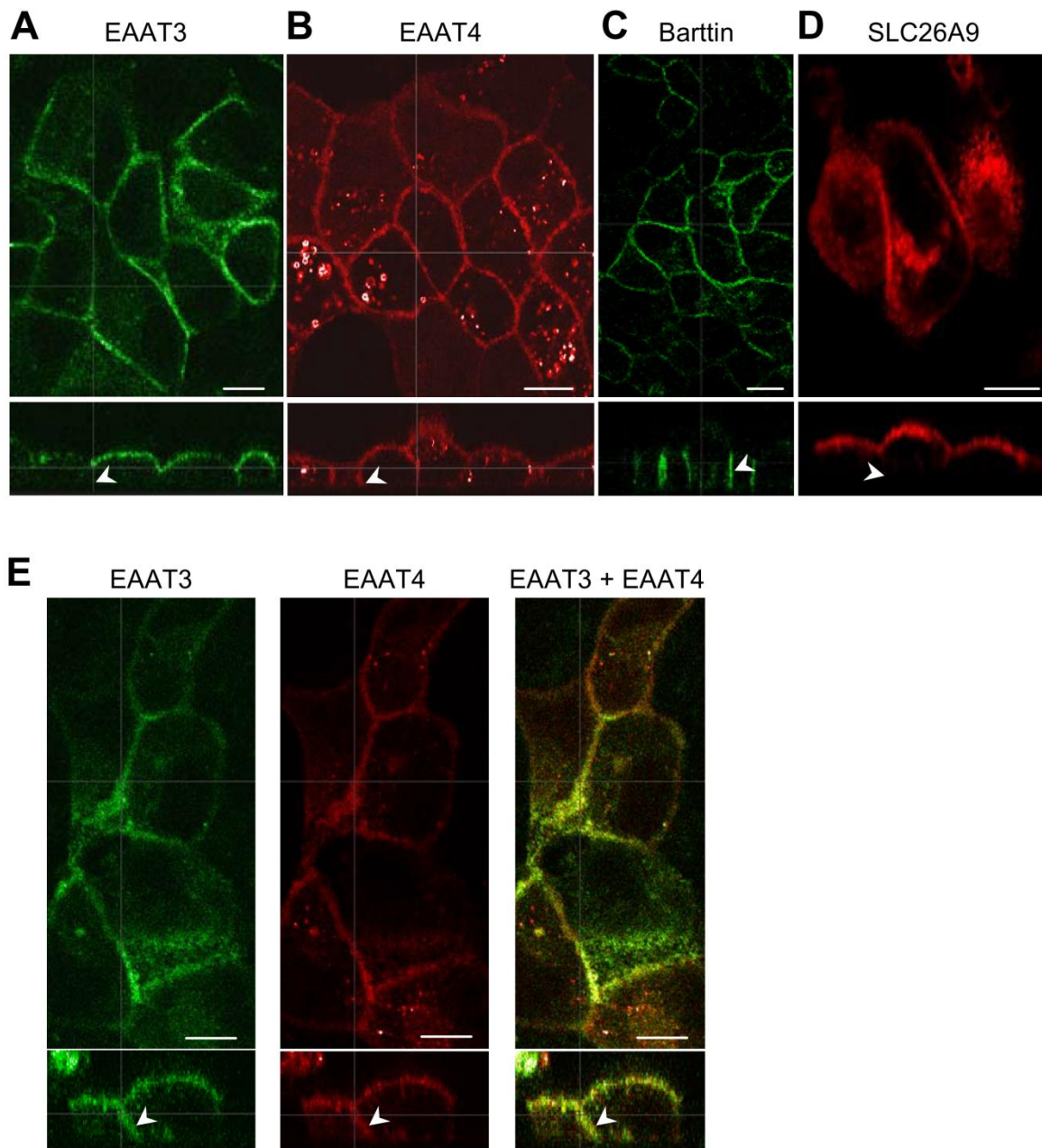
To test for potential subunit interactions during coupled substrate transport, we employed heterologous expression in mammalian cells and rapid application of glutamate with subsequent analysis of the relaxation of the transport-associated currents. This approach allows the resolution of early conformational changes in glutamate transporters (Figure 9.4). Because homotrimeric R501C *rEAAT4*s are insensitive to glutamate, differences in current responses of cells co-expressing WT *hEAAT3* and R501C *rEAAT4* from cells expressing *hEAAT3* alone will indicate modification of the function of *hEAAT3* by adjacent *rEAAT4* subunits. We performed these experiments under two different intracellular ionic conditions, i.e. with MES^- or with SCN^- as the predominant intracellular anion. In both types of experiments, intracellular K^+ was replaced by Na^+ , eliminating the relocation of the K^+ -bound transporter. With internal MES^- , there are no contributions of EAAT anion channels, and currents reflect conformational changes in the Na^+ /glutamate homoexchange mode (33) (Figure 9.4A and B). SCN^- represents the anion with highest permeability through the EAAT anion pore (8, 25, 32), and in cells dialyzed with internal SCN^- , currents at negative potentials are dominated by EAAT-mediated anion currents.

Two kinetic components of the current signal in response to glutamate application are observed in *hEAAT3*-expressing cells, a fast component due to Na^+ binding and a conformational change subsequent to the association of glutamate with the transporter (35) and a slow component representing the translocation of Na^+ and glutamate (26). Homo- and heterotrimeric transporters display identical time constants and relative amplitudes of the two kinetic components (Figure 9.4B). The two kinetic processes can also be observed in the presence of internal SCN^- . In this case, sudden increases of the external glutamate concentration result in a biexponential activation of *hEAAT3* anion channels with the same time constants as observed in the absence of permeant anions (Figure 9.4C and D). Serine activates R501C *rEAAT4* anion channels and thus increases the current amplitude in cells expressing heterotrimers in the presence of internal SCN^- . However, the rate constants of current activation were not affected by the co-expression of R501C *rEAAT4*, either in the absence or in the presence of serine (Figure 9.4E and F). We conclude that, within heterotrimeric assemblies, individual EAAT subunits bind and transport amino acid substrates and sodium ions independently of each other.

9.4.4 Targeting of Heterotrimeric Transporters in Polarized Epithelial Cells

EAAT3 exhibits a unique sorting signal that targets transporters to the apical membrane of epithelial cells and into neuronal dendrites (27). EAAT1, EAAT2, and EAAT4 lack this signal and are therefore distributed differently in MDCK cells than *hEAAT3* (27). We used co-expression of fluorescent protein-tagged *hEAAT3* and *rEAAT4*, confocal imaging (Figure 9.5) and surface biotinylation (Figure 9.6) to study whether hetero-trimerization affects epithelial sorting.

Figure 9.5
Epithelial sorting of homo- and heterotrimeric EAATs observed by confocal imaging



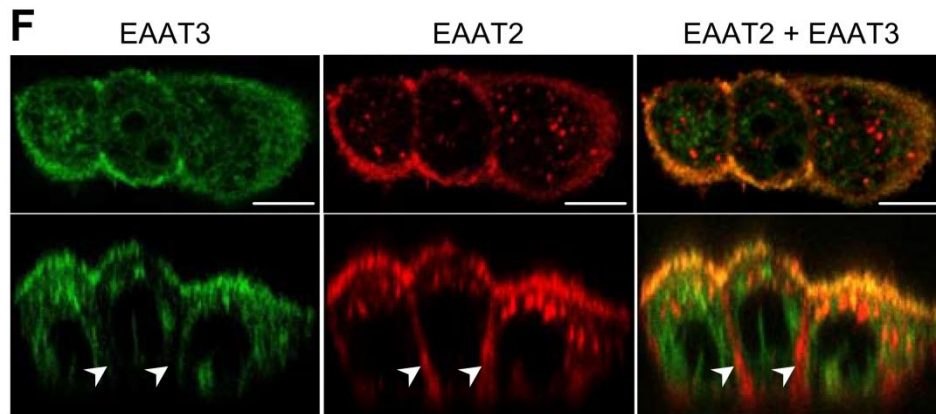


Figure 9.5: Epithelial sorting of homo- and heterotrimeric EAATs observed by confocal imaging.

A-D, confocal images of MDCK cells that transiently express CFP-*hEAAT3* (*A*), YFP-*rEAAT4* (*B*), barttin-YFP (*C*), or hSLC26A9-YFP (*D*). *E*, co-expression of CFP-*EAAT3* and YFP-*rEAAT4*. CFP is shown in *green*, and YFP is shown in *red*. This color code results in an *orange* coloring of regions where both proteins overlap. Individual YFP and CFP fluorescences are added to demonstrate co-localization of *hEAAT3* and *rEAAT4*. *F*, co-expression of GFP-*hEAAT3* and mCherry-*hEAAT2*. GFP is shown in *green*, and mCherry is shown in *red*. GFP and mCherry fluorescences are added to demonstrate co-localization of *hEAAT3* and *hEAAT2*. Arrows indicate basolateral membranes. x-y projections (*front view*) are given in the upper part, x-z projections (*side view*) in the lower part. Scale bar, 5 μm .

We first performed confocal imaging in confluent monolayers to study alteration of epithelial sorting (Figure 9.5). Whereas CFP-*hEAAT3* alone is predominantly inserted into the apical dome (Figure 9.5*A*), YFP-*rEAAT4* is visible in the apical and in the basolateral membranes (Figure 9.5*B*). We used barttin as basolateral (28, 36) (Fig. 9.5*C*) and SLC26A9 as apical marker (Figure 9.5*D*) (29). Co-transfection of CFP-*hEAAT3* and YFP-*rEAAT4* results in the appearance of *hEAAT3* and *rEAAT4* in apical as well as in basolateral (*arrows*) domains (Figure 9.5*E*). As expected for hetero-oligomerizing subunits, YFP and CFP fluorescence co-localizes. In contrast, co-transfection of GFP-*hEAAT3* with mCherry-*hEAAT2* that does not result in the formation of heterotrimers (Figure 9.1) fails to route *hEAAT3* to the basolateral domain (Figure 9.5*F*, *arrows*).

To quantify this alteration of epithelial sorting, we performed surface biotinylation in confluent monolayers of MDCK cells grown on filters (Figure 9.6). Figure 9.6*A* displays the fluorescent scan of a SDS-polyacrylamide gel with purified membrane-inserted GFP-*hEAAT3* after biotin application to the apical or the basolateral site of

cells expressing GFP-*hEAAT3* alone or co-expressing GFP-*hEAAT3* and *rEAAT4* or *hEAAT2*.

Figure 9.6
Epithelial sorting of homo- and heterotrimeric EAATs studied by cell surface biotinylation

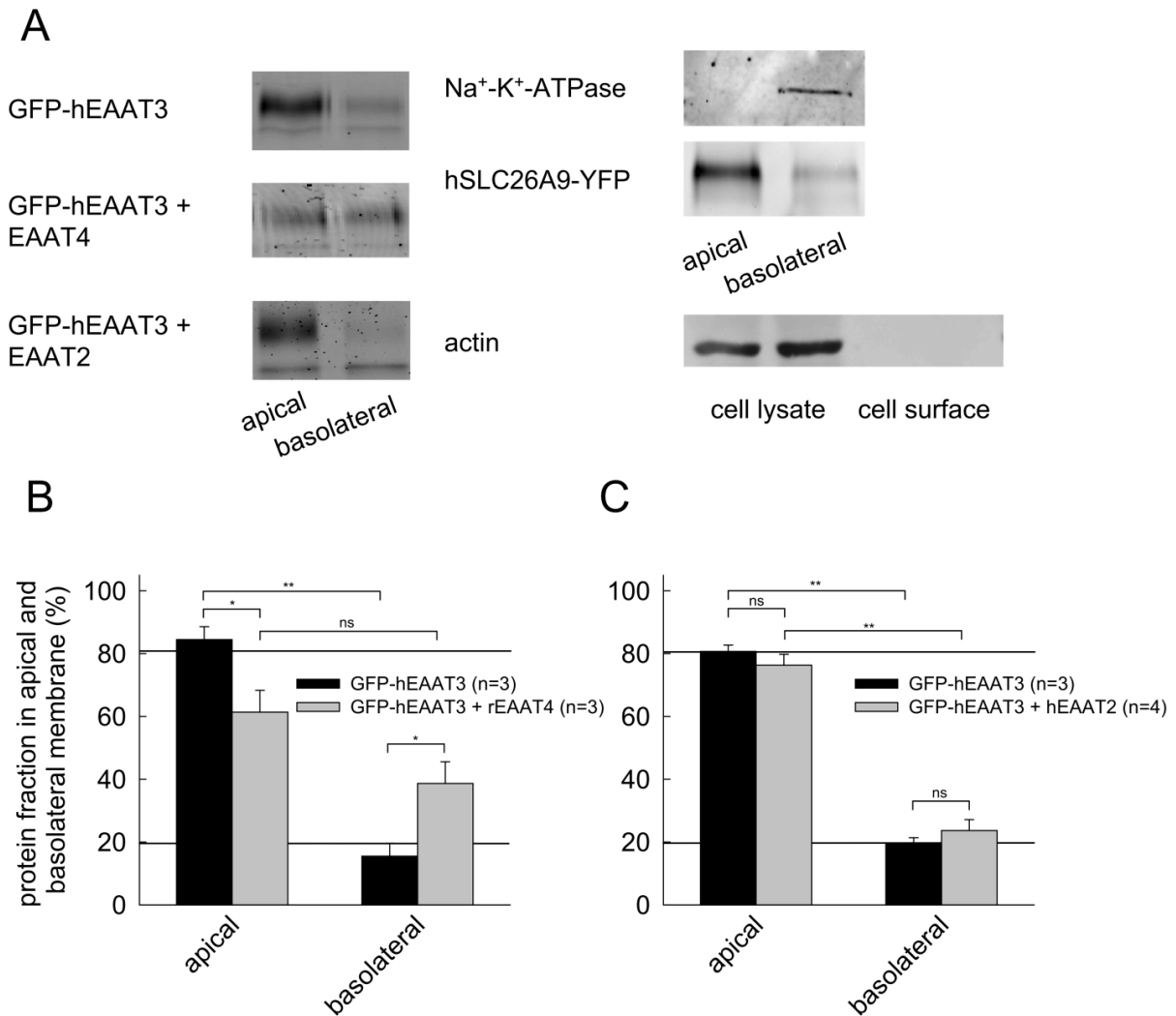


Figure 9.6: Epithelial sorting of homo- and heterotrimeric EAATs studied by cell surface biotinylation.

A, fluorescent scans of SDS-PAGE of GFP-*hEAAT3* purified by surface biotinylation from basolateral and apical membranes of MDCK cells expressing GFP-*hEAAT3* alone or together with untagged *rEAAT4* or *hEAAT2*. Control blots show that Na^+, K^+ -ATPase is detected at the basolateral but not the apical cell surface fraction, whereas heterologously expressed SLC26A9-mYFP is predominantly present in the apical membrane. Actin was only detected in the intracellular fraction. B and C, relative amounts of EAAT3 protein in the apical and the basolateral membrane when expressed alone or together with *rEAAT4* (B) or *hEAAT2* (C). GFP-EAAT3 was surface-biotinylated from the apical or the basolateral membrane, quantified by GFP fluorescence, and given as relative amount of the total surface fluorescence. Data represent means \pm S.E. (error bars) from three experiments. Level of significance: *, $p < 0.05$; **, $p < 0.01$. Solid lines give the proportion of the apical marker protein hSLC26A9 in basolateral or apical fractions.

In all cases, the majority of biotinylated EAAT3 protein is complex-glycosylated. Endogenous Na⁺,K⁺-ATPase and hSLC26A9-YFP were used as basolateral or apical controls.

Figure 9.6B shows the relative amounts of biotinylated GFP-*hEAAT3* after biotin application to the apical or the basolateral site, when expressed alone or co-expressed with nonfluorescent *rEAAT4*. Whereas *hEAAT3* homotrimers preferentially inserts into the apical membrane, hetero-trimerization results in equal distribution of *hEAAT3* in the apical and the basolateral membrane. Co-expression with *hEAAT2* does not modify the polarized expression of *hEAAT3* (Figure 9.6C). We conclude that *hEAAT3* is targeted to distinct regions as homotrimer or as a *hEAAT3/rEAAT4* heterotrimer.

9.5 Discussion

We here demonstrate that EAAT3 and EAAT4, but neither EAAT1 and EAAT2 nor EAAT2 and EAAT3, co-assemble into stable heterotrimers in heterologous expression systems. EAAT3 and EAAT4 co-express in several cell types of the mammalian brain (37, 38), and heterotrimers might, thus, represent a significant portion of the native transporters. BN-PAGE demonstrates the existence of stable heterotrimers, providing compelling evidence for a direct interaction of EAAT3 and EAAT4 (Figure 9.1). There are no indications for dimers and monomers or for higher order oligomers, *i.e.* the linkage of two trimers via interacting proteins.

Recent reports have demonstrated that co-expression of WT and mutant EAAT subunits results in a superposition of WT and mutant glutamate transport and anion currents, in full agreement with functionally independent subunits (17–19). We extended these studies by measuring substrate dependences (Figure 9.3) as well as early conformational changes (Figure 9.4) in heterotrimeric glutamate transporters. Our results support the idea that individual subunits function independently within the hetero-oligomeric assembly. The substrate concentration dependences of *hEAAT3* and R501C *rEAAT4* anion currents are similar in homo- and in heterotrimeric assemblies (Figure 9.3). Pre-steady-state kinetics of *hEAAT3* are unaffected by the presence of R501C *rEAAT4* in the heteromultimer (Figure 9.4). Co-expression of

*h*EAAT3 and serine-sensitive R501C *r*EAAT4 results in uptake currents that are identical to the superposition of currents mediated by *h*EAAT3 and R501C *r*EAAT4 (Figure 9.2G). For EAAT-associated anion currents, we observed slight deviations from the expectations of complete independence of individual subunits (Figure 9.2G). Structural evidence from the bacterial EAAT homolog Glt_{Ph} (39) suggested that substrate transport requires a major conformational change. Comparison of high resolution structures of Glt_{Ph} in the outward-facing (15) and in the inward-facing conformation (39) demonstrated a largely immobile “trimerization domain” (containing TM1, TM2, TM4, and TM5) and a “transport domain” undergoing substantial movements during the glutamate transport process (39). This transport mechanism requires trimerization for normal transport and suggests that monomeric Glt_{Ph} subunits might be unable to transport, in contrast to other multimeric transporter families (40). The apparent independence of EAAT subunits indicates that any transmission of conformational changes to other subunits through the trimerization domain may be minor.

Neither the glial transporters EAAT1 and EAAT2 nor EAAT2 and EAAT3 or EAAT2 and EAAT4 have the ability to co-assemble (Figure 9.1). Hetero-trimerization is, therefore, not a common feature of different EAAT isoforms. At present, we can only speculate about the biological significance of the hetero-oligomerization of EAAT3 and EAAT4. EAAT3 and EAAT4 are co-expressed in certain neurons of the central nervous system. Cooperation of different targeting signals might result in the insertion of heteromultimers in cell regions that exclude homotrimers. Hetero-trimerization results in close proximity of low affinity/high capacity (EAAT3) and high affinity/low capacity (EAAT4) transporter (30), allowing tight regulation of the external glutamate concentration. Because EAAT anion channels possibly modulate neuronal excitability (2, 11), relative expression levels of EAAT3 and EAAT4 will result in distinct pattern of neuronal excitability and its regulation by glutamate.

9.6 Acknowledgments

We thank Dr. M. Hediger, Dr. J. Rothstein, Dr. T. Rauen, Dr. W. Stoffel, Dr. Rainer Schreiber, and Dr. Karl Kunzelmann for providing the expression constructs for *hEAAT2*, *hEAAT3*, *rEAAT4*, *rEAAT3*, *rEAAT1*, and *hSLC26A9*; Dr. Patricia Hidalgo for helpful discussions; and Birgit Begemann for excellent technical assistance.

9.7 References

1. Danbolt, N. C. (2001) *Prog. Neurobiol.* **65**, 1–105
2. Amara, S. G., and Fontana, A. C. (2002) *Neurochem. Int.* **41**, 313–318
3. Levy, L. M., Warr, O., and Attwell, D. (1998) *J. Neurosci.* **18**, 9620–9628
4. Zerangue, N., and Kavanaugh, M. P. (1996) *Nature* **383**, 634–637
5. Wadiche, J. I., Amara, S. G., and Kavanaugh, M. P. (1995) *Neuron* **15**, 721–728
6. Fairman, W. A., Vandenberg, R. J., Arriza, J. L., Kavanaugh, M. P., and Amara, S. G. (1995) *Nature* **375**, 599–603
7. Watzke, N., and Grewer, C. (2001) *FEBS Lett.* **503**, 121–125
8. Melzer, N., Biela, A., and Fahlke, Ch. (2003) *J. Biol. Chem.* **278**, 50112–50119
9. Tanaka, K., Watase, K., Manabe, T., Yamada, K., Watanabe, M., Takahashi, K., Iwama, H., Nishikawa, T., Ichihara, N., Kikuchi, T., Okuyama, S., Kawashima, N., Hori, S., Takimoto, M., and Wada, K. (1997) *Science* **276**, 1699–1702
10. Watase, K., Hashimoto, K., Kano, M., Yamada, K., Watanabe, M., Inoue, Y., Okuyama, S., Sakagawa, T., Ogawa, S., Kawashima, N., Hori, S., Takimoto, M., Wada, K., and Tanaka, K. (1998) *Eur. J. Neurosci.* **10**, 976–988
11. Melzer, N., Torres-Salazar, D., and Fahlke, Ch. (2005) *Proc. Natl. Acad. Sci. USA*, **102**, 19214–19218

12. Veruki, M. L., Mørkve, S. H., and Hartveit, E. (2006) *Nat. Neurosci.* **9**, 1388–1396
13. Haugeto, O., Ullensvang, K., Levy, L. M., Chaudhry, F. A., Honoré, T., Nielsen, M., Lehre, K. P., and Danbolt, N. C. (1996) *J. Biol. Chem.* **271**, 27715–27722
14. Gendreau, S., Voswinkel, S., Torres-Salazar, D., Lang, N., Heidtmann, H., Detro-Dassen, S., Schmalzing, G., Hidalgo, P., and Fahlke, Ch. (2004) *J. Biol. Chem.* **279**, 39505–39512
15. Yernool, D., Boudker, O., Jin, Y., and Gouaux, E. (2004) *Nature* **431**, 811–818
16. Koch, H. P., and Larsson, H. P. (2005) *J. Neurosci.* **25**, 1730–1736
17. Grewer, C., Balani, P., Weidenfeller, C., Bartusel, T., Tao, Z., and Rauen, T. (2005) *Biochemistry* **44**, 11913–11923
18. Leary, G. P., Stone, E. F., Holley, D. C., and Kavanaugh, M. P. (2007) *J. Neurosci.* **27**, 2938–2942
19. Koch, H. P., Brown, R. L., and Larsson, H. P. (2007) *J. Neurosci.* **27**, 2943–2947
20. Torres-Salazar, D., and Fahlke, C. (2006) *J. Neurosci.* **26**, 7513–7522
21. Deleted in proof
22. Detro-Dassen, S., Schänzler, M., Lauks, H., Martin, I., zu Berstenhorst, S. M., Nothmann, D., Torres-Salazar, D., Hidalgo, P., Schmalzing, G., and Fahlke, Ch. (2008) *J. Biol. Chem.* **283**, 4177–4188
23. Nicke, A., Bäumert, H. G., Rettinger, J., Eichele, A., Lambrecht, G., Mutschler, E., and Schmalzing, G. (1998) *EMBO J.* **17**, 3016–3028
24. Trotti, D., Peng, J. B., Dunlop, J., and Hediger, M. A. (2001) *Brain Res.* **914**, 196–203
25. Torres-Salazar, D., and Fahlke, Ch. (2007) *J. Biol. Chem.* **282**, 34719–34726
26. Watzke, N., Bamberg, E., and Grewer, C. (2001) *J. Gen. Physiol.* **117**, 547–562
27. Cheng, C., Glover, G., Banker, G., and Amara, S. G. (2002) *J. Neurosci.* **22**, 10643–10652

28. Janssen, A. G., Scholl, U., Domeyer, C., Nothmann, D., Leinenweber, A., and Fahlke, Ch. (2009) *J. Am. Soc. Nephrol.* **20**, 145–153
29. Lohi, H., Kujala, M., Makela, S., Lehtonen, E., Kestila, M., Saarialho-Kere, U., Markovich, D., and Kere, J. (2002) *J. Biol. Chem.* **277**, 14246–14254
30. Mim, C., Balani, P., Rauen, T., and Grewer, C. (2005) *J. Gen. Physiol.* **126**, 571–589
31. Bendahan, A., Armon, A., Madani, N., Kavanaugh, M. P., and Kanner, B. I. (2000) *J. Biol. Chem.* **275**, 37436–37442
32. Wadiche, J. I., and Kavanaugh, M. P. (1998) *J. Neurosci.* **18**, 7650–7661
33. Grewer, C., Watzke, N., Wiessner, M., and Rauen, T. (2000) *Proc. Natl. Acad. Sci. USA*, **97**, 9706–9711
34. Kovermann, P., Machtens, J. P., Ewers, D., and Fahlke, Ch. (2010) *J. Biol. Chem.* **285**, 23676–23686
35. Mim, C., Tao, Z., and Grewer, C. (2007) *Biochemistry* **46**, 9007–9018
36. Estévez, R., Boettger, T., Stein, V., Birkenhäger, R., Otto, E., Hildebrandt, F., and Jentsch, T. J. (2001) *Nature* **414**, 558–561
37. Furuta, A., Rothstein, J. D., and Martin, L. J. (1997) *J. Neurosci.* **17**, 8363–8375
38. Furuta, A., Martin, L. J., Lin, C. L., Dykes-Hoberg, M., and Rothstein, J. D. (1997) *Neuroscience* **81**, 1031–1042
39. Reyes, N., Ginter, C., and Boudker, O. (2009) *Nature* **462**, 880–885
40. Robertson, J. L., Kolmakova-Partensky, L., and Miller, C. (2010) *Nature* **468**, 844–847

10 Neutralizing aspartate 83 modifies substrate translocation of Excitatory Amino Acid Transporter 3 (EAAT3) glutamate transporters^{*s}

Jasmin Hotzy[‡], Jan-Philipp Machtens[‡], and Christoph Fahlke^{‡§1}

From the [‡] Institut für Neurophysiologie, Medizinische Hochschule Hannover, D-30625 Hannover, Germany and

[§] Zentrum für Systemische Neurowissenschaften Hannover (ZSN), D-30559 Hannover, Germany

* This work was supported by Deutsche Forschungsgemeinschaft Grant FA301/9 (to Ch. F.).

^s This article contains supplemental Figs. 1-3.

¹ To whom correspondence should be addressed: Inst. für Neurophysiologie, Medizinische Hochschule Hannover, Carl-Neuberg-Str. 1, D-30625 Hannover, Germany. Tel.: 49-511-532-2777; Fax: 49-511-532-2776; E-mail: fahlke.christoph@mh-hannover.de.

² The abbreviations used are: EAAT, excitatory amino acid transporter; TM, transmembrane domain; HP, hairpin.

This research was originally published in *J. Biol. Chem.*. Jasmin Hotzy[‡], Jan-Philipp Machtens[‡], and Christoph Fahlke^{‡§1}. Neutralizing aspartate 83 modifies substrate translocation of Excitatory Amino Acid Transporter 3 (EAAT3) glutamate transporters^{*s}. *J. Biol. Chem.*, 2012, 287: 20016-20026 © the American Society for Biochemistry and Molecular Biology.

Background: Neutralizing a conserved aspartate between TM2 and TM3 affects gating of EAAT anion channels.

Results: Voltage clamp fluorometry demonstrates that the analogous mutation alters EAAT3 substrate translocation.

Conclusion: Altered substrate translocation is sufficient to explain anion channel gating in D83A EAAT3.

Significance: Dissection of transport and anion channel gating defines an intimate relationship between these two EAAT transport functions.

10.1 Abstract

Excitatory amino acid transporters (EAATs) terminate glutamatergic synaptic transmission by removing glutamate from the synaptic cleft into neuronal and glial cells. EAATs are not only secondary-active glutamate transporters, but also function as anion channels. Gating of EAAT anion channels is tightly coupled to transitions within the glutamate uptake cycle, resulting in Na⁺- and glutamate-dependent anion currents. A point mutation neutralizing a conserved aspartic acid within the intracellular loop close to the end of transmembrane domain 2 (TM2) was recently shown to modify the substrate dependence of EAAT anion currents. To distinguish whether this mutation affects transitions within the uptake cycle, or directly modifies opening/closing of the anion channel, we employed voltage clamp fluorometry. Using three different sites for fluorophore attachment, V120C, M205C and A430C, we observed time-, voltage- and substrate-dependent alterations of EAAT3 fluorescence intensities. The voltage and substrate dependence of fluorescence intensities can be described by a 15-state model of the transport cycle in which several states are connected to branching anion channel states. D83A-mediated changes of fluorescence intensities, anion currents and secondary-active transport can be explained by exclusive modifications of substrate translocation rates. In contrast, sole modification of anion channel opening and closing is insufficient to account for all experimental data. We conclude that D83A has direct effects on the glutamate transport cycle, and that these effects result in changed anion channel function.

10.2 Introduction

Excitatory amino acid transporters (EAATs) are secondary-active transporters that mediate the stoichiometrically coupled transport of one glutamate, three sodium ions and one proton while one potassium ion is counter-transported (1; 2). They are necessary for termination of glutamatergic synaptic transmission and for maintenance of low resting glutamate levels (3-5). There are five different mammalian EAATs with distinct physiological roles. Genetic removal of mouse EAAT2 results in pronounced hyperexcitability and neurodegeneration (6) demonstrating the crucial role of this isoform for glutamate homeostasis in the central nervous system. Mouse models that lack other EAATs exhibit much milder phenotypes with certain impairment of motor coordination, behavioural abnormalities, or age-dependent neurodegeneration (7-10). EAAT3 is not only expressed in the central nervous tissue, but also mediates glutamate and aspartate reabsorption in the renal proximal tubule (8). Naturally occurring mutations in the gene encoding EAAT3 cause human dicarboxylic aminoaciduria (11).

EAATs are not only glutamate transporters, but also conduct a pore-mediated anion current (12-15). EAAT anion currents have been postulated to be involved in the regulation of cell excitability (16; 17), but so far, the physiological importance of this transport function is not sufficiently understood. EAAT anion currents are thought to be conducted through an anion pathway that is opened and closed in response to conformational changes underlying glutamate transport (18; 19). However, how this anion pore is formed and how opening and closing occur is unclear. In a systematic screen for mutations affecting EAAT1 anion channel function, D112A was found to abolish the glutamate dependence of EAAT1 anion currents (20). The corresponding mutation D117A was later shown to change unitary anion current amplitudes and relative anion selectivities of EAAT4 anion channels (19), suggesting close proximity of this residue to the EAAT4 anion conduction pathway. In addition to modifying EAAT1 anion currents, D112A reduces EAAT1 glutamate uptake rates by 40%.

So far, anion permeation through EAATs was thought not to affect glutamate transport (13). A mutation that changes anion conduction and coupled glutamate transport thus promises insights into the interdependence of the two EAAT transport functions, and thus, we decided to further study this mutation using voltage clamp fluorometry. Voltage clamp fluorometry combines electrophysiological and fluorescence measurements and has been used to monitor conformational changes

in diverse transport proteins (21-23). We inserted the homologous mutation D83A into EAAT3 and applied voltage clamp fluorometry to separate the effects on coupled transport and on anion channel function. EAAT3 has already been studied using voltage clamp fluorometry, permitting detection of conformational rearrangements during coupled transport (23-26). Moreover, EAAT3 effectively transports glutamate (12; 27), thus permitting additional direct insights into the effects of neutralizing D83 on coupled transport.

We found that D83A changes the time, substrate and voltage dependence of EAAT3 fluorescence signals. Moreover, similar to earlier data on D112A EAAT1 and D117A EAAT4, D83A enlarges EAAT3 anion currents in the absence of glutamate, but reduces glutamate-sensitive current amplitudes. It reduces coupled transport by about 50%. The data on fluorescence amplitudes and transport function can be described by a kinetic scheme in which only transitions within the uptake cycle are modified by the mutation, whereas the likelihood of anion channel opening was not changed in mutant transporters.

10.3 Experimental Procedures

10.3.1 Expression of WT and mutant *hEAAT3* transporters in *Xenopus laevis* oocytes

Point mutations were introduced into pTLN2-*hEAAT3* (28; 29) (kindly provided by Dr. Matthias Hediger (University of Bern, Switzerland)) using the QuikChange mutagenesis kit (Stratagene, La Jolla, CA, USA). Capped cRNA was synthesized from *MluI*-/*NheI*-linearized pTLN2-*hEAAT3* through use of MESSAGE machine kits (Ambion, Austin, TX, USA). Collagenase-treated, defolliculated stage IV-V oocytes were microinjected with 10 ng of RNA (Nanoliter 2000, World Precision Instruments, Sarasota, FL, USA) and incubated at 18°C in ND96 (in mM: 96 NaCl, 2 KCl, 1.8 CaCl₂, 1 MgCl₂, 5 HEPES, pH 7.6, supplemented with 2.5 sodium pyruvate and 50 µg/ml gentamycin sulfate). Experiments were performed 3-7 days after injection.

10.3.2 Electrophysiology

Currents were recorded through two-electrode voltage clamp using a CA-1B amplifier (Dagan Corporation, Minneapolis, MN, USA) and digitized at 5 kHz using an ITC-18 Computer Interface in combination with Patchmaster (HEKA Elektronik, Lambrecht, Germany) (30). Experiments were performed under constant perfusion using a PF-8 8-Channel Perfusion System (Abimek-Zech electronic, Göttingen, Germany) with Ringer's solution (in mM: 98.5 Choline-Cl or NaCl/NO₃/gluconate, 1.8 CaCl₂/gluconate, and 1 MgCl₂/gluconate, 5 Hepes pH 7.5, ± 1 glutamate). Oocytes were held at 0 mV for at least 2 s between voltage steps.

10.3.3 Voltage clamp fluorometry

For fluorescence experiments, oocytes were labeled for 2-3 h with 10 μM of the fluorescent maleimide probe, AlexaFluor546 (Life Technologies Corporation, Invitrogen, Carlsbad, CA, USA). A short arc mercury lamp (HBO 103W/2, Osram, München, Germany) combined with a Uniblitz shutter (VS25S2ZMOR1-24 shutter, VCM-D1 shutter driver, Uniblitz, Vincent Associates, Rochester, NY, USA) was used as light source. Fluorescence was monitored under voltage clamp by a photodiode (PIN020-A, AMS Technologies AG, Martinsried, Germany) and a rhodamine filter cube (HQ535/50x, Q565LP, HQ610/75m, Chroma Technology Corp., Bellows Falls, VT, USA) attached to an inverted fluorescence microscope (IX71, Olympus, Hamburg, Germany). Fluorescence signals were amplified with a DLPCA-200 amplifier (Femto Messtechnik, Berlin, Germany) and low pass-filtered at 2 kHz (LPF-8, Low Pass Bessel Filter, Warner Instruments, Hamden, CT, USA). Representative fluorescence recordings were obtained by averaging ten consecutive measurements.

10.3.4 Data analysis

Electrophysiological and fluorescence data were analyzed with a combination of Patchmaster (HEKA Elektronik, Lambrecht,), pClamp10 (Molecular Devices, Sunnyvale, CA, USA), MATLAB (The MathWorks, Natick, MA, USA) and SigmaPlot (Jandel Scientific, San Rafael, CA, USA). For statistical evaluations, Student's t-test

and paired t-test with $p \leq 0.05$ (*) as the level of significance were used ($p \leq 0.01$ (**), $p \leq 0.001$ (***)). The data are given as means \pm S.E..

10.3.5 Kinetic modeling

Voltage and substrate dependence of EAAT3 fluorescence was simulated by solving differential equations at steady-state according to a previously developed 15-state model of EAAT2 extended by channel states branching from the uptake cycle (19; 23; 31). Rate constants of the uptake cycle were adopted from earlier work on cysteine-substituted EAAT3 (23). Anion channel open probabilities were estimated by optimizing the model against cysteine-substituted WT steady-state fluorescence data using the genetic algorithm as implemented in MATLAB (The MathWorks, Natick, MA, USA). The overall fluorescence was calculated as sum of the products of relative fluorescence and probability of occupation for every state. This model was then adapted to D83A EAAT3 - either by modifying translocation rates (reactions 8, 15, 17) or anion channel open probabilities. In all cases, detailed balance was preserved, and fitting parameters were simultaneously optimized against experimentally determined relative glutamate uptake and anion current amplitudes. For kinetic modeling we assumed intracellular concentrations of $[\text{Na}^+] = 10$ mM, $[\text{K}^+] = 70$ mM, $[\text{glu}] = 12$ mM and a $\text{pH} = 7.3$ (1), extracellular concentrations were set to experimental conditions.

10.4 Results

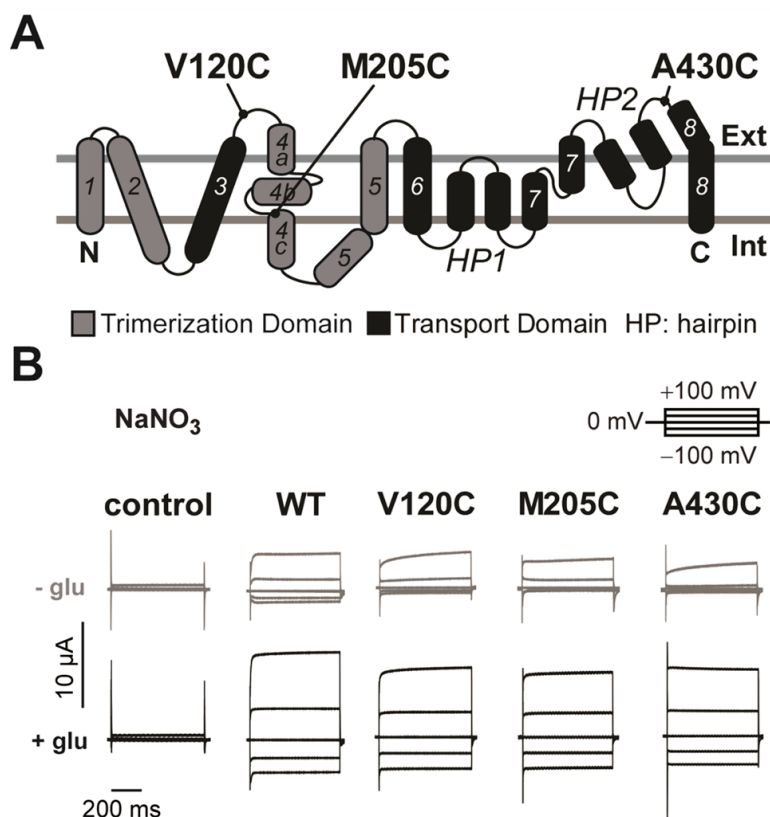
10.4.1 Time, substrate and voltage dependence of EAAT-associated currents and fluorescence signals

To permit site-directed fluorescence labeling of EAAT3 we introduced single cysteines into human EAAT3 and expressed WT and cysteine-substituted transporters in *Xenopus* oocytes (Figure 10.1). We chose three reporter mutations localized in different parts of the transporter, V120C (3-4 loop), M205C (TM4c) and A430C (7-8 loop) (Figure 10.1A) to observe fluorescence changes due to conformational changes in more than one protein region. M205C and A430C has

already been used in earlier studies (23; 25), whereas V120C has not been reported to date. Since the fluorophore attachment site Cys120 is localized nearby an accessible endogenous cysteine, we additionally mutated Cys158 to serine in all our constructs, to prevent possible modifications by fluorophore application.

For each reporter mutation, the time course of fluorescence labeling was tested to define incubation times sufficient for maximum labeling (Suppl. Figure 10.8). V120C, M205C and A430C EAAT3 injected oocytes exhibit higher levels of fluorescence intensities as uninjected oocytes or oocytes expressing C158S EAAT3 (data not shown). Moreover, oocytes expressing V120C, M205C or A430C EAAT3 displayed fluorescence changes upon voltage or substrate alterations (Suppl. Figure 10.9) that were absent in uninjected oocytes or those expressing C158S EAAT3, indicating that cysteine-substituted EAAT3 are specifically labeled with the fluorescent dye.

Figure 10.1
Reporter mutations do not affect the function of EAAT3 associated currents



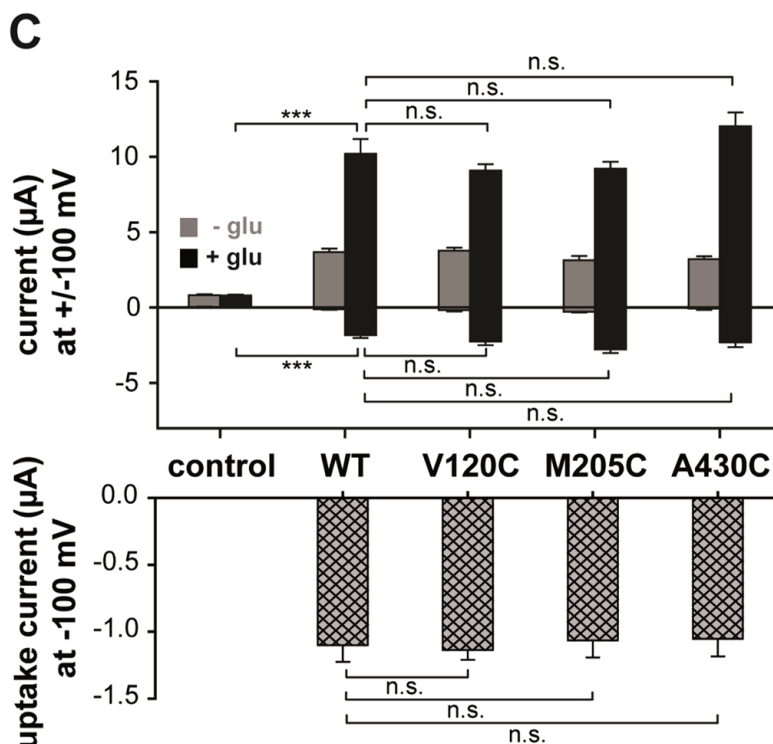


Figure 10.1: Reporter mutations do not affect the function of EAAT3 associated currents.

A, localization of the fluorescence reporter mutations, V120C, M205C and A430C on the transmembrane topology model of EAAT3. The trimerization domain is shown in grey, the transport domain and the hairpins are in black. B, representative current traces recorded from *X. laevis* oocytes expressing WT, V120C, M205C or A430C EAAT3. C, averaged absolute current amplitudes at ± 100 mV (top) and averaged uptake current amplitudes at -100 mV (bottom) calculated by the difference of measurements in sodium gluconate with and without glutamate. n.s.: not significantly different $p > 0.05$, ***, $p \leq 0.001$. Data are given as means \pm S.E.; $n \geq 7$. Int, internal; Ext, external; glu, glutamate.

To test whether cysteine insertions change glutamate transport or anion conduction we studied WT and cysteine-substituted EAAT3 currents using two-electrode voltage clamp (Figure 10.1B). Application of glutamate resulted in a pronounced increase of current amplitudes at negative as well as at positive voltages. In the absence as well as in the presence of glutamate, current amplitudes in oocytes expressing V120C, M205C, or A430C EAAT3 were not statistically different from those of WT EAAT3, illustrating comparable expression levels. EAAT3 currents consist of two components, glutamate uptake currents due to electrogenic transport and EAAT3-associated anion currents. Glutamate uptake current can be separated from anion currents after substituting permeant anions with impermeant gluconate and measured as the difference of currents in the presence and in the absence of glutamate (2; 13; 33). Glutamate uptake is strongly voltage-dependent and

decreases to values around zero at positive potentials (2). Thus, currents at positive voltages predominantly represent anion currents. The use of NO_3^- as main external anion results in EAAT3 currents that are significantly larger than endogenous currents of uninjected oocytes and permit accurate measurements of EAAT3 anion currents (Figure 10.1B) (33). For all tested constructs, glutamate uptake currents and anion currents at saturating glutamate concentrations were not statistically different from WT values, illustrating that none of the cysteine substitutions modify functional properties of EAAT3 (23;25) (Figure 10.1B and C).

Figure 10.2 shows representative fluorescence recordings from V120C, M205C or A430C EAAT3 in the absence (*top*) or in the presence (*bottom*) of 1 mM L-glutamate. Oocytes were held at 0 mV, and voltage steps between -150 mV and +150 mV were applied in 50 mV intervals. In the absence of glutamate hyperpolarizing voltage steps caused a slow reduction of V120C EAAT3 fluorescence that could be fit with a monoexponential function ($\tau_{(-150 \text{ mV})} = 46.7 \pm 4.3 \text{ ms}$, $n = 3$) (Figure 10.2A). M205C and A430C EAAT3 exhibited fluorescence amplitudes that, in the absence of glutamate, increased upon membrane depolarization and decreased upon hyperpolarization (Figure 10.2B and C). The time course of these voltage-dependent changes was significantly faster than for V120C ($\tau_{(\text{M205C}, -150/+150\text{mV})} = 4.3 \pm 0.4/7.1 \pm 0.9 \text{ ms}$, $n = 3$; $\tau_{(\text{A430C}, -150/+150\text{mV})} = 10.5 \pm 0.6/8 \pm 1.2 \text{ ms}$, $n = 3$). For M205C EAAT3, the initial rise upon membrane depolarization was followed by a much slower decay (Figure 10.2).

Application of glutamate increased fluorescence intensities of V120C EAAT3 and decreased these values for M205C and A430C EAAT3. Glutamate modified the voltage dependences of fluorescence signals for all cysteine-substituted EAAT3 (Figure 10.2). Application of L-glutamate accelerated the time course of fluorescence change ($\tau_{(+150 \text{ mV})} = 16 \pm 0.5 \text{ ms}$, $n = 3$) and modified its voltage dependence for V120C EAAT3 (Figure 10.2A). For M205C and A430C EAAT3 (Figure 10.2B and C), fluorescence showed lowest intensity around 0 mV and increased upon positive as well as negative membrane potentials. In the presence of glutamate, fluorescence increased on a slow time course upon depolarization as well as upon hyperpolarization ($\tau_{(\text{M205C}, +150\text{mV})} = 87.2 \pm 3.2 \text{ ms}$, $n = 3$; $\tau_{(\text{A430C}, +150\text{mV})} = 59.2 \pm 4.2 \text{ ms}$, $n = 2$).

Figure 10.2
Voltage- and substrate-dependent conformational changes of EAAT3

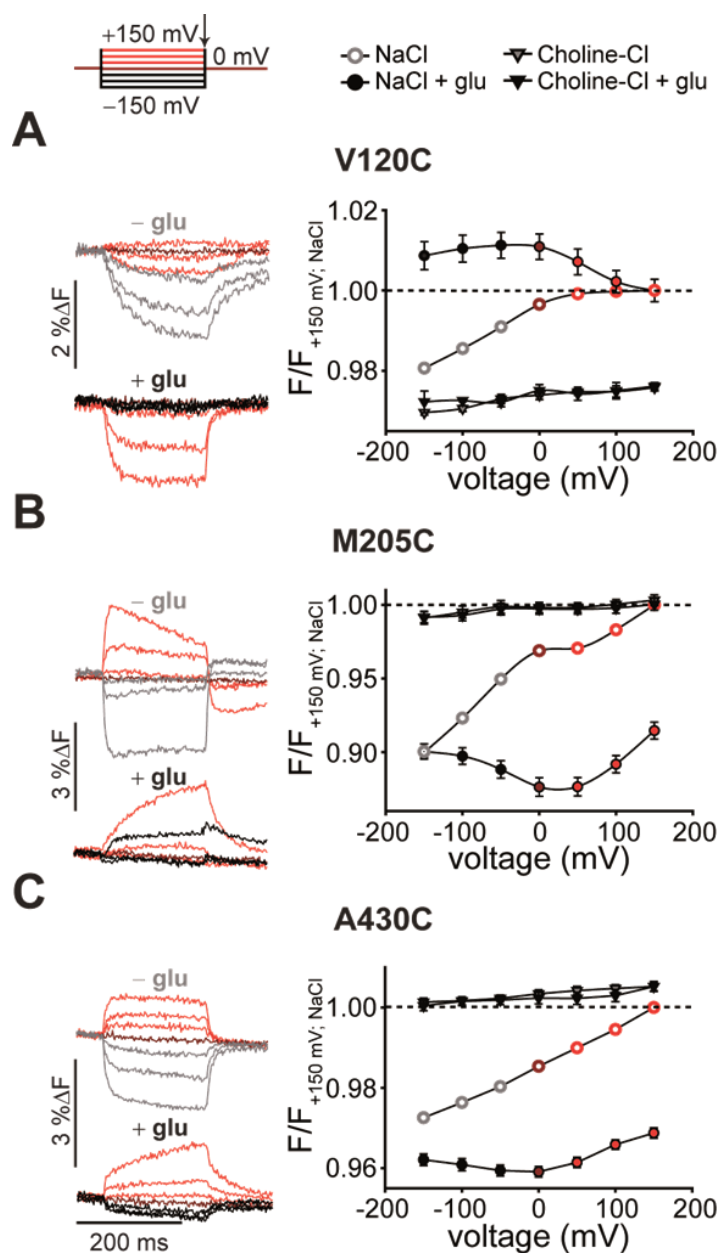


Figure 10.2: Voltage- and substrate-dependent conformational changes of EAAT3.

Representative fluorescence traces (left column) recorded from *X. laevis* oocytes expressing V120C (A), M205C (B) and A430C EAAT3 (C) and averaged voltage dependence of late (arrow) relative fluorescence changes (right column) in the presence of different substrates are shown. Fluorescence signals were measured in NaCl Ringer's solution during 200-ms voltage steps between +150 mV and -150 mV. Fluorescence amplitudes were normalized to the fluorescence generated at +150 mV in NaCl solution. Measurements in NaCl at voltages above 0 mV are shown in red, 0 mV is in dark red, and negative voltages in the absence of 1 mM glutamate are shown in light grey and in the presence of 1 mM glutamate are shown in black. Fluorescence data from at least six oocytes are reported as means \pm S.E.. F, fluorescence; glu, glutamate.

EAAT-mediated glutamate transport is based on a series of substrate association steps and related conformational changes. Three Na⁺ ions, one H⁺ and one glutamate associate with the outward facing transporter with an open extracellular gate (hairpin 2; HP2). After closure of HP2 and movement of the translocation domain to the inside (34), Na⁺, H⁺ and glutamate are released by opening of the intracellular gate (hairpin 1; HP1), and the uptake cycle is completed by retranslocation after association of K⁺ or Na⁺. Modification of the uptake cycle by removal of certain substrates or application of EAAT-specific blockers allows testing of the specificity of the observed signals. For all constructs, substitution of Na⁺ by choline⁺ abolished the voltage dependence of fluorescence signals and changed the fluorescence intensity (Figure 10.2). A specific blocker of EAAT transporters, DL-threo-benzyloxyaspartate (35; 36) inhibited fluorescence changes in the absence and in the presence of glutamate by about 90%, supporting the notion that fluorescence changes are due to conformational rearrangements in the glutamate transporter (Suppl. Figure 10.9).

EAAT4 anion channel gating depends on anion concentrations on both membrane sites (19; 33). To test whether EAAT3 fluorescence intensities undergo anion-dependent alterations, we studied all cysteine-substituted EAAT3 constructs after substitution of the external anion by gluconate. Chloride removal did not change the intensity or voltage dependence of fluorescence signals (Suppl. Figure 10.10A-C). We conclude that fluorescence changes of fluorophores added to V120C, M205C and A430C report on conformational changes within the EAAT3 uptake cycle that require external Na⁺ but do not depend on the anion composition.

To test whether EAAT3

10.4.2 Voltage clamp fluorometry reveals additional slow conformational changes

In addition to the initial rise upon depolarization, fluorescence intensities of M205C EAAT3 exhibited voltage-dependent changes with very slow time course. Figure 10.3 shows such current and fluorescence recordings of M205C EAAT3 on an extended time scale. In the absence of glutamate, a depolarizing voltage step to +50 mV caused a very slow fluorescence decay ($\tau_{(+50\text{mV})} = 6.7 \pm 1.2 \text{ s}$, $n = 6$). This process is

not due to bleaching, since we observed slow fluorescence recovery upon return to the holding potential of 0 mV (Figure 10.3A). Application of glutamate shifted the voltage dependence of these slow processes so that relaxation of these signals was observed upon voltage steps to -100 mV ($\tau_{(-100\text{mV})} = 4.0 \pm 1.2$ s, $n = 11$) (Figure 10.3A).

Figure 10.3
Slow conformational changes in EAAT3

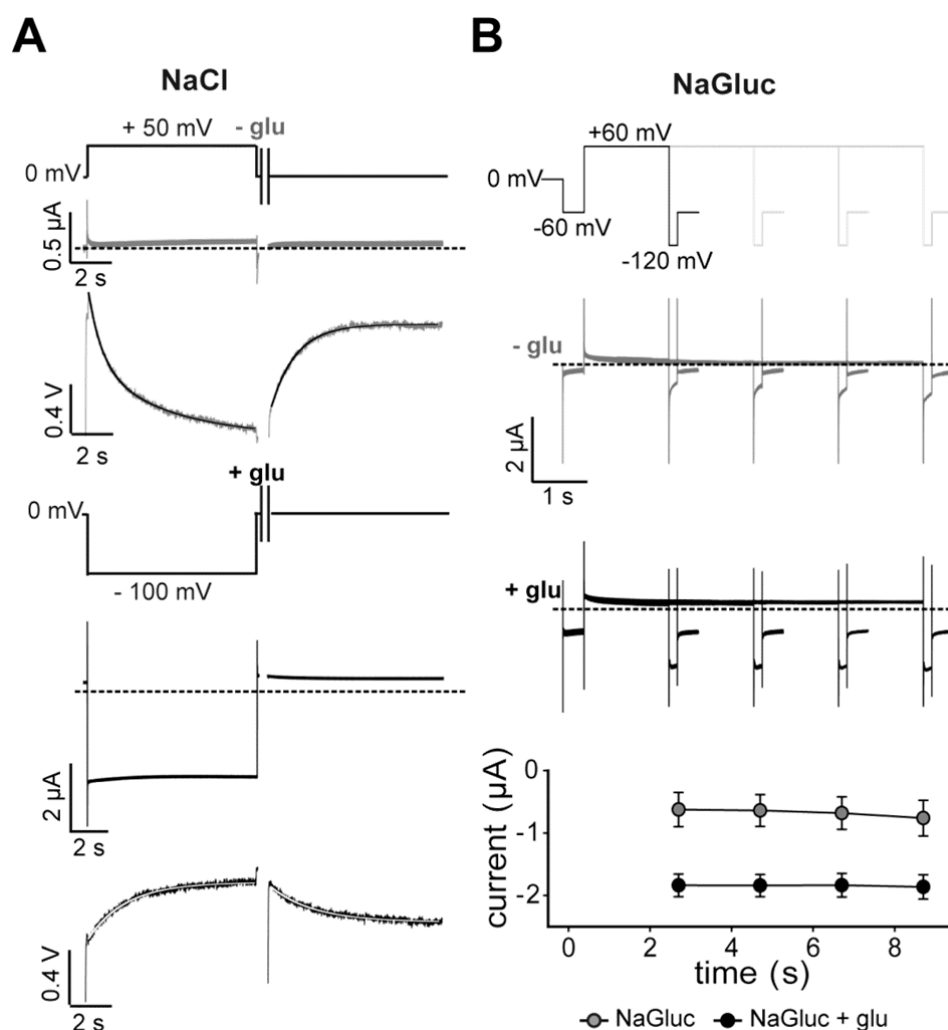


Figure 10.3: Slow conformational changes in EAAT3.

A, representative current and fluorescence traces recorded from *X. laevis* oocytes expressing M205C EAAT3 in response to long voltage steps to +50 mV in the absence of glutamate (*light grey, top*) or to -100 mV in the presence of glutamate (*black, bottom*) and the recovery back to the holding potential of 0 mV. B, current responses to voltage steps to +60 mV of increasing durations followed by fixed test steps to -120 mV in the absence of glutamate (*light grey, top*) and in the presence of glutamate (*black, middle*). Averaged current amplitudes (*bottom*) are given as means \pm S.E.; $n = 4$. glu, glutamate; NaGluc, sodium gluconate.

These fluorescence changes are too slow to represent transitions within the uptake cycle. However, we did not observe slow fluorescence changes in the absence of transport substrates or in the presence of DL-threo-benzyloxyaspartate (Suppl. Figure 10.9), suggesting that the slow fluorescence signal also reflects conformational changes coupled to the uptake cycle. A possible explanation might be a conformational change occurring from certain states of the uptake cycle. Such a kinetic scheme predicts that occupation of this novel state will prevent progress of the uptake cycle and thus result in concomitant slow alterations of transport rates. We tested for slow voltage-dependent changes of glutamate transport rates by studying glutamate uptake currents after prepulses to positive voltages. These experiments were performed in external gluconate after incubation of oocytes in Cl⁻-free solution (13). For various pulse protocols, we did not observe any time- or voltage-dependent changes in transport current amplitudes (Figure 10.3B). These data indicate that slow fluorescence changes cannot be represented as transitions branching from the uptake cycle.

10.4.3 D83A modifies EAAT3 glutamate transport, anion currents and fluorescence amplitudes

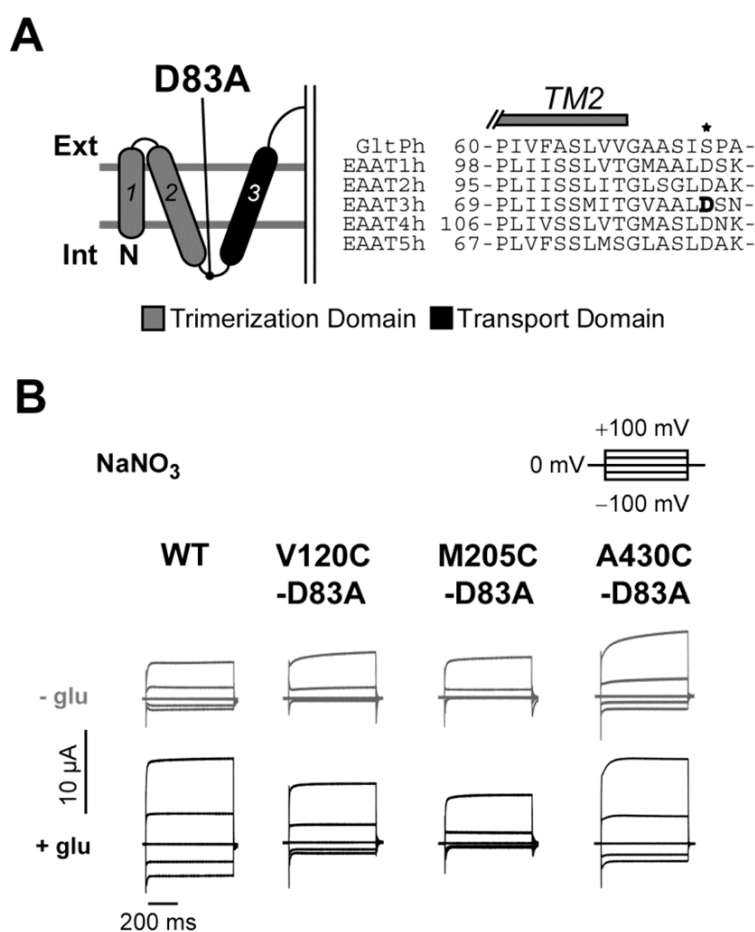
We next inserted the D83A mutation into each cysteine-substituted EAAT3 construct and studied the functional effects of this mutation using voltage clamp analysis. D83 is localized between TM2 and TM3 and is highly conserved among mammalian EAATs (Figure 10.4A). Because homologous mutations in EAAT1 (20) and EAAT4 (19) alter glutamate transport and anion conduction, D83A might allow insights into how conformational changes underlying coupled transport open and close the anion channel.

At positive membrane potentials in the absence of glutamate, D83A EAAT3 currents were statistically larger than WT or cysteine-substituted EAAT3 currents (Figure 10.4B and C) (WT ($3.7 \pm 0.2 \mu\text{A}$) compared to V120C-D83A ($7.7 \pm 0.3 \mu\text{A}$): $p < 0.001$, compared to M205C-D83A ($6.1 \pm 0.5 \mu\text{A}$): $p = 0.006$, and compared to A430C-D83A ($9.5 \pm 0.5 \mu\text{A}$): $p < 0.001$; $n > 10$). The glutamate-induced current increase was less pronounced in D83A EAAT3 than in WT EAAT3 (Figure 10.4C, *top*). This is due to virtually glutamate-independent anion current amplitudes (Figure 10.4C, *middle*).

Moreover, D83A reduced uptake current amplitudes to values between 30% and 50% for all reporter mutations (Figure 10.4C, *bottom*).

Voltage clamp fluorometry revealed D83A-induced changes in the voltage and substrate sensitivity of the fluorescence signals for each fluorophore attachment site (Figure 10.5). V120C-D83A and A430C-D83A EAAT3 fluorescence signals increased during depolarization and decreased during hyperpolarization (Figure 10.5A and C). However, D83A modified the time course of hyperpolarization-induced fluorescence decreases ($(\tau_{(V120C-D83A, -150mV)} = 18.2 \pm 2.6 \text{ ms}, n = 2; \tau_{(A430C-D83A, -150/+150mV)} = 12.7 \pm 2.6/11.5 \pm 2.8 \text{ ms}, n = 4)$). The voltage dependence of M205C EAAT3 fluorescence was dramatically altered by D83A. Without external glutamate, D83A EAAT3 fluorescence amplitudes displayed minimum levels around +50 mV and increased with depolarization and hyperpolarization to nearly the same intensity as in sodium-free conditions (Figure 10.5B).

Figure 10.4
D83A changes substrate dependence of EAAT3 current amplitudes



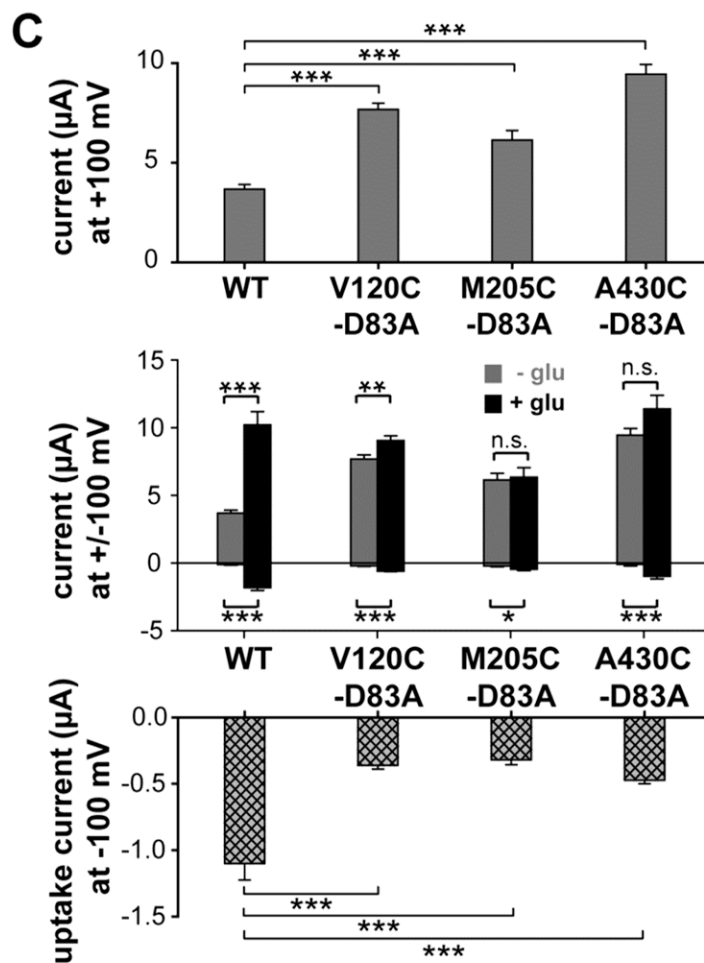


Figure 10.4: D83A changes substrate dependence of EAAT3 current amplitudes.

A, Localization of the mutation D83A in the transmembrane topology model. The trimerization domain is shown in *grey*, the transport domain is shown in *black*. The amino acid sequence alignment of Glt_{ph} and EAAT1-5 shows the TM2-3 region. D83 of EAAT3 is highlighted in *black*. B, representative current traces recorded from *X. laevis* oocytes expressing V120C-, M205C- or A430C-D83A EAAT3. C, averaged absolute current amplitudes at ± 100 mV with and without glutamate (*top*), averaged relative glutamate-induced current increase at +100 mV (*middle*) calculated by division of the current in presence by the current absence of glutamate, and averaged uptake current amplitudes at -100 mV (*bottom*) calculated by the difference of currents in sodium gluconate with and without glutamate from oocytes expressing WT or mutant EAAT3. n.s.: not significant different $p > 0.05$; *, $p \leq 0.05$ **, $p \leq 0.01$; ***, $p \leq 0.001$. Data are given as means \pm S.E.; $n \geq 10$. Int, internal; Ext, external; glu, glutamate.

Figure 10.5

Voltage- and substrate-dependent conformational changes of D83A EAAT3

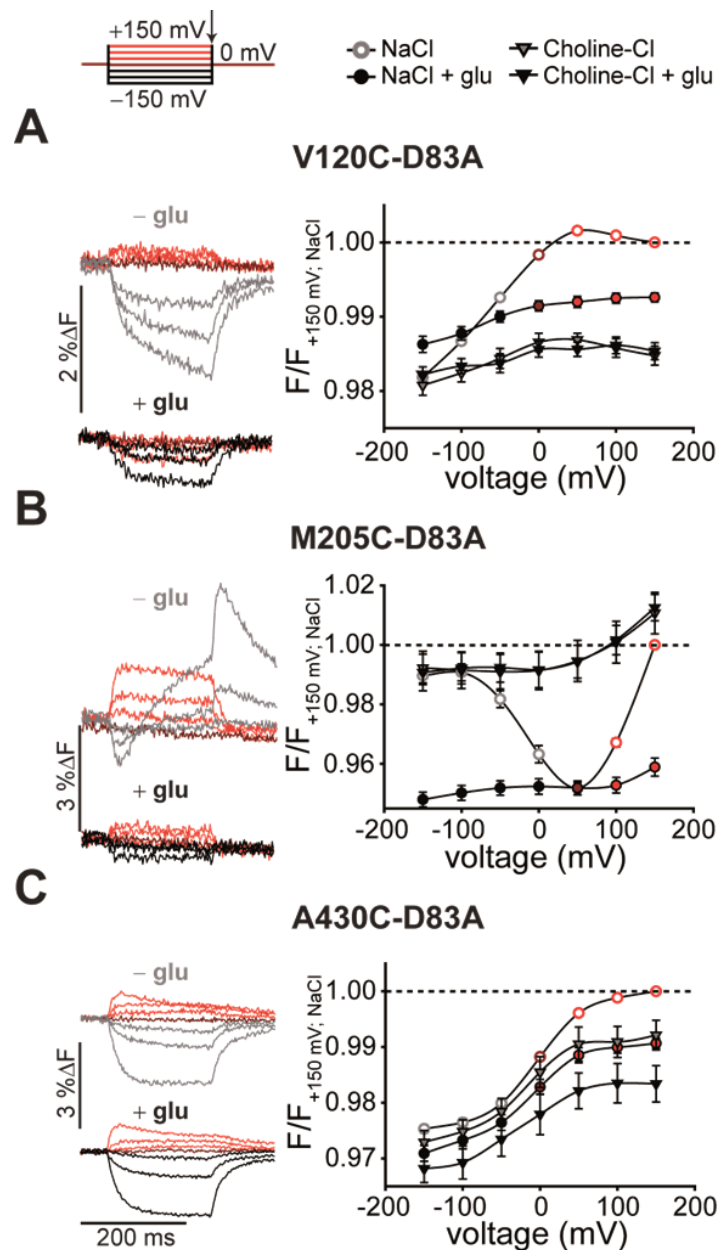


Figure 10.5: Voltage- and substrate-dependent conformational changes of D83A EAAT3.

Representative fluorescence traces (left column) recorded from *X. laevis* oocytes expressing V120C- (A), M205C- (B) and A430C-D83A EAAT3 (C) and averaged voltage dependence of late (arrow) relative fluorescence changes (right column) in the presence of different substrates are shown. Fluorescence signals were measured in NaCl Ringer's solution during 200-ms voltage steps between +150 mV and -150 mV and. Fluorescence amplitudes were normalized to the fluorescence generated at +150 mV in NaCl solution. Measurements in NaCl at voltages above 0 mV are shown in red, 0 mV is shown in dark red, and negative voltages in the absence of 1 mM glutamate are shown in light grey and in the presence of 1 mM glutamate are shown in black. Fluorescence data from at least 6 oocytes are reported as means \pm S.E.. F, fluorescence; glu, glutamate.

Furthermore, the maximum change of fluorescence intensity by applying different membrane potentials was less pronounced than for M205C EAAT3 (5% instead of 10%). Glutamate decreased fluorescence intensity of V120C-D83A and M205C-D83A EAAT3 and modified their voltage dependences (Figure 10.5A and B). Whereas fluorescence signals of V120C-D83A and M205C-D83A EAAT3 require external Na^+ , A430C-D83A EAAT3 voltage-dependent fluorescence changes seemed to be less substrate-dependent (Figure 10.5C). Removal of external permeant anions did not affect the intensity or the voltage dependence of fluorescence signals of D83A EAAT3 (Suppl. Figure 10.10D-F), similar to our results on EAAT3 with an aspartate at position 83.

10.4.4 Kinetic modeling reveals changes in the glutamate uptake cycle in D83A EAAT3

Glutamate transport by EAATs can be described with a kinetic scheme that encompasses subsequent substrate association/dissociation and translocation steps between inward and outward facing conformations (14; 31; 37) (Figure 10.6). Anion channel gating is tightly coupled to these transitions and can be represented by adding branching open anion channel states (19; 38; 39). Because the transport cycle can only proceed from closed channel states (19; 38), opening of EAAT anion channels prevents progression of the uptake cycle. Changes in the distribution between open and closed anion channel states will therefore affect the uptake cycle. D83A could alter EAAT3 function by directly modifying substrate association/dissociation or transporter translocation rates. Alternatively, D83A might modify apparent transitions within the uptake cycle by changing anion channel opening and closing transitions. To distinguish between the two possibilities, sole modification of transitions within the uptake cycle or modification by changed anion channel open probabilities, we modeled voltage-dependent fluorescence data from WT and D83A EAAT3 with a kinetic model that is based on a scheme developed to describe EAAT3 fluorescence data (23).

We modified this model by increasing the number of different fluorescence levels for each fluorescently labeled transporter from three to four. The four fluorescence levels

of our kinetic scheme correspond to four structurally distinct conformations (Figure 10.6).

Figure 10.6
Kinetic model and transport scheme of wildtype and mutant EAAT3

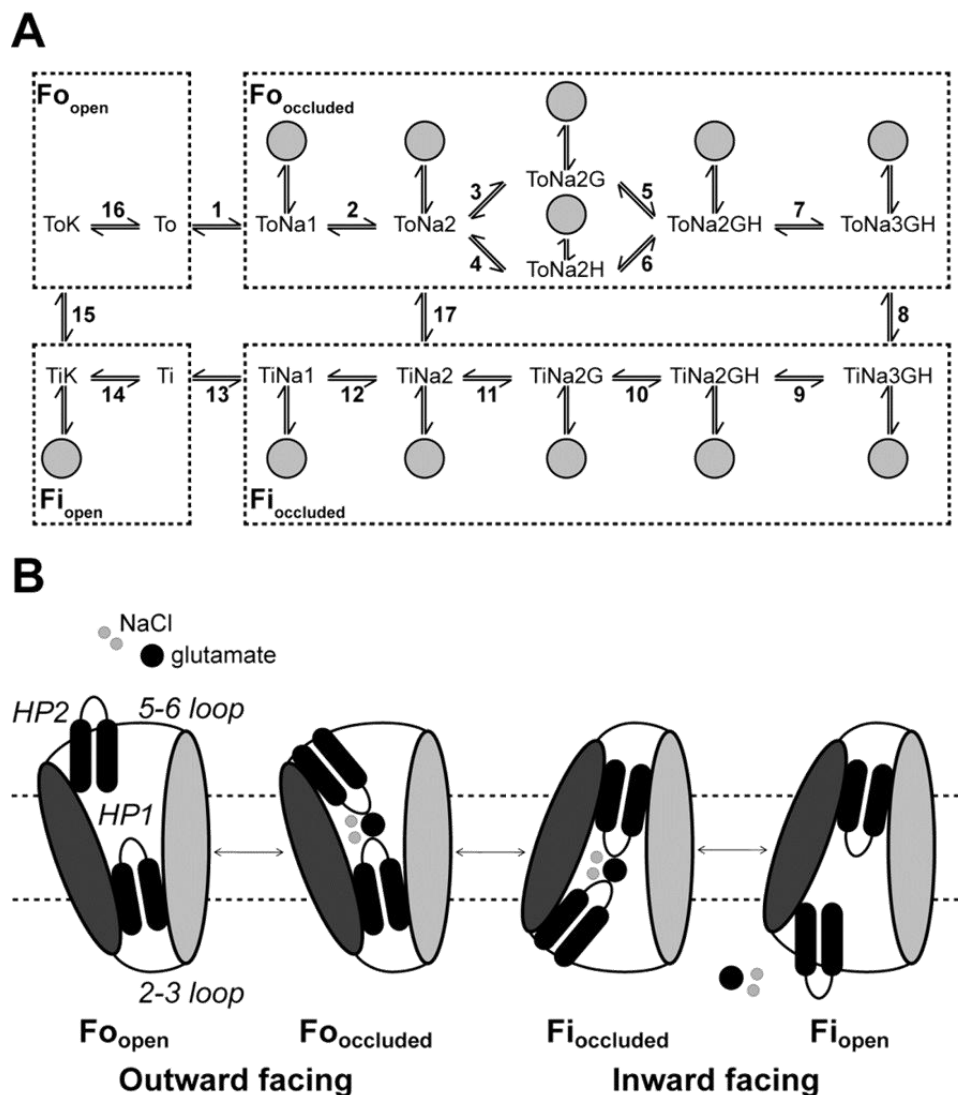


Figure 10.6: Kinetic model and transport scheme of wildtype and mutant EAAT3.

A, modified 15-state model extended by anion channel states branching from state 2-12 and state 14 (grey circles) (16; 28) used to simulate the fluorescence data. B, schematic transport mechanism. Shown is a single protomer. The isomerization between the outward and inward facing occluded states occurs upon movement of the whole transport domain (dark grey) relative to the trimerization domain (light grey). The inward facing open state has not been structurally characterized and is hypothetical. (modified from Reyes *et al.* (34)).

The empty transporter resides in an outward facing state with HP2 open and the substrate binding sites exposed to the extracellular space (F_{o_open} : ToK, To).

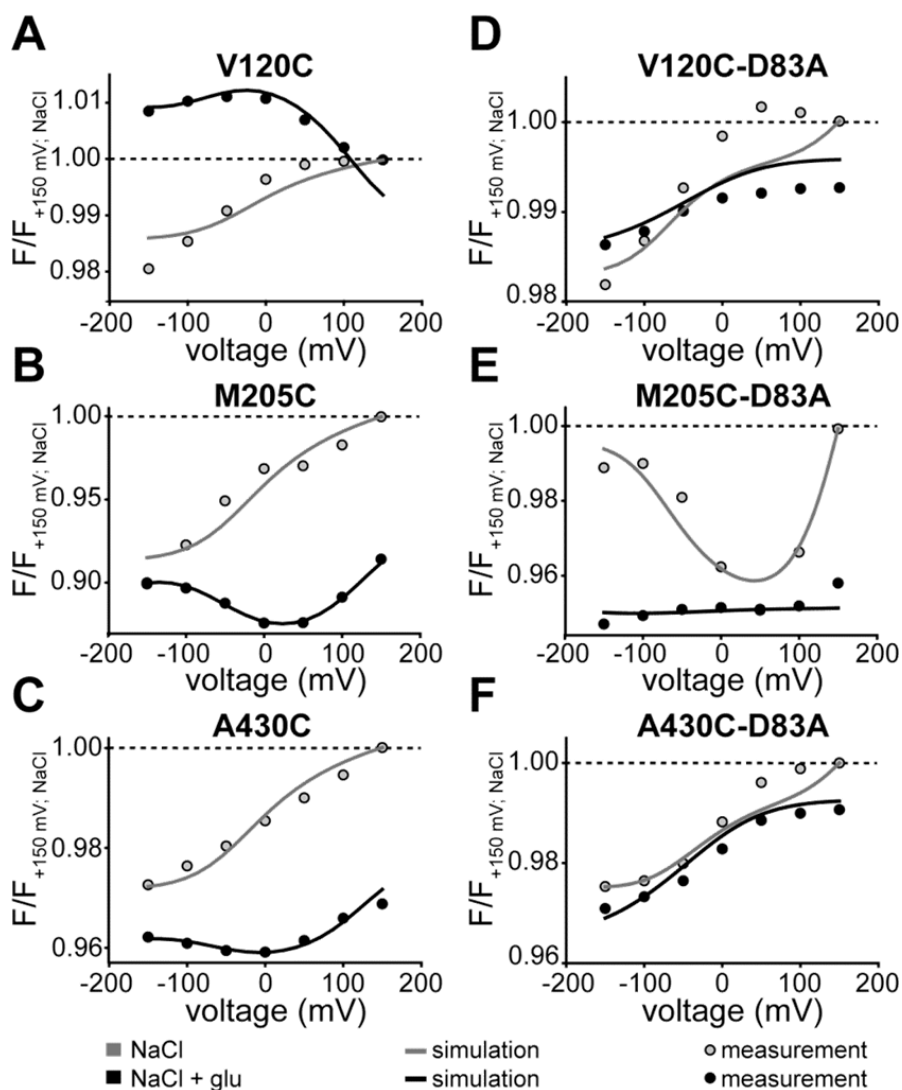
Glutamate uptake is initiated by association of three Na^+ ions, one H^+ and one glutamate. Association of these substrate causes closure of HP2 ($F_{\text{occluded: ToNa1}}$, ToNa2 , ToNa2G , ToNa2H , ToNa2GH , ToNa3GH), and a large piston-like movement of the “translocation domain” results in the inward-facing conformation ($F_{\text{occluded: TiNa3GH}}$, TiNa2GH , TiNa2G , TiNa2 , TiNa1) (26). Opening of HP1 is followed substrate release and exposure of the binding sites to the intracellular solution ($F_{\text{open: Ti}}$, TiK) (23). Retranslocation after association of internal K^+ completes the uptake cycle. The Gating of EAAT anion channels can be represented by adding branching open channel states from the uptake cycle (Figure 10.6A and B) (19; 38). Anion channel opening and closing are assumed to be fast compared with transitions in the uptake cycle, and therefore, we only use probabilities of anion channel opening from a particular state. These state-specific open probabilities are the ratio of the number of transporters in one transporter state with an open anion channel to the number of transporters in this particular state with either open or closed states.

To obtain a kinetic scheme describing fluorescence values, anion currents and uptake currents for WT EAAT3 we used the same rate constants of the uptake cycle as determined in earlier work on cysteine-substituted EAAT3 (23). We determined anion channel open probabilities by fitting the model to the experimentally observed fluorescence of V120C, M205C and A430C EAAT3. The parameters were constrained to correctly describe experimentally determined relative glutamate-induced current amplitudes at +100 mV and to preserve detailed balance (Figure 10.7G). The so-obtained fitting parameters (Table 10.1, 2 and 3) demonstrated a good agreement of the simulated and observed fluorescence-voltage relationship under different substrate conditions (Figure 10.7A-C). However, they predicted a transport rate of about 4 transported glutamate per second at -100 mV (Figure 10.7H), which is lower than in previously published data relating to EAAT1, -2 or -3 (27; 40). We did not succeed in modifying fit parameters in order to increase transport rates. All attempts impaired the compatibility with the experimentally observed voltage dependence of fluorescence. Because unitary transport currents are extremely difficult to measure directly, we accepted this deviation between published and predicted results and only used the relative decrease of glutamate uptake currents by D83A in the optimization procedure.

We then modified the thus established kinetic model to account for the fluorescence signals and transport properties of D83A EAAT3. We initially tested whether

modifying reactions in certain parts of the uptake cycle can qualitatively account for the observed D83A-mediated changes in fluorescence. There were two processes that resulted in such alterations, changes in anion channel open probability or changes in translocation rates. We first optimized all anion channel opening/closing reactions simultaneously against fluorescence intensities for all three reporter mutations combined with D83A. Glutamate-induced increases of anion current amplitudes at +100 mV, relative glutamate uptake currents at -100 mV, and detailed balance were again used as constraints.

Figure 10.7
Simulated voltage- and substrate-dependent conformational changes, open probabilities and transport currents of cysteine-substituted and D83A EAAT3



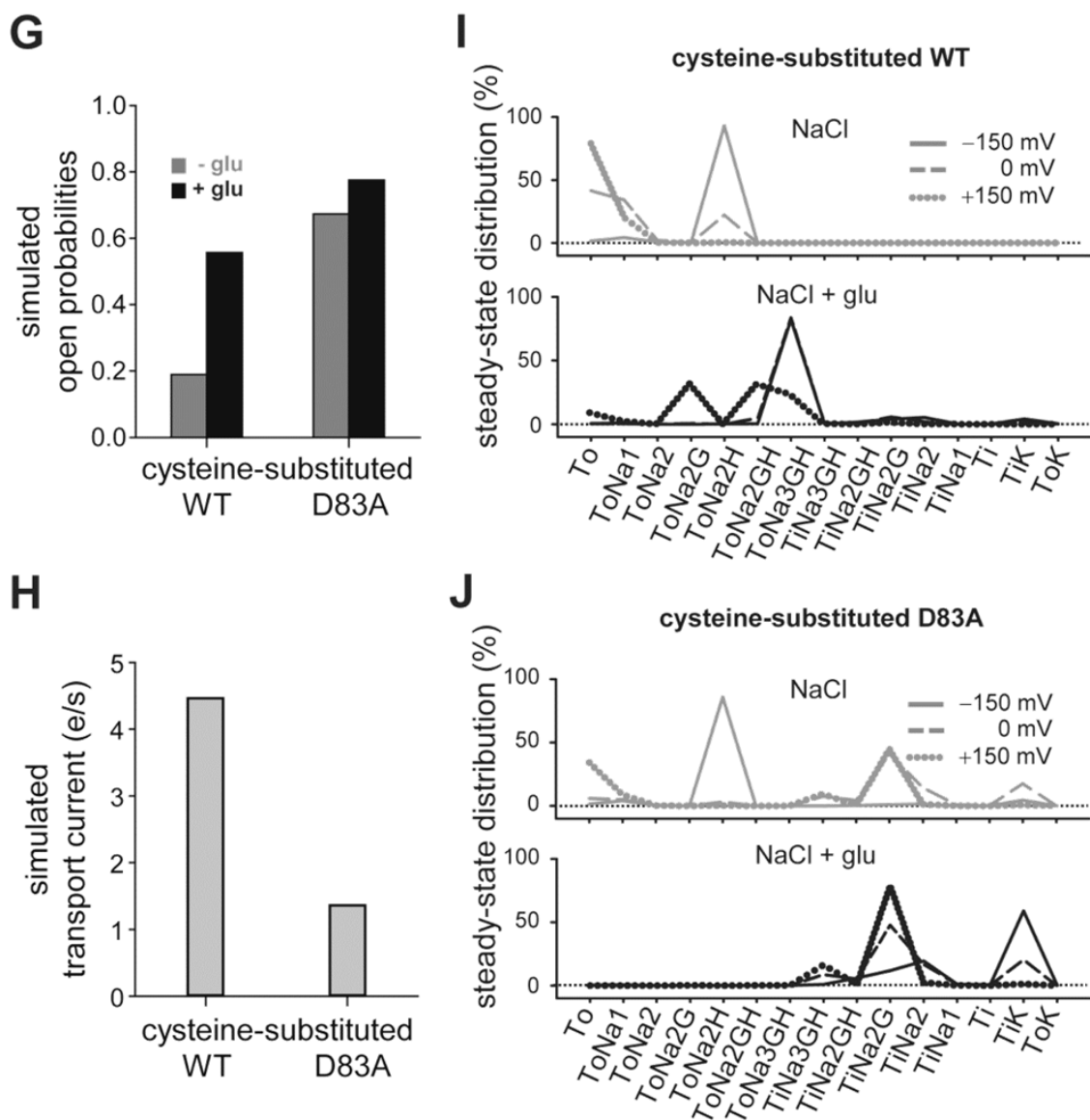


Figure 10.7: Simulated voltage- and substrate-dependent conformational changes, open probabilities and transport currents of cysteine-substituted and D83A EAAT3.

A-F, averaged voltage dependence of measured late fluorescence changes (fluorescence-voltage relationship) (*circles*) and simulated fluorescence changes (*solid lines*) in the absence (*grey*) or in the presence of 1 mM glutamate (*black*). Fluorescence amplitudes were normalized to the fluorescence generated at +150 mV in NaCl solution. G and H, simulated open probabilities (G) at +100 mV of cysteine-substituted WT and D83A EAAT3 without (*grey*) and in the presence of glutamate (*black*) and simulated transport currents (H) at -100 mV from the data given in Table 10.1 and 10.3. I and J, simulated residence probability of cysteine-substituted WT (I) and D83A EAAT3 (J) calculated from the data given in Table 10.1 without (*grey*) and in the presence of glutamate (*black*) for three different voltages, +150 mV (*solid line*), 0 mV (*dashed line*) and +150 mV (*dotted line*). glu, glutamate; F, fluorescence.

During optimization of opening and closing rates of anion channels, global fitting yielded a set of parameters that well reproduced the fluorescence-voltage

relationship of D83A EAAT3 under different ionic conditions. However, these changes always predicted reduction of glutamate transport rates to negligible values. Therefore, we evaluated whether alterations of translocation rates within the uptake cycle can account for D83A fluorescence and function. In these fitting procedures, only the three translocation reactions were adjusted. The fitting procedure revealed altered translocation rates of the K^+ -bound (reaction 15), the Na^+ -bound (reaction 17) and the Na^+ - and glutamate-bound transporter (reaction 8). Whereas inward translocation from ToNa3GH to TiNa3GH was promoted, D83A stimulated the outward translocation for the two other processes (Table 10.1-3). These alterations resulted in predicted fluorescence data that resemble experimental data on D83A EAAT3 (Figure 10.7D-F) (Table 10.1-3).

The kinetic model permits prediction of the steady-state probability that the transporter resides in a given state of the transport cycle. We next calculated the residence probability of each states of the uptake cycle under steady-state conditions for the cysteine-substituted WT (Figure 10.7I) or D83A EAAT3 (Figure 10.7J). In the presence as well as in the absence of glutamate, D83A EAAT3 was predicted to reside with higher likelihood in the inward facing conformation than cysteine-substituted EAAT3.

Table 10.1
Parameters of the EAAT3 model

reaction	forward	backward	z δ	changed parameters for D83A	
				forward	backward
1	$1.00 \cdot 10^{+04} \text{ M}^{-1} \text{ s}^{-1}$	$2.50 \cdot 10^{+03} \text{ s}^{-1}$	0.20		
2	$1.00 \cdot 10^{+04} \text{ M}^{-1} \text{ s}^{-1}$	$2.50 \cdot 10^{+03} \text{ s}^{-1}$	0.20		
3	$6.80 \cdot 10^{+06} \text{ M}^{-1} \text{ s}^{-1}$	$3.00 \cdot 10^{+02} \text{ s}^{-1}$	-0.40		
4	$6.00 \cdot 10^{+11} \text{ M}^{-1} \text{ s}^{-1}$	$7.00 \cdot 10^{+02} \text{ s}^{-1}$			
5	$6.00 \cdot 10^{+11} \text{ M}^{-1} \text{ s}^{-1}$	$7.00 \cdot 10^{+02} \text{ s}^{-1}$	0.40		
6	$6.80 \cdot 10^{+06} \text{ M}^{-1} \text{ s}^{-1}$	$3.00 \cdot 10^{+02} \text{ s}^{-1}$			
7	$1.00 \cdot 10^{+04} \text{ M}^{-1} \text{ s}^{-1}$	$1.00 \cdot 10^{+03} \text{ s}^{-1}$	0.55		
8	$5.50 \cdot 10^{+02} \text{ s}^{-1}$	$5.00 \cdot 10^{+02} \text{ s}^{-1}$		$1.00 \cdot 10^{+05} \text{ s}^{-1}$	6.59 s^{-1}
9	$8.00 \cdot 10^{+02} \text{ s}^{-1}$	$4.00 \cdot 10^{+04} \text{ M}^{-1} \text{ s}^{-1}$	0.45		
10	$6.00 \cdot 10^{+03} \text{ s}^{-1}$	$9.00 \cdot 10^{+10} \text{ M}^{-1} \text{ s}^{-1}$			
11	$3.00 \cdot 10^{+03} \text{ s}^{-1}$	$4.00 \cdot 10^{+05} \text{ M}^{-1} \text{ s}^{-1}$			
12	$5.00 \cdot 10^{+02} \text{ s}^{-1}$	$2.00 \cdot 10^{+05} \text{ M}^{-1} \text{ s}^{-1}$			
13	$4.00 \cdot 10^{+03} \text{ s}^{-1}$	$1.00 \cdot 10^{+06} \text{ M}^{-1} \text{ s}^{-1}$	0.20		
14	$1.00 \cdot 10^{+06} \text{ M}^{-1} \text{ s}^{-1}$	$1.00 \cdot 10^{+03} \text{ s}^{-1}$			
15	50 s^{-1}	5.00 s^{-1}	0.40	131.45 s^{-1}	$1.00 \cdot 10^{+05} \text{ s}^{-1}$
16	$8.00 \cdot 10^{+02} \text{ s}^{-1}$	$1.00 \cdot 10^{+04} \text{ M}^{-1} \text{ s}^{-1}$			
17	0.80 s^{-1}	$1.00 \cdot 10^{-02} \text{ s}^{-1}$		0.11 s^{-1}	19.19 s^{-1}

Table 10.1: Parameters of the EAAT3 model.

Rate constants of the transport process and channel opening/closing at -70 mV are shown. Electrogenic reactions are defined by z δ values, which correspond to the product of the charge and the fraction of the electric field the charge is moved across the membrane. Clockwise transitions in the model scheme are denoted as “forward reactions”.

Table 10.2
Fluorescence intensities used for simulations of cysteine-substituted wildtype and mutant EAAT3 fluorescence voltage relationships

fluorescence state	V120C	M205C	A430C	V120C-D83A	M205C-D83A	A430C-D83A
F _{Oopen}	1.00	1.00	1.00	1.00	1.00	1.00
F _{Ooccluded}	0.98	0.89	0.96	0.97	0.92	0.96
F _{Ioccluded}	1.32	0.29	0.79	0.98	0.88	0.97
F _{Iopen}	0.52	2.44	1.25	0.97	0.88	0.93

Table 10.2: Fluorescence intensities used for simulations of cysteine-substituted wildtype and mutant EAAT3 fluorescence voltage relationships.

Fluorescence intensities of fluorescence states F_{Oopen/occluded} and F_{Iopen/occluded} of cysteine-substituted and D83A EAAT3 used to simulate the overall fluorescence-voltage relationship were normalized to the fluorescence intensity of F_{Oopen}.

Table 10.3
State-specific open probabilities for channel opening from the respective state used in the kinetic modeling of cysteine-substituted wildtype and mutant EAAT3

anion channel state branching from:	open probability
ToNa1	0.722
ToNa2	$9.999 \cdot 10^{-05}$
ToNa2G	$9.999 \cdot 10^{-05}$
ToNa2H	$9.999 \cdot 10^{-05}$
ToNa2GH	$1.321 \cdot 10^{-04}$
ToNa3GH	0.988
TiNa3GH	0.826
TiNa2GH	0.713
TiNa2G	$1.275 \cdot 10^{-04}$
TiNa2	$1.008 \cdot 10^{-04}$
TiNa1	0.765
TiK	$1.357 \cdot 10^{-04}$

Table 10.3: State-specific open probabilities for channel opening from the respective state used in the kinetic modeling of cysteine-substituted wildtype and mutant EAAT3.

10.5 Discussion

Here, we studied the functional consequences of neutralizing a conserved aspartate at position 83 in EAAT3. Homologous mutations have already been studied in EAAT1 and EAAT4 (19; 20) and were reported to result in dramatic alterations of EAAT anion channel opening and closing for both isoforms. Investigating the effects of this point mutation on conformational changes promised insights into the interaction of transporter and anion channel function of EAAT glutamate transporters.

In our experiments transporter proteins were labeled with fluorophores, and fluorescence intensities were measured upon changes in membrane voltages or in substrate concentrations (22; 41). We used three different cysteine substitutions, V120C, M205C and A430C for these experiments. Labeling of cysteine-substituted EAAT3 was specific because the same procedures on oocytes expressing EAAT3 that lack cysteines for fluorophore attachment resulted in background fluorescence levels (Suppl. Figure 10.8 and Suppl. Figure 10.9). For each reporter mutant, voltage steps caused changes in fluorescence amplitudes that were modified by concentrations of transporter substrates, such as Na^+ and glutamate (Figure 10.2).

Moreover, application of DL-threo-benzyloxyaspartate abolished our observed fluorescence changes (Suppl. Figure 10.9). Because DL-threo-benzyloxyaspartate is known to lock EAATs into an outward facing conformation with HP2 open (35) and thus to prevent substrate-binding and subsequent voltage-dependent conformational changes, this result further supports the notion that fluorescence signals arise from conformational changes of the EAAT3 transporter.

Because EAATs are dual function proteins, the observed fluorescence changes might report on transitions within the uptake cycle or on anion channel opening and closing. We found that the voltage and substrate dependence of EAAT3 fluorescence signals can be well described by a kinetic model that is based on the glutamate transport cycle and in which opening and closing transitions of anion channels are voltage-independent (Figure 10.6) (5; 23; 34). Moreover, fluorescence is modified by transport substrates that affect the transport cycle, but do not directly affect the anion channel opening and closing (42). Taken together, these results indicate that the observed fluorescence changes are not directly linked to opening and closing of the anion channel.

Time courses of fluorescence changes are therefore expected to reflect rate constants of transitions between individual states of the uptake cycle. However, we observed different kinetics but very similar voltage dependences of fluorescence changes of M205C and A430C (Figure 10.2B and C). The time dependences of fluorescence amplitudes obviously depend not only on global conformational changes of the EAAT proteins but also on additional region-specific changes of the environment. We therefore did not use the time dependence of fluorescence amplitudes to deduce information about rate constants within the uptake cycle.

For M205C EAAT3, we observed very slow changes in the fluorescence amplitude upon depolarizing voltage steps in the absence of external glutamate and upon membrane hyperpolarization after application of glutamate (Figure 10.3). The time dependence of this process can be well described with a single time constant of around 7 s without glutamate, and around 4 s in the presence of the substrate. Turnover rates of individual EAAT3 have been determined to be well above 10/s (27), and such slow time constants thus indicate a conformational change outside the transport cycle. Because ultraslow fluorescence changes are voltage-dependent (Figure 10.3A) and because glutamate modifies this voltage dependence, one might speculate about the existence of a branching connection from one of the states of the

uptake cycle. After entering such a branching state, the transport cycle is interrupted and can only resume after having left this particular long-lasting state. We tested the existence of such branching connection by measuring time-dependent changes in glutamate transport currents. The existence of long-lasting branching states requires that glutamate transport rates are changed with the same time constant as the fluorescence signal. However, we did not observe any time- or voltage-dependent changes in the glutamate-dependent current, indicating that there are no branching connections from one of the uptake cycle states of the transporter (Figure 10.3). Slow fluorescence changes are thus due to conformational changes that occur in certain states of EAAT3 but do not interfere with the uptake cycle. At present, we can only speculate about the molecular basis and functional consequences of this finding. A possible explanation of these slow processes might be large collective motions as recently reported by Jiang *et al.* (43). An alternative assumption is that these very slow fluorescence changes correspond to a slow gating process within the EAAT anion channel. This gating process has been initially described in EAAT4 where slow changes in the anion to cation selectivity occur upon membrane depolarization. We also observed similar processes for EAAT3 (unpublished observation) and the time and voltage dependence of these gating processes resemble the observed slow changes of the fluorescence signals (17).

Due to the slow changes of fluorescence amplitudes, it was impossible to obtain and to interpret steady-state fluorescence values. We therefore determined fluorescence values at the end of a 200-ms pulse. After this time period, all processes within the uptake cycle will have reached steady-state conditions. Moreover, the additional slow processes that occur outside the uptake cycle and thus should not contribute to the measured fluorescence values will not have caused major alterations of the fluorescence levels.

We recently performed a detailed analysis of the effects of D117A on EAAT4 anion currents (19). Noise analysis demonstrated reduced unitary current amplitudes of D117A EAAT4 anion channels, and reversal potential measurements under bionic conditions indicated altered anion selectivity. These functional alterations supported direct modification of the EAAT4 anion conduction pathway by D117A. We reasoned that D117 is in close proximity to the anion conduction pathway and that D117A alters anion channel open probabilities by directly modifying opening and closing transitions. We optimized rate constants in the kinetic scheme that is closely similar

to the one shown in Figure 10.6 against experimentally determined absolute open probabilities for WT and D117A EAAT4 at different voltages. This procedure revealed that the effect of D117A on EAAT4 gating can be well reproduced by exclusive modification of anion channel open probabilities.

We now studied the effects of the homologous mutation on EAAT3 using voltage clamp fluorometry. The use of EAAT3 permits direct measurements of glutamate uptake currents, and this parameter turned out to be crucial for our interpretation of the effects of D83A. Cysteine-substituted EAAT3 fluorescence, glutamate transport and anion currents can be well represented by a kinetic scheme that is based on a model developed in a recent voltage clamp fluorometry study (23). We optimized this scheme by inserting anion channel states branching from certain states of the glutamate transport cycle. For WT EAAT3, rate constants within the uptake cycle were not modified. The glutamate transport cycle consists of many different steps, and some of them are outside the temporal resolution of our system. Moreover, the kinetic scheme encompasses too many rate constants to be accurately determined in separation. The resulting scheme is in good agreement with all our experimental data on WT. However, there is one published feature of EAAT3 the kinetic model fails to account for. It is not capable to correctly predict the high transport rates of EAAT3 for reverse transport at high external K^+ (44). Since our experiments were performed in the absence of external K^+ , we accepted this limitation of the kinetic scheme.

The effects of D83A on fluorescence and anion current could be explained by modifying anion channel gating. However, these alterations predicted a reduction of the glutamate uptake rates to very low values and are thus in disagreement with experimental data (Figure 10.4). Only by modification of translocation rates in the uptake cycle were we able to accurately describe all existing data, glutamate transport, anion currents, and fluorescence data. Our data thus indicate that D83A modifies translocation rates. These changes in translocation are supported by available crystal structures that place the homologous residue of D83/D117 to the TM2-TM3 loop between the trimerization and the transport domains. By altering the hinge function of this region (19; 34; 45) D83A/D117 might affect the isomerisation between inward and outward facing conformations.

The different outcome of the two studies on EAAT3 and EAAT4 is most likely not due to isoform-specific differences in anion channel function but rather caused by the separate experimental approaches. Anion channel properties are very well conserved

between EAAT3 and EAAT4 with closely similar unitary conductance, selectivity and open probabilities (33). EAAT4 differs from EAAT3 in very low glutamate transport rates (27). Changes in translocation processes might have less influence on anion channel gating in EAAT4 than in EAAT3. D83A is thus expected to exert effects on EAAT3 anion channels similar to those of D117A on EAAT4 anion channels. We conclude that D83A/D117A modifies substrate translocation and anion channel opening as well as anion conduction by EAAT3/EAAT4.

At present, the molecular basis of anion conduction in EAAT glutamate transporters is insufficiently understood. So far, only one point mutation, D117A, has been shown to modify unitary anion conduction rates in the outward (35) as well as in the inward facing conformation (34). S74, the Glt_{Ph} residue homologous to D83/D117, projects into surrounding lipids rather than into possible conduction pathways. Moreover, D117A reduces unitary current amplitudes of EAAT4 anion channels by removing a negative charge. These two findings argue against a direct effect of D83A/D117A on anion conduction. A possible scenario that accounts for the effects of D83A on substrate translocation in EAAT3 and of D117A on anion conduction in EAAT4 is that anion channel formation is closely related to translocation. One might speculate that the anion pore opens upon moving the translocation domain between outward to inward facing conformations. Indeed, a recently reported high resolution structure of an intermediate conformation of Glt_{Ph} revealed an aqueous conduction pathway that might permit permeation of anions (32). By altering the translocation trajectory, D83A/D117A could not only affect substrate translocation and anion channel opening/closing, but also the anion conduction pathway itself.

10.6 Acknowledgments

We would like to thank Dr. M. Hediger for providing the expression construct for *hEAAT3*. We appreciate helpful discussions with Drs. Alexi Alekov, David Ewers, Peter Kovermann, Gabriel Stölting and Nicole Schneider.

10.7 Reference List

1. Zerangue, N. and Kavanaugh, M. P. (1996) *Nature* **383**, 634-637
2. Levy, L. M., Warr, O., and Attwell, D. (1998) *J Neurosci* **18**, 9620-9628
3. Danbolt, N. C. (2001) *Progress in Neurobiology* **65**, 1-105
4. Kanner, B. I. (2006) *J Membr. Biol.* **213**, 89-100
5. Grewer, C., Gameiro, A., Zhang, Z., Tao, Z., Braams, S., and Rauen, T. (2008) *IUBMB. Life* **60**, 609-619
6. Tanaka, K., Watase, K., Manabe, T., Yamada, K., Watanabe, M., Takahashi, K., Iwama, H., Nishikawa, T., Ichihara, N., Kikuchi, T., Okuyama, S., Kawashima, N., Hori, S., Takimoto, M., and Wada, K. (1997) *Science* **276**, 1699-1702
7. Watase, K., Hashimoto, K., Kano, M., Yamada, K., Watanabe, M., Inoue, Y., Okuyama, S., Sakagawa, T., Ogawa, S., Kawashima, N., Hori, S., Takimoto, M., Wada, K., and Tanaka, K. (1998) *European Journal of Neuroscience* **10**, 976-988
8. Peghini, P., Janzen, J., and Stoffel, W. (1997) *EMBO J* **16**, 3822-3832
9. Aoyama, K., Suh, S. W., Hamby, A. M., Liu, J., Chan, W. Y., Chen, Y., and Swanson, R. A. (2006) *Nat. Neurosci.* **9**, 119-126
10. Huang, Y. H., Dykes-Hoberg, M., Tanaka, K., Rothstein, J. D., and Bergles, D. E. (2004) *J. Neurosci.* **24**, 103-111
11. Bailey, C. G., Ryan, R. M., Thoeng, A. D., Ng, C., King, K., Vanslambrouck, J. M., Auray-Blais, C., Vandenberg, R. J., Broer, S., and Rasko, J. E. (11 A.D.) *J. Clin. Invest.* **121**, 446-453
12. Fairman, W. A., Vandenberg, R. J., Arriza, J. L., Kavanaugh, M. P., and Amara, S. G. (1995) *Nature* **375**, 599-603
13. Wadiche, J. I., Amara, S. G., and Kavanaugh, M. P. (1995) *Neuron* **15**, 721-728
14. Grewer, C., Watzke, N., Wiessner, M., and Rauen, T. (2000) *Proc. Natl. Acad. Sci. USA* **97**, 9706-9711

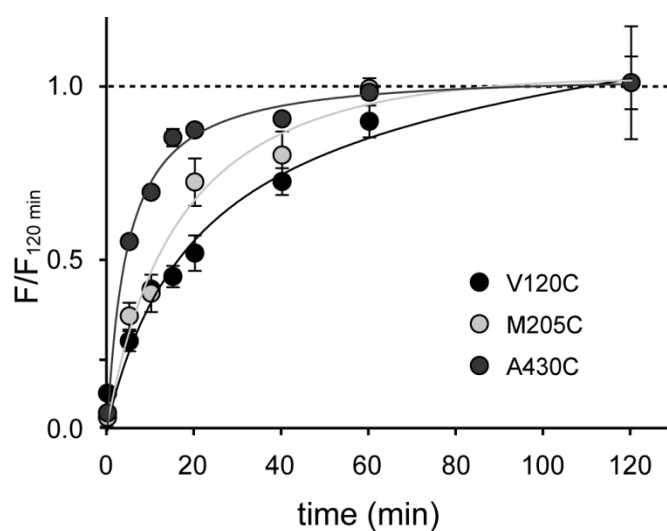
15. Melzer, N., Biela, A., and Fahlke, Ch. (2003) *J. Biol. Chem.* **278**, 50112-50119
16. Fairman, W. A. and Amara, S. G. (1999) *Am. J. Physiol* **277**, F481-F486
17. Melzer, N., Torres-Salazar, D., and Fahlke, C. (2005) *Proc. Natl. Acad. Sci. USA*, **102**, 19214-19218
18. Vandenberg, R. J., Huang, S., and Ryan, R. M. (2008) *Channels (Austin.)* **2**, 51-58
19. Kovermann, P., Machtens, J. P., Ewers, D., and Fahlke, C. (2010) *J. Biol. Chem.* **285**, 23676-23686
20. Ryan, R. M., Mitrovic, A. D., and Vandenberg, R. J. (2004) *J. Biol. Chem.* **279**, 20742-20751
21. Mannuzzu, L. M., Moronne, M. M., and Isacoff, E. Y. (1996) *Science* **271**, 213-216
22. Cha, A. and Bezanilla, F. (1997) *Neuron* **19**, 1127-1140
23. Larsson, H. P., Tzingounis, A. V., Koch, H. P., and Kavanaugh, M. P. (2004) *Proc. Natl. Acad. Sci. USA*, **101**, 3951-3956
24. Koch, H. P. and Larsson, H. P. (2005) *J. Neurosci.* **25**, 1730-1736
25. Koch, H. P., Hubbard, J. M., and Larsson, H. P. (2007) *J. Biol. Chem.* **282**, 24547-24553
26. Larsson, H. P., Wang, X., Lev, B., Bacongus, I., Caplan, D. A., Vyleta, N. P., Koch, H. P., ez-Sampedro, A., and Noskov, S. Y. (2010) *Proc. Natl. Acad. Sci. USA*, **107**, 13912-13917
27. Mim, C., Balani, P., Rauen, T., and Grewer, C. (2005) *J. Gen. Physiol.* **126**, 571-589
28. Lorenz, C., Pusch, M., and Jentsch, T. J. (1996) *Proc. Natl. Acad. Sci. USA* **93**, 13362-13366
29. Trotti, D., Rolfs, A., Danbolt, N. C., Brown, R. H., Jr., and Hediger, M. A. (1999) *Nature Neuroscience* **2**, 427-433
30. Torres-Salazar, D. and Fahlke, C. (2006) *J. Neurosci.* **26**, 7513-7522
31. Bergles, D. E., Tzingounis, A. V., and Jahr, C. E. (2002) *J. Neurosci.* **22**,

10153-10162

32. Verdon, G. and Boudker, O. (2012) *Nat. Struct. Mol. Biol.* **19**, 355-357
33. Torres-Salazar, D. and Fahlke, C. (2007) *J. Biol. Chem.* **282**, 34719-34726
34. Reyes, N., Ginter, C., and Boudker, O. (2009) *Nature* **462**, 880-885
35. Boudker, O., Ryan, R. M., Yernool, D., Shimamoto, K., and Gouaux, E. (2007) *Nature* **445**, 387-393
36. Shimamoto, K., Lebrun, B., Yasuda-Kamatani, Y., Sakaitani, M., Shigeri, Y., Yumoto, N., and Nakajima, T. (1998) *Mol. Pharmacol.* **53**, 195-201
37. Kanner, B. I. and Bendahan, A. (1982) *Biochemistry* **21**, 6327-6330
38. Machtens, J. P., Fahlke, C., and Kovermann, P. (2011) *Channels (Austin.)* **5**, 468-472
39. Leinenweber, A., Machtens, J. P., Begemann, B., and Fahlke, C. (2011) *J. Biol. Chem.* **286**, 1927-1937
40. Wadiche, J. I. and Kavanaugh, M. P. (1998) *J. Neurosci.* **18**, 7650-7661
41. Gandhi, C. S. and Olcese, R. (2008) *Methods Mol. Biol.* **491**, 213-231
42. Machtens, J. P., Kovermann, P., and Fahlke, C. (2011) *J. Biol. Chem.* **286**, 23780-23788
43. Jiang, J., Shrivastava, I. H., Watts, S. D., Bahar, I., and Amara, S. G. (2011) *Proc. Natl. Acad. Sci. USA*, **108**, 15141-15146
44. Zhang, Z., Tao, Z., Gameiro, A., Barcelona, S., Braams, S., Rauen, T., and Grewer, C. (2007) *Proc. Natl. Acad. Sci. USA*, **104**, 18025-18030
45. Yernool, D., Boudker, O., Jin, Y., and Gouaux, E. (2004) *Nature* **431**, 811-818

10.8 Supplemental Figures

Suppl. Figure 10.8
Time course of fluorescence labeling of cysteine-substituted EAAT3

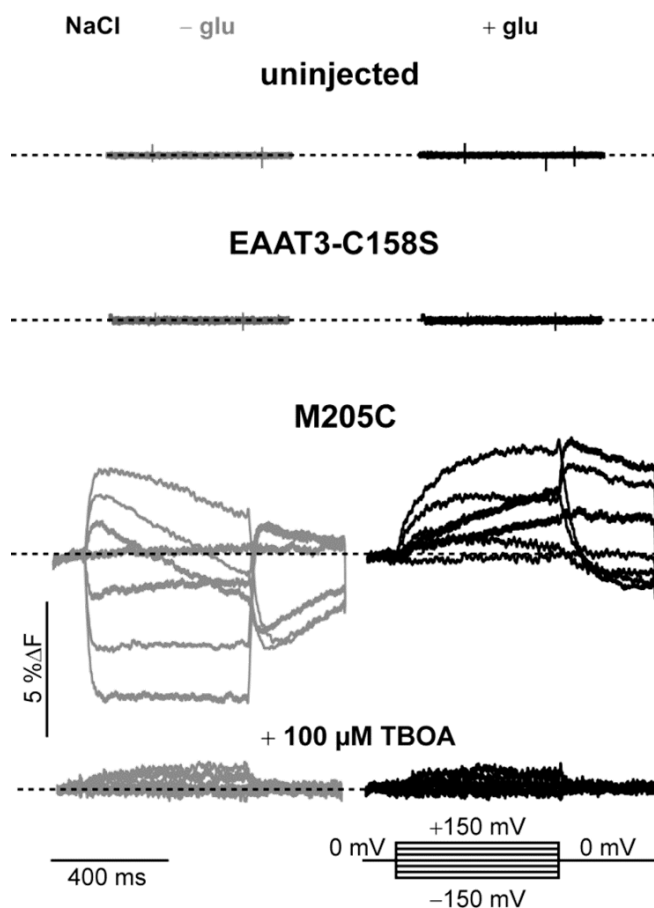


Suppl. Figure 10.8: Time course of fluorescence labeling of cysteine-substituted EAAT3.

Averaged time-dependent fluorescence change of *Xenopus laevis* oocytes expressing V120C, M205C or A430C EAAT3 from at least 5 oocytes is reported as means \pm S.E..

Suppl. Figure 10.9

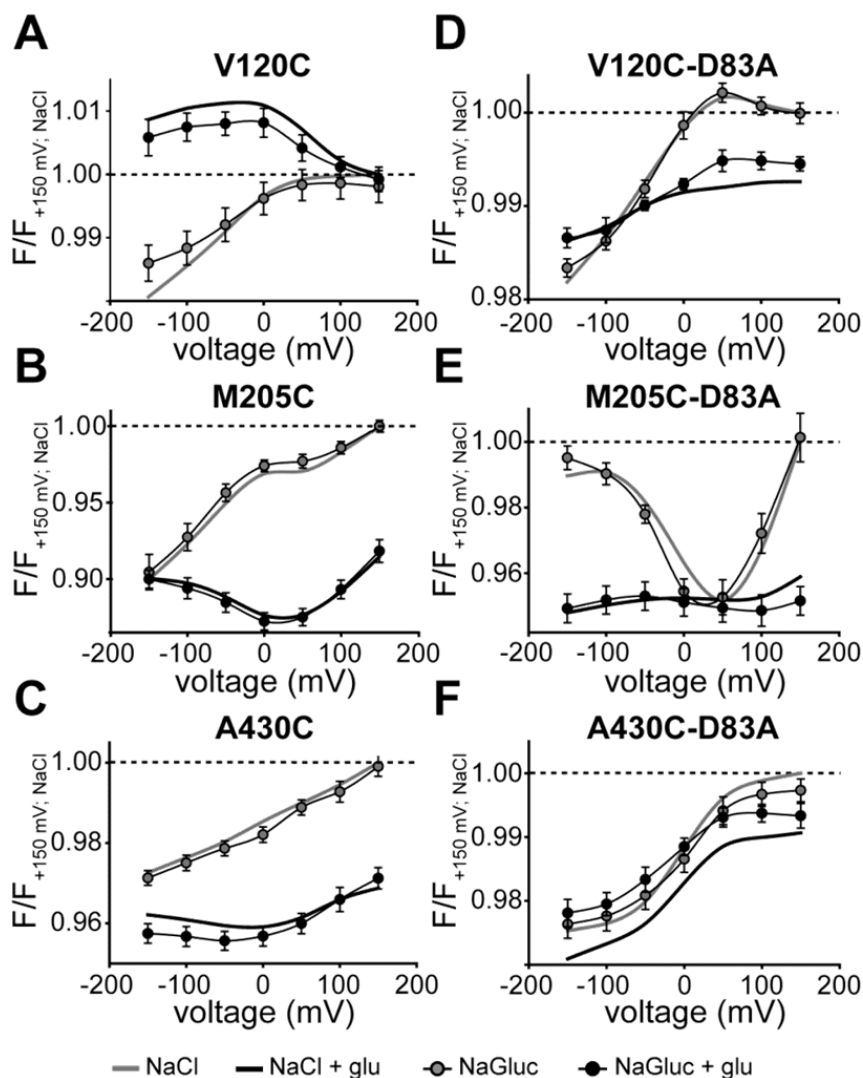
Voltage-dependent conformational changes are due to EAAT3 and are blocked by TBOA



Suppl. Figure 10.9: Voltage-dependent conformational changes are due to EAAT3 and are blocked by TBOA.

Representative fluorescence traces recorded from *Xenopus laevis* oocytes, either uninjected or expressing C158S, and M205C EAAT3. Fluorescence recordings were generated by 0.3 – 0.6 s voltage steps between +150 mV and -150 mV and measured in NaCl Ringer's solution in the absence of 1 mM glutamate (*grey*) or in the presence of 1 mM glutamate (*black*). The block by application of 100 μM TBOA was the same oocyte as shown above.

Suppl. Figure 10.10
Anion independence of cysteine-substituted WT and D83A EAAT3



Suppl. Figure 10.10: Anion independence of cysteine-substituted WT and D83A EAAT3.

Averaged voltage dependence of late relative fluorescence changes of cysteine-substituted WT (A-C) and D83A EAAT3 (D-F) in the presence of different substrates. Fluorescence signals were measured during 200 ms voltage steps between +150 mV and -150 mV. Fluorescence amplitudes are normalized to the fluorescence measured at +150 mV in NaCl solution. Measurements were done either in NaCl (*solid lines*) or in anion-substituted NaGluconate solution (*circles*) in the absence of 1 mM glutamate (*grey*) or in the presence of 1 mM glutamate (*black*). Fluorescence data from at least 6 oocytes are reported as means \pm S.E..

11 A mutation causing Episodic Ataxia modifies sodium association to EAAT glutamate transporters

Jasmin Hotzy¹, Nicole Schneider^{1,2}, Peter Kovermann¹ and Christoph Fahlke^{1,2}

¹Institut für Neurophysiologie, Medizinische Hochschule Hannover, Germany and

²Zentrum für Systemische Neurowissenschaften Hannover (ZSN), Germany.

Correspondence should be addressed to Ch.F. (fahlke.christoph@mh-hannover.de)

11.1 Abstract

The episodic ataxias (EA) are inherited human syndromes characterized by paroxysmal cerebellar incoordination. One type, episodic ataxia type 6, is associated with mutations in *SLC1A3* - the gene encoding the glial glutamate transporter *hEAAT1*. We here use voltage clamp fluorometry to functionally evaluate one EA6-associated mutation that predicts the substitution of a conserved proline in the hinge of transmembrane domain 5 (TM5) by arginine, P290R. Since P290R *hEAAT1* did not express at sufficient levels to permit fluorescence measurements, we studied the homologous mutation P259R in another EAAT transporter, *hEAAT3*. P259R inverts the voltage dependence, changes the sodium dependence and drastically decelerates the kinetics of EAAT3 fluorescence signals. Analysis of these results and kinetic modelling defined altered sodium-binding to mutant transporters as molecular basis of reduced glutamate uptake and increased anion conduction of EAAT transporters in episodic ataxia type 6.

11.2 Introduction

Episodic ataxia (EA) is a rare autosomal dominant human disease characterized by imbalance and paroxysmal cerebellar incoordination associated with additional other neurological symptoms. There are six episodic ataxia syndromes with distinct clinical features and underlying genetic origins¹. Episodic ataxia type 6 differs from other forms of episodic ataxia in long duration of attacks, epilepsy and absent myokymia, nystagm, and tinnitus¹. It is caused by mutations in *SLC1A3*, the gene encoding EAAT1, the major glutamate transporter in cerebellar Bergmann glia^{2, 3}. So far, two disease-associated mutations have been reported, and one of them predicts a substitution of a highly conserved proline by arginine at position 290 in EAAT1². P290R reduces EAAT1 expression levels and surface membrane insertion² and also modifies transport functions of EAAT1⁴.

EAATs are secondary-active glutamate transporter, coupling glutamate transport to the co-transport of three sodium ions, one proton and to the countertransport of one potassium ion. The effective glutamate transport by EAATs ensures tightly regulated synaptic communication and is the basis of low extracellular glutamate concentrations in the synaptic cleft that are necessary to prevent glutamate

excitotoxicity. Furthermore, EAATs mediate a glutamate-activated anion flux which is thought to be conducted through an anion pathway transiently generated during conformational changes coupled to glutamate transport⁵⁻⁸. EAAT anion currents have been suggested to regulate neuronal excitability, but so far, the physiological importance of this transport function is not sufficiently understood. P290R was shown to exert distinct effects on both EAAT functions. It diminishes individual glutamate transport rates and increases EAAT1-associated anion currents⁴.

We here employed “voltage clamp fluorometry” (VCF) to define which particular steps in the transport cycle are affected by this disease-associated mutation. Voltage clamp fluorometry combines current recordings with fluorescence measurements under voltage clamp and permits insights into the substrate and voltage dependences of various conformational changes underlying EAAT function. Using the related isoform EAAT3⁹⁻¹³, we demonstrate that alteration of Na⁺-association and dissociation prior to glutamate-binding to the outward facing transporter and to the inward facing transporter represents the molecular basis of transporter dysfunction in episodic ataxia type 6.

11.3 Results

11.4 P259R EAAT3 is a reliable model to study transport dysfunction of P290R EAAT1

To permit cysteine-specific fluorescence labeling for subsequent fluorescence analysis we inserted the mutation V238C into WT and P290R *hEAAT1* and expressed both constructs in *Xenopus* oocytes. V238C *hEAAT1* is homologous to M205C *hEAAT3* (Figure 11.1A), a reporter mutation that results in prominent changes of fluorescence amplitudes with substrate concentration and voltage when labeled with the cysteine-specific dye AlexaFluor546^{11, 13}. Unfortunately, oocytes expressing V238C-P290R *hEAAT1* did not show fluorescence signals of sufficient amplitude to permit quantitative analysis. The low fluorescence amplitude levels of V238C-P290R *hEAAT1* are consistent with earlier reports that P290R reduces the

surface density of *hEAAT1*^{2, 4}. Since P290 is highly conserved within the whole EAAT family, we studied the functional effects of the disease-associated mutation in the related glutamate transporter EAAT3. EAAT3 expresses robustly in oocytes¹⁴ and has already been successfully analyzed using voltage clamp fluorometry^{9, 12, 13}. We initially tested the suitability of P259R *hEAAT3* as model for P290R *hEAAT1* by measuring P259R *hEAAT3* glutamate transport and anion currents after expression in *Xenopus* oocytes or in mammalian cells and comparing the results to those on P290R *hEAAT1*.

To quantify WT and mutant *hEAAT1/3* glutamate transport oocytes expressing WT, M205C, or M205C-P259R *hEAAT3* and WT or P290R *hEAAT1* were incubated in Cl⁻-free medium, and differences in current amplitudes before and after glutamate application were measured (Figure 11.1B and Suppl. Figure 11.5B). The thus determined current amplitudes reveal comparably reduced uptake currents for P259R *hEAAT3* (WT: $I_{\text{uptake}} = -1.17 \pm 0.14 \mu\text{A}$; M205C: $I_{\text{uptake}} = -1.07 \pm 0.13 \mu\text{A}$; M205C-P259R: $I_{\text{uptake}} = -0.18 \pm 0.04 \mu\text{A}$; $n \geq 13$; $p_{\text{WT:P259R}} \leq 0.001$) as well as for P290R *hEAAT1* (WT: $I_{\text{uptake}} = -0.75 \pm 0.07 \mu\text{A}$; P290R: $I_{\text{uptake}} = -0.11 \pm 0.03 \mu\text{A}$; $n \geq 8$; $p_{\text{WT:P290R}} \leq 0.001$) (Suppl. Figure 11.5B). Lyotropic anions such as NO₃⁻ or SCN⁻ greatly increase EAAT anion currents and permit observation of these current components without significant contaminations with glutamate uptake currents^{8, 15}. However, oocytes expressing P259R *hEAAT3* mediated large anion currents that are neither TBOA nor Na⁺-dependent and thus represent endogenous anion currents. We therefore studied the effect of P259R on *hEAAT3* anion currents through whole-cell patch clamp measurements in transfected mammalian cells (Figure 11.1C and D). In these experiments, cells were internally dialyzed with high [K⁺] to permit all physiologically occurring transitions in the glutamate uptake cycle⁵. In the absence as well as in the presence of glutamate, cells expressing P259R *hEAAT3* display significantly larger current amplitudes in the negative voltage range when compared to WT. P259R did not only modify EAAT3 anion current amplitudes, but also the voltage and time dependence of these currents. Upon hyperpolarizing voltage steps P259R *hEAAT3* currents display time-dependent increases that are more pronounced in the presence of glutamate than in its absence. The novel gating results in inwardly rectifying currents associated with mutant *hEAAT3*.

Figure 11.1
P259R changes EAAT1- and EAAT3-associated anion- and uptake currents

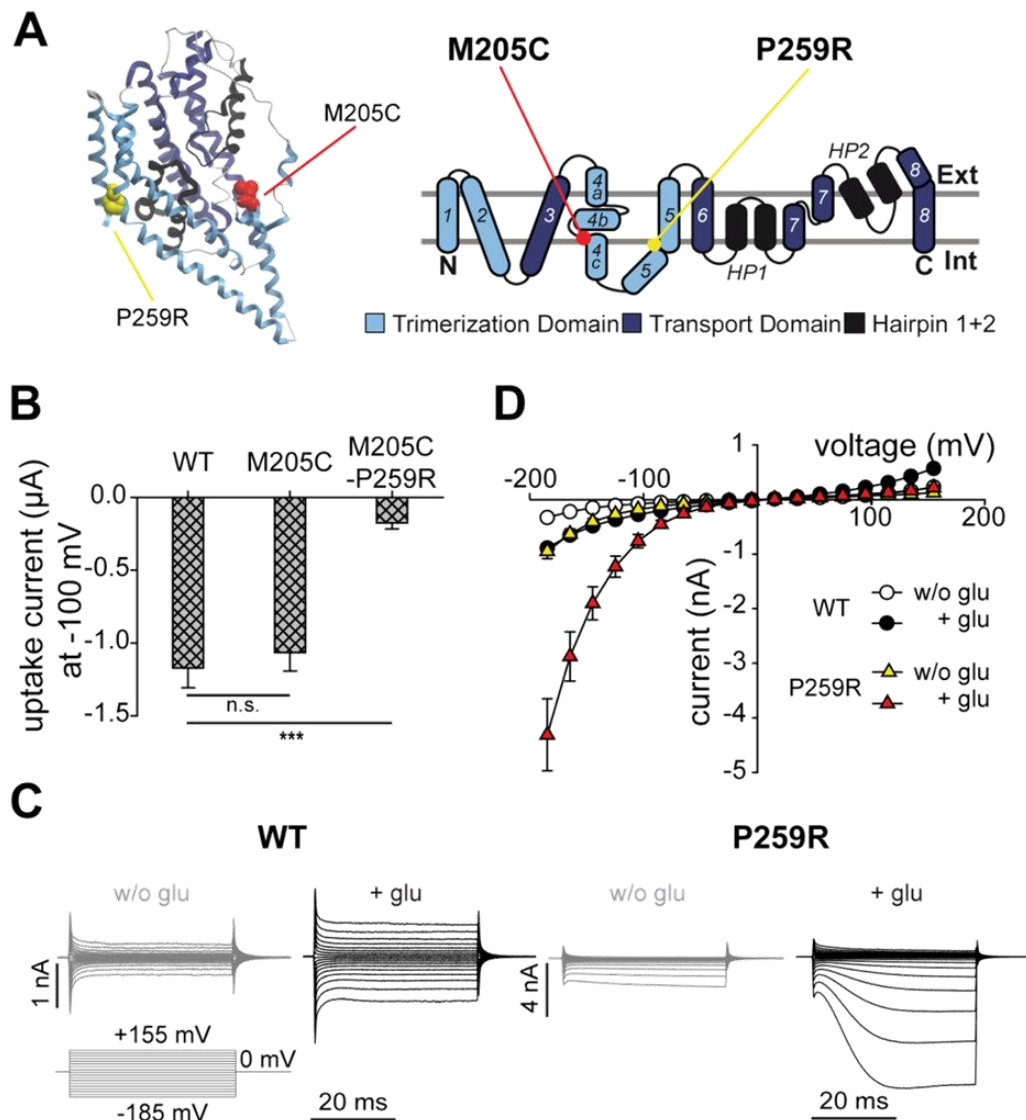


Figure 11.1: P259R changes EAAT1- and EAAT3-associated anion- and uptake currents.

A, Localization of M205C and P259R on the transmembrane topology model of EAAT3 and on the monomeric structure shown in a ribbon representation viewed in the plane of the membrane. B, averaged glutamate uptake currents at -100 mV of oocytes expressing WT, M205C- or M205C-P259R EAAT3. Uptake currents were calculated as difference of current amplitudes with and without glutamate measured in a chloride-free solution. Student's t-test and paired t-test with $p \leq 0.05$ (*) as the level of significance were used ($p \leq 0.01$ (**), $p \leq 0.001$ (***)). The data are given as the means \pm S.E.; $n \geq 13$. C, representative current recordings from tsA201 cells expressing WT or P259R EAAT3 with standard KNO₃-based internal solution and a NaNO₃-based external solution before (light grey) and after application of 1mM glutamate (black) and the corresponding I-V plot (D) with WT-data (circles), either in the absence (white) or in the presence of glutamate (black) and P259R EAAT3 data (triangles), either in the absence (yellow) or in the presence of glutamate (red); $n \geq 4$.

Under similar experimental conditions, WT *hEAAT3* anion currents display comparable anion conductances at positive and at negative voltages with only minor time-dependent relaxations. The effects of P259R on *hEAAT3* anion current amplitudes resemble those of P290R on *hEAAT1* (Suppl. Figure 11.5A). P259R *hEAAT3* and P290R *hEAAT1*, both open upon negative membrane potentials on a slow time course (Suppl. Figure 11.5A). Since openings and closings of EAAT anion channels are tightly coupled to transitions within the uptake cycle^{6, 16, 17}, these similarity in gating indicates that P290R and P259R cause comparable changes in the glutamate uptake cycle of *hEAAT1* and *hEAAT3*. We conclude that P259R *hEAAT3* represent a reliable model protein to study the effects of the disease-associated mutation P290R on *hEAAT1* function.

11.4.1 P259R modifies conformational changes of M205C *hEAAT3*

We used M205C for fluorophore attachment to P259R *hEAAT3* (Figure 11.1A). This reporter mutation is known to preserve functional properties of *hEAAT3* and to generate fluorescence signals that report on EAAT3-specific conformational changes^{11, 13}. Figure 11.2A shows representative fluorescence recordings of M205C or M205C-P259R EAAT3 in absence (*top*) and in the presence of glutamate (*bottom*). Oocytes were held at 0 mV, and voltage steps between -150 mV and +150 mV were applied in 50 mV intervals. EAAT3 carrying only the fluorophore attachment site M205C displays pronounced voltage- and substrate-dependent fluorescence signals (Figure 11.2, *left column*). Application of glutamate decreases fluorescence intensity of M205C EAAT3 over the whole tested voltage-range and furthermore changes the voltage dependence of the fluorescence signal (Figure 11.2B, *left column*)¹³. P259R inverts the voltage dependence and modifies the substrate dependence of these fluorescence signals (Figure 11.2A and B, *right column*). M205C-P259R *hEAAT3* fluorescence intensities increase upon membrane hyperpolarization, and positive membrane potentials lead to slight decreases. Glutamate decreases fluorescence intensities at negative voltages and leaves them unaffected at positive potentials (Figure 11.2B, *right column*).

Figure 11.2
Voltage-, substrate- and time-dependent conformational changes of M205C and M205C-P259R EAAT3

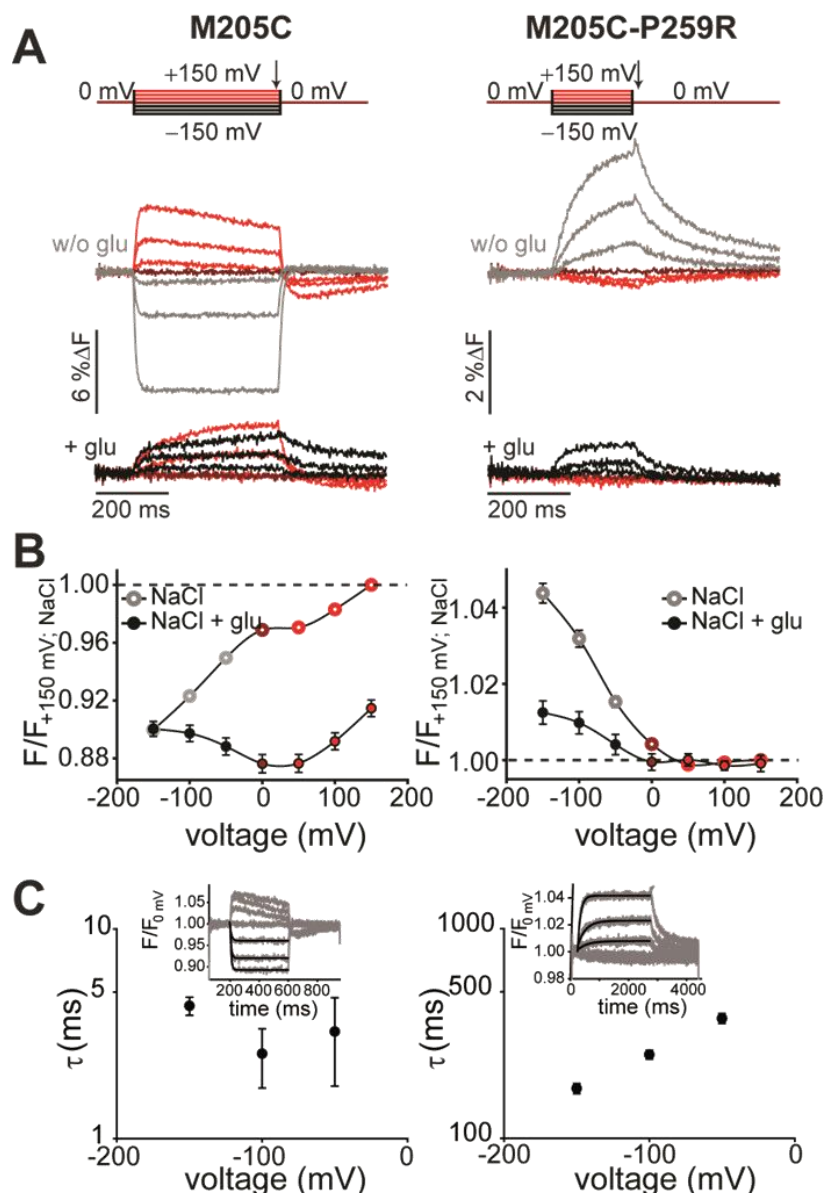


Figure 11.2: Voltage-, substrate- and time-dependent conformational changes of M205C and M205C-P259R EAAT3.

A, fluorescence recordings of M205C (left column) or M205C-P259R EAAT3 (right column) expressing oocytes. B, averaged voltage dependence of fluorescence changes. Voltages above 0 mV were shown in red, 0 mV in dark red and negative voltages without (light grey) or with glutamate (black). Fluorescence amplitudes are normalized to the fluorescence generated at +150 mV in NaCl solution. C, averaged time constants determined from monoexponential fits of the fluorescence change at a voltage jump from 0 mV to -150 mV (black) of fluorescence traces of M205C (left column) or M205C-P259R EAAT3 (right column) expressing oocytes shown as insets. Fluorescence amplitudes are normalized to the fluorescence generated at 0 mV. $n \geq 4$ in B and $n \geq 3$ in C. Fluorescence data are reported as means \pm S.E..

P259R does not only modify the voltage dependence of M205C *h*EAAT3 fluorescence signals, but also their time course. Hyperpolarizing voltage steps cause fast reductions of M205C EAAT3 fluorescence that can be fit with monoexponential functions resulting in time constants of around 3 ms (Figure 11.2C, *left column*). For M205C-P259R EAAT3, time constants of fluorescence increases upon hyperpolarization are between 170 and 370 ms (Figure 11.2C, *right column*), changing upon the voltage, whereas M205C EAAT3 values change only little within the tested voltage-range.

11.4.2 P259R alters the sodium dependence of M205C *h*EAAT3 conformational changes

M205C EAAT3 fluorescence changes report on sodium-binding in absence of glutamate^{11, 13} and the pronounced effects of P259R on these signals suggest that the disease-associated mutation modifies these particular substrate association steps within the EAAT transport cycle. Figure 11.3A gives the voltage dependence of averaged fluorescence intensities of M205C EAAT3 at various external [Na⁺]. Reduction of external sodium results in larger fluorescence amplitudes at negative voltages, whereas values at positive potentials were unaffected. Complete substitution of Na⁺ by choline⁺ nearly abolishes the voltage dependence of fluorescence signals. We next fitted the sodium dependences of fluorescence amplitudes at certain membrane potentials with Hill equations (Figure 11.3A, *inset*) to obtain apparent dissociation constants (K_D) and Hill coefficients (n_H) for sodium-binding and subsequent protein movements. M205C *h*EAAT3 exhibits apparent dissociation constants in the range of 11 - 14 mM (Table 11.1). P259R increases apparent K_D 's about fivefold (Table 11.1). Even doubling of [Na⁺] to 197 mM was insufficient to reach saturation for M205C-P259R *h*EAAT3 (Figure 11.3A, *right column*). For M205C and for M205C-P259R *h*EAAT3, apparent K_D 's decrease slightly with hyperpolarizing voltages. For WT as well as for P259R *h*EAAT3, Hill coefficients are above one (Table 11.1) - in agreement with the notion that two Na⁺ associate prior to glutamate^{5, 12, 18}.

Figure 11.3
Sodium dependence of M205C and M205C-P259R EAAT3 conformational changes

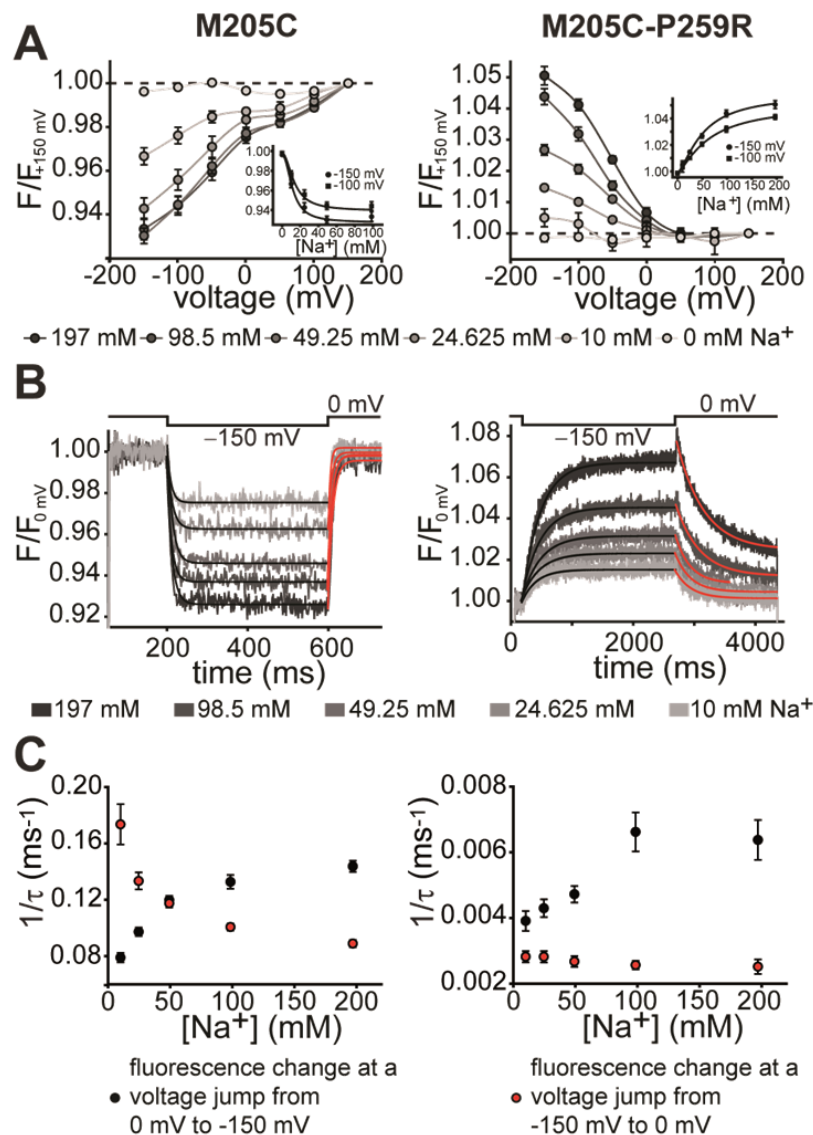


Figure 11.3: Sodium dependence of M205C and M205C-P259R EAAT3 conformational changes.

A, averaged voltage dependence of fluorescence changes of M205C (*left column*) or M205C-P259R EAAT3 (*right column*) measured at different $[\text{Na}^+]$ (197, 98.5, 49.25, 24.625, 10, 0 mM) and corresponding dose-response curves were shown as insets. Fluorescence amplitudes are normalized to the fluorescence generated at +150 mV. B, fluorescence traces of M205C (*left column*) or M205C-P259R EAAT3 (*right column*) expressing oocytes at different $[\text{Na}^+]$ (197, 98.5, 49.25, 24.625, 10 mM) with monoexponential fits of the fluorescence change at a voltage jump from 0mV to -150 mV (*black*) and from -150 mV to 0 mV (*red*). Fluorescence amplitudes are normalized to the fluorescence generated at 0 mV. C, corresponding averaged time constants. $n \geq 4$. Fluorescence data are reported as means \pm S.E..

Table 11.1
Apparent dissociation constants and hill coefficients of M205C and M205C-P259R EAAT3 sodium dependence

voltage (mV)	M205C		M205C-P259R	
	K _D (mM)	n _H	K _D (mM)	n _H
-150	11.7 ± 4	1.9 ± 0.9	50.7 ± 7.7	1.5 ± 0.2
-100	13.4 ± 4.6	2 ± 1.3	63.7 ± 2.4	1.3 ± 0.04

Table 11.1: Apparent dissociation constants and hill coefficients of M205C and M205C-P259R EAAT3 sodium dependence.

K_D's and n_H at different applied voltages were calculated by fitting the fluorescence data with the Hill equation.

Changes in external [Na⁺] also modify the time courses of M205C as well as of M205C-P259R hEAAT3 fluorescence changes upon voltage steps to -150 mV (Figure 11.3B). For M205C hEAAT3, time constants of the fluorescence decrease - that report on Na⁺-binding and binding-associated conformational rearrangements^{9, 11, 13} - accelerate with increasing sodium concentrations from about 13 ms to 7 ms (Figure 11.3C, *left column*). For M205C-P259R hEAAT3, the time constants decrease from 280 to 180 ms upon increasing [Na⁺] (Figure 11.3C, *right column*). Fluorescence increases upon subsequent voltage steps back to the holding potential are due to sodium-dissociation and related conformational changes and can be described with a single time constant that changes with [Na⁺]. M205C hEAAT3 conformational changes display time constants from around 6 ms to 11 ms (Figure 11.3C, *left column*) and P259R M205C hEAAT3 conformational changes display time constants between 370 ms to 440 ms with increasing [Na⁺]. For M205C as well as for M205C-P259R EAAT3 we observed a saturating Na⁺ dependence for fluorescence time constants. This deviation from a linear [Na⁺] dependence indicates that the fluorescence signal does not only result from a one step association of Na⁺ to the transporter. The saturation behavior rather suggest that there is an additional reaction limiting the overall rate at high [Na⁺] once all sodium binding sites are saturated.

Within the EAAT transport cycle two Na⁺ bind prior to glutamate association and a third one to the glutamate-bound transporter^{5, 12, 18}. The data presented so far indicate altered Na⁺-association to the glutamate-unliganded transporter. Since glutamate reduces fluorescence signals of M205C and M205C-P259R *hEAAT3* (Figure 11.2), we analyzed current amplitudes upon varying [Na⁺] in the presence of saturating glutamate concentrations in order to test whether P259R also affects this third sodium binding step. Under these conditions WT, M205C and M205C-P259R *hEAAT3* display sodium dependences with similar apparent dissociation constants and Hill coefficients that agree well with published data¹⁹ (Suppl. Figure 11.6).

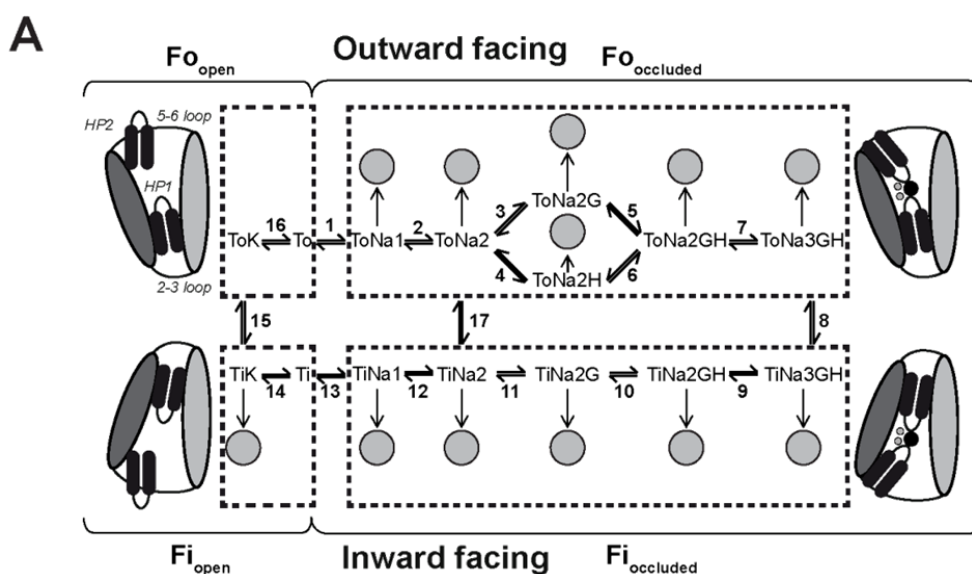
11.4.3 Kinetic modeling reveals altered sodium-binding to P259R *hEAAT3*

We next performed kinetic simulations of P259R *hEAAT3* fluorescence data using a model we recently developed to describe EAAT3 currents and fluorescence values. The scheme is based on the EAAT transport cycle⁹ and was supplemented with additional branching open channel states^{9, 13, 15} (Figure 11.4A, *displayed as grey circles*). To describe fluorescence signals, four major fluorescence levels were assigned to four distinct conformations²⁰⁻²² (Figure 11.4A, *displayed as dotted boxes*). This model describes well the fluorescence-voltage relationship and the current characteristics of cysteine-substituted WT¹³ *hEAAT3* (Table 11.2-4, Figure 11.4).

The complexity of this kinetic scheme prevents direct determination of P259R-modified rate constants by a global fitting procedure. We therefore used an iterative approach to quantify possible changes in the transport cycle and/or anion channel opening in P259R *hEAAT3*. We initially tested whether modifying reactions in certain parts of the uptake cycle can simulate the effects of P259R on *hEAAT3* fluorescence signals (Figure 11.2 and Figure 11.3). We found that adjusting reactions 1 and 2 resulted in most promising preliminary results. Since P290R modifies anion channel open probabilities of *hEAAT1*⁴, we also attempted to describe our data by exclusively varying anion channel opening and closing. However, we could neither describe the fluorescence-voltage relationship nor the current characteristics of P259R *hEAAT3* by modification of anion channel opening and closing rates alone.

We then optimized rate constants of reaction 1 and 2 versus fluorescence data, experimentally determined relative current amplitudes at -100 mV and relative glutamate uptake currents at -100 mV. Since preservation of detailed balance turned out to be impossible under these conditions, and since it appears unlikely that only sodium association to the outward-facing, but not to the inward-facing transporter is altered by P259R, we also optimized reactions 12 and 13 during the fitting process. The resulting kinetic scheme predicts drastic deceleration of binding as well as unbinding of the first and second sodium in the outward facing conformation (Table 11.2). Furthermore, unbinding of the second (reaction 12) from the inward facing state of EAAT is enhanced and unbinding of the first sodium (reaction 13) is reduced, whereas other rates are just slightly changed (Table 11.2). The reduced sodium binding rates are consistent with the experimentally observed deceleration of fluorescence time constants. The kinetic scheme does not only reproduce the fluorescence-voltage relationship with and without glutamate, the sodium dependence and the corresponding apparent fluorescence dissociation constants and Hill coefficients of M205C and M205C-P259R EAAT3 (Figure 11.4B-C, Table 11.2-5), but also the decreased uptake current and increased anion conductance in the absence of glutamate by P259R are correctly calculated by the kinetic simulation (Figure 11.4D-E).

Figure 11.4
Kinetic model and simulated conformational changes and currents of M205C and M205C-P259R EAAT3



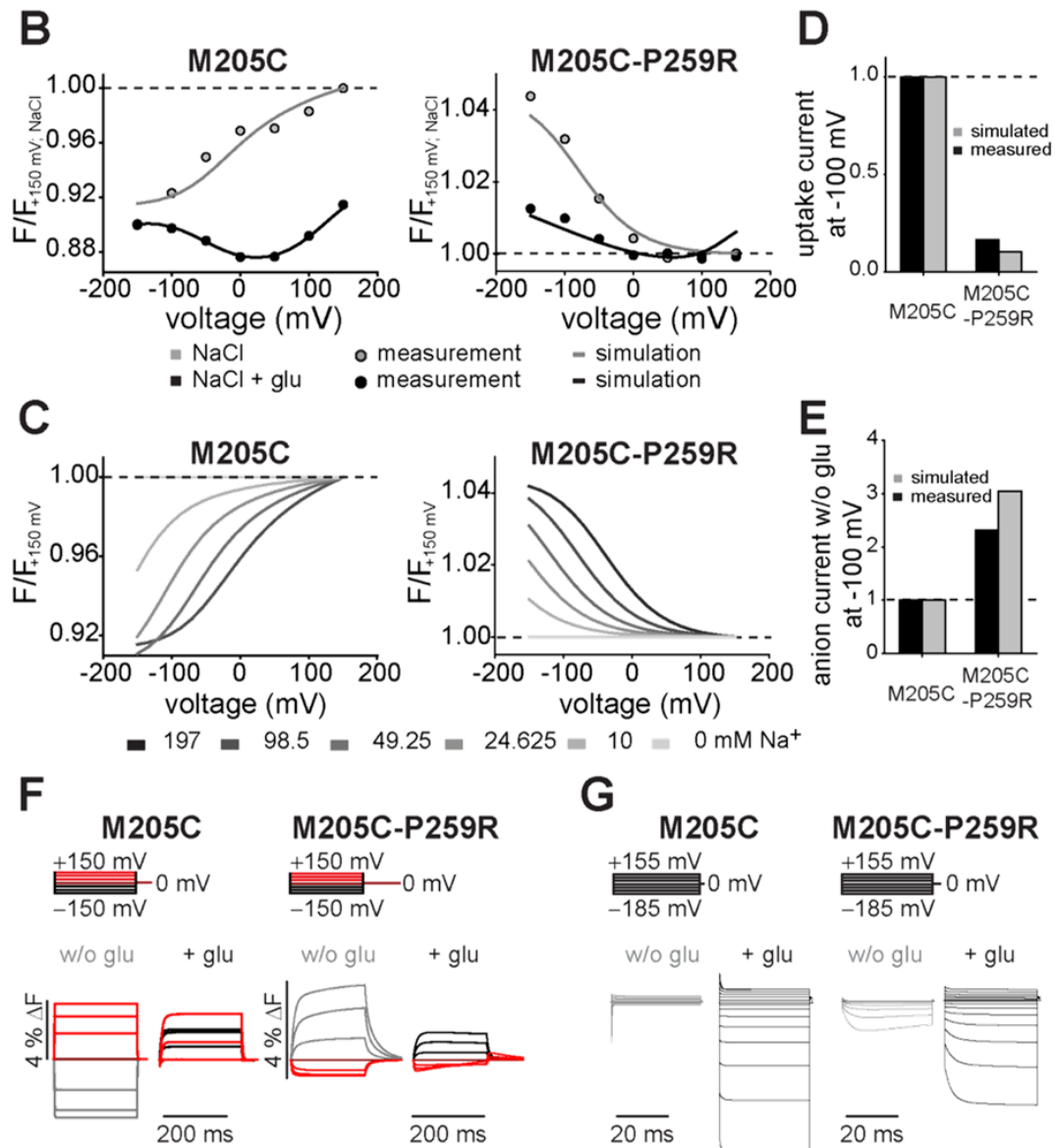


Figure 11.4: Kinetic model and simulated conformational changes and currents of M205C and M205C-P259R EAAT3.

A, 15-state model with branching anion channel states (*grey circles*), grouped into 4 fluorescence states (*dotted boxes*), corresponding to 4 conformations shown as protomers (modified from 20). B, voltage dependence of measured (*circles*) or simulated fluorescence changes (*solid lines*) without (*grey*) or with glutamate (*black*). C, simulated fluorescence changes at different $[\text{Na}^+]$ (197, 98.5, 49.25, 24.625, 10, 0 mM). D, E Comparison of the simulated (*grey*) and measured (*black*) glutamate uptake (D) and anion currents (E) at -100 mV, normalized to the current amplitudes of M205C. F, G time-dependent simulation fluorescence changes (F) and current amplitudes (G) upon the indicated voltage steps for M205C or M205C-P259R EAAT3 either in the absence or in the presence of 1 mM glutamate.

However, assuming identical voltage dependence for Na⁺ association to M205C and M205C-P259R EAAT3, the model failed to predict the slow activation of P259R hEAAT3 upon hyperpolarizing voltage steps, but rather predicted time-independent current responses. We thus manually optimized the voltage dependence of Na⁺ association for P259R hEAAT3 and found that increasing the apparent electrical distance $z\delta$ of reaction 1 from 0.2 to 0.5 and adjusting $z\delta$ of reaction 2 from 0.2 to -0.1 resulted in an improved agreement of simulated time-dependent fluorescence responses and anion currents with experimental data without affecting the predictions for other parameters (Figure 11.4F and G). The altered voltage dependence of Na⁺ association also accounts for the different voltage dependences of the time constants of fluorescence changes upon hyperpolarizing voltage steps (Figure 11.2).

Table 11.2
Parameters of the EAAT3 model

reaction	<u>changed parameters for P259R</u>					
	forward	backward	$z\delta$	$z\delta$	forward	backward
1	$1.00 \cdot 10^{+04} \text{ M}^{-1} \text{ s}^{-1}$	$2.50 \cdot 10^{+03} \text{ s}^{-1}$	0.20	0.50	$80 \text{ M}^{-1} \text{ s}^{-1}$	51.73 s^{-1}
2	$1.00 \cdot 10^{+04} \text{ M}^{-1} \text{ s}^{-1}$	$2.50 \cdot 10^{+03} \text{ s}^{-1}$	0.20	-0.10	$55 \text{ M}^{-1} \text{ s}^{-1}$	78.61 s^{-1}
3	$6.80 \cdot 10^{+06} \text{ M}^{-1} \text{ s}^{-1}$	$3.00 \cdot 10^{+02} \text{ s}^{-1}$	-0.40			
4	$6.00 \cdot 10^{+11} \text{ M}^{-1} \text{ s}^{-1}$	$7.00 \cdot 10^{+02} \text{ s}^{-1}$				
5	$6.00 \cdot 10^{+11} \text{ M}^{-1} \text{ s}^{-1}$	$7.00 \cdot 10^{+02} \text{ s}^{-1}$	0.40			
6	$6.80 \cdot 10^{+06} \text{ M}^{-1} \text{ s}^{-1}$	$3.00 \cdot 10^{+02} \text{ s}^{-1}$				
7	$1.00 \cdot 10^{+04} \text{ M}^{-1} \text{ s}^{-1}$	$1.00 \cdot 10^{+03} \text{ s}^{-1}$	0.55			
8	$5.50 \cdot 10^{+02} \text{ s}^{-1}$	$5.00 \cdot 10^{+02} \text{ s}^{-1}$				
9	$8.00 \cdot 10^{+02} \text{ s}^{-1}$	$4.00 \cdot 10^{+04} \text{ M}^{-1} \text{ s}^{-1}$	0.45			
10	$6.00 \cdot 10^{+03} \text{ s}^{-1}$	$9.00 \cdot 10^{+10} \text{ M}^{-1} \text{ s}^{-1}$				
11	$3.00 \cdot 10^{+03} \text{ s}^{-1}$	$4.00 \cdot 10^{+05} \text{ M}^{-1} \text{ s}^{-1}$				
12	$5.00 \cdot 10^{+02} \text{ s}^{-1}$	$2.00 \cdot 10^{+05} \text{ M}^{-1} \text{ s}^{-1}$			$7.57 \cdot 10^{+04} \text{ s}^{-1}$	$4.64 \cdot 10^{+03} \text{ M}^{-1} \text{ s}^{-1}$
13	$4.00 \cdot 10^{+03} \text{ s}^{-1}$	$1.00 \cdot 10^{+06} \text{ M}^{-1} \text{ s}^{-1}$	0.20		2.20 s^{-1}	$2.39 \cdot 10^{+05} \text{ M}^{-1} \text{ s}^{-1}$
14	$1.00 \cdot 10^{+06} \text{ M}^{-1} \text{ s}^{-1}$	$1.00 \cdot 10^{+03} \text{ s}^{-1}$				
15	50 s^{-1}	5.00 s^{-1}	0.40			
16	$8.00 \cdot 10^{+02} \text{ s}^{-1}$	$1.00 \cdot 10^{+04} \text{ M}^{-1} \text{ s}^{-1}$				
17	0.80 s^{-1}	$1.00 \cdot 10^{-02} \text{ s}^{-1}$				

Table 11.2: Parameters of the EAAT3 model.

Rate constants of the transport process and channel opening/closing at -70 mV. Electrogenic reactions are defined by $z\delta$ values, which correspond to the product of the charge, and the fraction of the electric field the charge is moved across the membrane. Clockwise transitions in the model scheme are denoted as “forward reactions”.

Table 11.3
Open probabilities used in the kinetic modeling of cysteine-substituted wildtype and mutant EAAT3

anion channel state branching from:	open probability
ToNa1	0.7224
ToNa2	$9.9990 \cdot 10^{-05}$
ToNa2G	$9.9990 \cdot 10^{-05}$
ToNa2H	$9.9990 \cdot 10^{-05}$
ToNa2GH	$1.3214 \cdot 10^{-04}$
ToNa3GH	0.9881
TiNa3GH	0.8264
TiNa2GH	0.7133
TiNa2G	$1.2749 \cdot 10^{-04}$
TiNa2	$1.0081 \cdot 10^{-04}$
TiNa1	0.7652
TiK	$1.3570 \cdot 10^{-04}$

Table 11.3: Open probabilities used in the kinetic modeling of cysteine-substituted wildtype and mutant EAAT3.

Table 11.4
Fluorescence intensities used for simulations of cysteine-substituted wildtype and mutant EAAT3 fluorescence voltage relationships

fluorescence state	M205C	M205C-P259R
F_{open}	1.00	1.00
F_{occluded}	0.89	1.05
F_{open}	0.29	0.99
F_{occluded}	2.44	2.81

Table 11.4: Fluorescence intensities used for simulations of cysteine-substituted wildtype and mutant EAAT3 fluorescence voltage relationships.

Fluorescence intensities of fluorescence states $F_{\text{open/occluded}}$ and $F_{\text{open/occluded}}$ of cysteine-substituted and M205C-P259R EAAT3 used to simulate the overall fluorescence voltage relationship were normalized to the fluorescence intensity of F_{open} .

Table 11.5
Simulated dissociation constants and hill coefficients of M205C and M205C-P259R EAAT3 sodium dependence

voltage (mV)	M205C		M205C-P259R	
	K _D (mM)	n _H	K _D (mM)	n _H
-150	9.5 ± 0.8	2.8 ± 1.1	27 ± 1.2	1.3 ± 0.06
-100	17.2 ± 1.6	1.8 ± 0.3	71 ± 1.2	1.2 ± 0.05

Table 11.5: Simulated dissociation constants and hill coefficients of M205C and M205C-P259R EAAT3 sodium dependence.

K_D's and n_H at -150 and -100 mV were calculated by fitting the simulated fluorescence data with the Hill equation.

11.5 Discussion

EAAT transporters fulfill diverse cellular functions in the central nervous system, in sensory organs as well as in the kidney²³. The physiological impact of this class of glutamate transporters is illustrated by several hereditary diseases caused by naturally occurring mutations in the *SLC1A* gene family that encodes EAAT glutamate transporters. Apart from the mutations in *SLC1A3* in episodic ataxia^{2, 3}, *SLC1A2* mutations have been identified in rare hereditary forms of amyotrophic lateral sclerosis²⁴, and *SLC1A1* mutations associated with human dicarboxylic aminoaciduria²⁵. Studying “transporteropathies” does not only provide insights into the physiological roles of affected transporters or does not only improve the understanding of certain rare human diseases, but also serves as tool to decipher the molecular basis of transporter function. Random sequence alterations that are known to impair transporter function permit unexpected insights into structure-function relationship and thus provide an alternative approach to identify sequence determinants of EAAT functions. We here show that a combination of voltage clamp fluorometry and kinetic modelling permits identification of the underlying molecular mechanism of the EAAT “transporteropathy” episodic ataxia type 6 for one disease-associated mutation, P290R.

In these experiments, we used the related isoform *hEAAT3* for voltage clamp fluorometry experiments since P290R *hEAAT1* did not express at levels sufficiently

high to allow current and fluorescence measurements. EAAT1 and EAAT3 share basic mechanisms of glutamate transport and exhibit similar anion conduction properties^{26-27, 28}. The homologous mutations P259R and P290R both reduce glutamate uptake currents and increase the amplitudes of EAAT anion currents in the absence as well as in the presence of glutamate (Figure 11.1, Suppl. Figure 11.5). Moreover, we observed comparable modifications of the time and voltage dependence of P259R *h*EAAT3 and P290R *h*EAAT1 anion currents (Figure 11.1, Suppl. Figure 11.5). These findings indicate that the function of both mutant transporters is comparably affected and that voltage clamp fluorometry on P259R EAAT3 permits insights into the dysfunction of P290R EAAT1.

We found that P259R inverts the voltage dependence of EAAT3 fluorescence intensities, changes the glutamate-induced fluorescence change and drastically decelerates the time dependence of these signals (Figure 11.2 and Figure 11.3). To describe the basis of these alterations we optimized a kinetic scheme developed to describe fluorescence signals as well as transport and anion currents of M205C *h*EAAT3⁹. By modifying reactions that report on Na⁺-association/-dissociation to the transporter prior to glutamate in the outward or in the inward facing state, we could simulate all functional alterations by P259R. The obtained kinetic scheme correctly predicts the voltage, substrate and [Na⁺] dependence of fluorescence signals of mutant transporters (Figure 11.4, Table 11.2-5). Moreover, it accounts for decreased glutamate uptake and increased anion conduction in the absence of glutamate and predicts qualitatively the deceleration in the time course of fluorescence signals and anion currents by P259R (Figure 11.4).

In EAAT3 three putative sodium binding sites have been identified as aspartate residues at position D368 (TM7), D440 and D455 (TM8)^{12, 18, 22, 29}. Since P259 is not in close proximity to any of those residues (C α -distances in the outward facing open conformation from P259 to: D368 = 26.3 Å, D440 = 21.2 Å, D455 = 24.4 Å), the structural basis for altered sodium binding to P259R *h*EAAT3 is not clear. Moreover, Na⁺-association should be a diffusion-controlled process, and the dramatic effect we observed for P259R on the Na⁺-association rates is difficult to imagine. We thus hypothesize that P259R does not affect the cation association itself, but rather an associated conformational change. This interpretation is supported by the saturating behaviour in the Na⁺ concentration dependence of time constants for M205C or M205C-P259R EAAT3 fluorescence changes. A possible Na⁺-associated

conformational change affected by P259R might be the opening of HP2 that is triggered by association of Na⁺ to the empty transporter¹².

Proline often acts as structural disruptor of α -helices and β -sheets, and the conserved proline P259 at the hinge of TM5 might represent the structural determinant of the kinked shape of TM5²⁰. P259R might abolish the TM5 kink and cause an overall structural change of the trimerization domain of mutant transporters. The resulting change in the orientation of the transport domain towards the trimerization domain might impair certain conformational changes within the transport domain. Moreover, it possibly could alter the position of Na⁺ binding sites within the electric field. This hypothesis can explain the inversed voltage dependence of conformational changes (Figure 11.2) and the increased electrical distances simulated for sodium binding (Table 11.2).

To quantitatively describe our results on P259R *hEAAT3* we used a kinetic scheme that was developed to describe fluorescence signals as well as transport and anion currents of *hEAAT3* carrying multiple reporter mutations. WT *hEAAT3* as well as P259R *hEAAT3* anion currents predicted by this scheme do not resemble measured currents. A possible explanation for this deviation is the complexity of EAAT transport functions and of the used kinetic scheme. For example, anion channel opening is coupled to transitions within the uptake cycle that can be directly observed by voltage clamp fluorometry⁹⁻¹³. However, it is currently not possible to determine anion channel opening and closing reactions experimentally.

P259R as well as P290R result in dramatically increased EAAT3 and EAAT1 anion currents in the absence as well as in the presence of glutamate. For P290R EAAT1, we demonstrated that the increased anion current of mutant EAAT1 is accompanied by a reduced number of transporters in the surface membrane⁴. This finding is incompatible with noise analysis measurements that reveal an absolute open probability larger than 0.5 for WT EAAT1⁴ or the very high absolute open probabilities predicted by the kinetic scheme developed here (Suppl. Figure 11.8). The approximately fourfold increase of EAAT3 anion currents by P259R will be only possible if noise analysis underestimates the number of active EAAT anion channels and thus overestimates their absolute open probability. We recently demonstrated a similar disagreement for the dual function anion transporter CIC-4, reporting that changes in the external [Cl⁻] alters the apparent number of CIC-4 channels determined by noise analysis without modifying the density of CIC-4 proteins in the

surface membrane³⁰. We explained this behaviour by proposing two functional states of CIC-4, one functioning as transporter and the other one as channel, and transitions between these functional modes are mediated by association of Cl⁻. If the rate constant of Cl⁻ binding is much faster than the opening transition of the channel, the proportions of CIC-4 without or with bound Cl⁻ will equilibrate into a semi-equilibrium distribution, and noise analysis will only report on opening and closing transitions of the anion channels. The state diagram proposed for CIC-4 resembles the kinetic scheme used to describe *hEAAT3*. Since Na⁺-association is very fast for WT *hEAAT3*, noise analysis might provide incorrectly high absolute open probabilities of *hEAAT3* anion channels via a similar mechanism.

Gameiro *et al.*³¹ recently studied EAAT5 glutamate transport and anion currents. They reported that EAAT5 anion currents activate slowly upon membrane hyperpolarization and identified slow Na⁺-association as basis for the slow activation time course and the very low glutamate transport rates. Our result that the high capacity glutamate transporters EAAT1 or EAAT3 carrying a disease-causing mutation functionally resemble the low capacity glutamate transporter EAAT5 beautifully illustrates the importance of the evolutionary optimization of EAAT isoform with distinct functional properties.

11.6 Methods

11.6.1 Expression of WT and mutant *hEAAT3* transporters in *Xenopus laevis* oocytes or mammalian cells

Point mutations were introduced into pTLN2-*hEAAT3*^{24, 32} (kindly provided by Dr. Matthias Hediger (University of Bern, Switzerland)) or into pTLN2-*hEAAT1* using the QuikChange mutagenesis kit (Stratagene, La Jolla, CA, USA). Capped cRNA was synthesized from *MluI*-/*NheI*-linearized pTLN2-*hEAAT* through use of MESSAGE machine kits (Ambion, Austin, TX, USA). Collagenase-treated, defolliculated stage IV-V oocytes were microinjected with 10 ng of RNA (Nanoliter 2000, World Precision Instruments, Sarasota, FL, USA) and incubated at 18°C in ND96 (in mM: 96 NaCl, 2 KCl, 1.8 CaCl₂, 1 MgCl₂, 5 HEPES, pH 7.6, supplemented with 2.5 sodium pyruvate

and 50 µg/ml gentamycine sulfate). Experiments were performed 3-7 days after injection.

For expression in mammalian cells point mutations were introduced into pcDNA3.1-*hEAAT1*³³ or pcDNA3.1-*hEAAT3*³⁴ and transiently transfected in tsA201 cells using the $\text{Ca}_3(\text{PO}_4)_2$ technique as described³³. For each construct, two independent recombinants from the same transformation were examined and shown to exhibit indistinguishable functional properties.

11.6.2 Voltage clamp fluorometry

Current amplitudes were measured under two-electrode voltage clamp using a CA-1B amplifier (Dagan Corporation, Minneapolis, MN, USA) and digitized at 5 kHz using an ITC-18 Computer Interface in combination with Patchmaster (HEKA Elektronik, Lambrecht, Germany). For fluorescence experiments, oocytes were labeled for 2-3 h with 10 µM of the fluorescent maleimide probe, AlexaFluor546 (Life Technologies Corporation, Invitrogen, Carlsbad, CA, USA). Incubation times were optimized for each construct as described¹³. A short arc mercury lamp (HBO 103W/2, Osram, München, Germany) combined with a Uniblitz shutter (VS25S2ZMOR1-24 shutter, VCM-D1 shutter driver, Uniblitz, Vincent Associates, Rochester, NY, USA) was used as light source. Fluorescence was monitored under voltage clamp by a photodiode (PIN020-A, AMS Technologies AG, Martinsried, Germany) and a rhodamine filter cube (HQ535/50x, Q565LP, HQ610/75m, Chroma Technology Corp., Bellows Falls, VT, USA) attached to an inverted fluorescence microscope (IX71, Olympus, Hamburg, Germany). Fluorescence signals were amplified with a DLPCA-200 amplifier (Femto Messtechnik, Berlin, Germany) and low pass-filtered at 2 kHz (LPF-8, Low Pass Bessel Filter, Warner Instruments, Hamden, CT, USA). Experiments were performed under constant perfusion using a PF-8 8-Channel Perfusion System (Abimek-Zech electronic, Göttingen, Germany) with Ringer's solution (in mM: 98.5 Choline-Cl or NaCl/NO₃/gluconate, 1.8 CaCl₂/gluconate, and 1 MgCl₂/gluconate, 5 Hepes pH 7.5, ± 1 glutamate). Oocytes were held at 0 mV for at least 2 s between voltage steps, and representative fluorescence recordings were obtained by averaging ten consecutive measurements.

To permit site-directed fluorescence labeling of EAAT3, we introduced a single cysteine into *hEAAT3* and expressed WT and cysteine-substituted transporters in *Xenopus* oocytes. We chose a mutation for fluorophore attachment localized in TM4c, M205C and additionally mutated the endogenous C158 to serine to prevent possible modifications by fluorophore application (for simplification further not nominated). Oocytes expressing M205C or M205C-P259R *hEAAT3* exhibited higher fluorescence intensities than uninjected oocytes or oocytes expressing corresponding *hEAAT3* without the reporter mutation (data not shown). Moreover, the fluorescence changes display characteristic voltage or substrate dependences¹³ and could be inhibited by the EAAT-specific transporter-blocker DL-threo-benzyloxyaspartate (TBOA) in the absence and in the presence of glutamate by about 90%¹³. These data strongly supports the notion that the studied fluorescence signals are specific for WT or mutant *hEAAT3*.

11.6.3 Electrophysiology

Standard whole-cell patch clamp recordings were performed using an Axopatch 200B amplifier (Molecular Devices, Sunnyvale, CA). We routinely compensated at least 80% of the series resistance by an analogue procedure to reduce voltage errors, filtered currents at 5 kHz and digitized with a sampling rate of 20 KHz using a Digidata AD/DA converter (Molecular Devices, Sunnyvale, CA). Borosilicate pipettes were pulled with resistances of 1.5–2.5 MΩ and cells with currents more than 10 nA were excluded from the analysis. We used an internal solution containing (mM) 115 KNO₃, 2 MgCl₂, 5 EGTA, 10 HEPES (pH = 7.4) and an external solution of (mM) 140 NaNO₃, 4 KCl, 2 CaCl₂, 1 MgCl₂, 5 HEPES (pH = 7.4) to study the effect of 1 mM external applied L-glutamate on WT EAAT1 and EAAT3 and mutant transporter-mediated currents. The pH of the internal and external solution was adjusted to 7.4, with KOH or NMDG, respectively.

11.6.4 Data analysis

Electrophysiological and fluorescence data were analyzed with a combination of Patchmaster (HEKA Elektronik, Lambrecht,), pClamp10 (Molecular Devices,

Sunnyvale, CA, USA), MATLAB (The MathWorks, Natick, MA, USA) and SigmaPlot (Jandel Scientific, San Rafael, CA, USA). For statistical evaluations, Student's t-test and paired t-test with $p \leq 0.05$ (*) as the level of significance were used ($p \leq 0.01$ (**), $p \leq 0.001$ (***)). The data are given as the means \pm S.E.. Apparent dissociation constants and hill coefficients were calculated by fitting the data with the Hill equation ($F/F_{+150mV} = y_0 + a * [Na^+]^{nH} / (K_D^{nH} + [Na^+]^{nH})$).

11.6.5 Kinetic modeling

We recently established a kinetic scheme for WT *hEAAT3* based on voltage- and substrate-dependent fluorescence signals, as well as on uptake currents and glutamate-sensitive relative current amplitudes¹³. Based on the idea of four major conformations (inward/outward facing and substrate-bound/-unbound), all states were grouped into four different subsets with distinct relative fluorescence intensities for each construct. The first conformation corresponds to an empty transporter residing in an outward facing state with HP2 being open and the substrate binding sites exposed to the extracellular space ($F_{o_{open}}$: ToK, To). Binding of sodium and glutamate causes closure of HP2 ($F_{o_{occluded}}$: ToNa1, ToNa2, ToNa2G, ToNa2H, ToNa2GH, ToNa3GH) which is followed by the large movement of the whole transport domain ($F_{i_{occluded}}$: TiNa3GH, TiNa2GH, TiNa2G, TiNa2, TiNa1). Opening of HP1 leads to substrate release and exposure of the binding sites to the intracellular solution ($F_{i_{open}}$: Ti, TiK). Whereas the first three conformations have been characterized at a structural level, the inward facing open state is at present only hypothetical. The overall fluorescence was calculated as sum of the products of relative fluorescence and probability of occupation for every state. Parameters for channel gating (open probabilities for leaving the cycle into the conducting state) were estimated by optimizing the model against WT steady-state fluorescence data using the genetic algorithm as implemented in MATLAB (The MathWorks, Natick, MA, USA). The so-determined model was then adapted to the P259R mutant by modifying sodium-binding rates (reactions 1, 2 and 12, 13) and electrical distances $z\delta$. In all cases, detailed balance was preserved, and fitting parameters were simultaneously optimized against experimentally determined relative glutamate uptake and relative glutamate-induced current amplitudes at -100 mV. For kinetic

modeling we assumed intracellular concentrations of $[Na^+] = 10$ mM, $[K^+] = 70$ mM, $[glu] = 12$ mM and a $pH = 7.3^{27}$, extracellular concentrations were set to experimental conditions.

11.7 Acknowledgements

We would like to thank Dr. M. Hediger for providing the expression construct for *hEAAT3*. We appreciate helpful discussions with Dr. Alexi Alekov, Dr. David Ewers, Dr. Martin Fischer, Gabriel Stöling, and Natalie Winter. These studies were supported by the Deutsche Forschungsgemeinschaft (FA301/ 9 to Ch. F.).

11.8 References

1. Jen, J.C. *et al.* Primary episodic ataxias: diagnosis, pathogenesis and treatment. *Brain* **130**, 2484-2493 (2007).
2. Jen, J.C., Wan, J., Palos, T.P., Howard, B.D., & Baloh, R.W. Mutation in the glutamate transporter EAAT1 causes episodic ataxia, hemiplegia, and seizures. *Neurology* **65**, 529-534 (2005).
3. de Vries, B. *et al.* Episodic ataxia associated with EAAT1 mutation C186S affecting glutamate reuptake. *Arch. Neurol.* **66**, 97-101 (2009).
4. Winter, N., Kovermann, P., & Fahlke, C. Gain-of-function of glial glutamate transporter-associated anion channels cause episodic ataxia. *Brain in revision*, (2010).
5. Watzke, N., Bamberg, E., & Grewer, C. Early intermediates in the transport cycle of the neuronal excitatory amino acid carrier EAAC1. *J Gen Physiol* **117**, 547-562 (2001).
6. Bergles, D.E., Tzingounis, A.V., & Jahr, C.E. Comparison of coupled and uncoupled currents during glutamate uptake by GLT-1 transporters. *J Neurosci* **22**, 10153-10162 (2002).
7. Vandenberg, R.J., Huang, S., & Ryan, R.M. Slips, leaks and channels in glutamate transporters. *Channels (Austin.)* **2**, 51-58 (2008).

8. Machtens,J.P., Kovermann,P., & Fahlke,Ch. Substrate-dependent Gating of Anion Channels Associated with Excitatory Amino Acid Transporter 4. *J Biol Chem* **286**, 23780-23788 (2011).
9. Larsson,H.P., Tzingounis,A.V., Koch,H.P., & Kavanaugh,M.P. Fluorometric measurements of conformational changes in glutamate transporters. *Proc. Natl. Acad. Sci. U. S. A* **101**, 3951-3956 (2004).
10. Koch,H.P. & Larsson,H.P. Small-scale molecular motions accomplish glutamate uptake in human glutamate transporters. *J Neurosci.* **25**, 1730-1736 (2005).
11. Koch,H.P., Hubbard,J.M., & Larsson,H.P. Voltage-independent sodium-binding events reported by the 4B-4C loop in the human glutamate transporter EAAT3. *J. Biol. Chem.* **282**, 24547-24553 (2007).
12. Larsson,H.P. *et al.* Evidence for a third sodium-binding site in glutamate transporters suggests an ion/substrate coupling model. *Proc. Natl. Acad. Sci. U. S. A* **107**, 13912-13917 (2010).
13. Hotzy,J., Machtens,J.P., & Fahlke,Ch. Neutralizing aspartate 83 modifies substrate translocation of EAAT3 glutamate transporters. *J Biol Chem*(2012).
14. Kanai,Y. & Hediger,M.A. Primary structure and functional characterization of a high-affinity glutamate transporter [see comments]. *Nature* **360**, 467-471 (1992).
15. Kovermann,P., Machtens,J.P., Ewers,D., & Fahlke,Ch. A conserved aspartate determines pore properties of anion channels associated with excitatory amino acid transporter 4 (EAAT4). *J Biol Chem* **285**, 23676-23686 (2010).
16. Tao,Z., Zhang,Z., & Grewer,C. Neutralization of the aspartic acid residue Asp-367, but not Asp-454, inhibits binding of Na⁺ to the glutamate-free form and cycling of the glutamate transporter EAAC1. *J Biol. Chem.* **281**, 10263-10272 (2006).
17. Machtens,J.P., Fahlke,Ch., & Kovermann,P. Noise analysis to study unitary properties of transporter-associated ion channels. *Channels (Austin.)* **5**, 468-472 (2011).
18. Tao,Z. & Grewer,C. Cooperation of the conserved aspartate 439 and bound amino acid substrate is important for high-affinity Na⁺ binding to the glutamate transporter EAAC1. *J Gen. Physiol* **129**, 331-344 (2007).
19. Rosental,N. & Kanner,B.I. A conserved methionine residue controls the substrate selectivity of a neuronal glutamate transporter. *J Biol Chem* **285**, 21241-21248 (2010).
20. Yernool,D., Boudker,O., Jin,Y., & Gouaux,E. Structure of a glutamate transporter homologue from *Pyrococcus horikoshii*. *Nature* **431**, 811-818 (2004).
21. Reyes,N., Ginter,C., & Boudker,O. Transport mechanism of a bacterial homologue of glutamate transporters. *Nature* **462**, 880-885 (2009).

22. Boudker,O., Ryan,R.M., Yernool,D., Shimamoto,K., & Gouaux,E. Coupling substrate and ion binding to extracellular gate of a sodium-dependent aspartate transporter. *Nature* **445**, 387-393 (2007).
23. Danbolt,N.C. Glutamate uptake. *Progress in Neurobiology* **65**, 1-105 (2001).
24. Trotti,D., Rolfs,A., Danbolt,N.C., Brown,R.H., Jr., & Hediger,M.A. SOD1 mutants linked to amyotrophic lateral sclerosis selectively inactivate a glial glutamate transporter *Nature Neuroscience* **2**, 427-433 (1999).
25. Bailey,C.G. *et al.* Loss-of-function mutations in the glutamate transporter SLC1A1 cause human dicarboxylic aminoaciduria. *J Clin. Invest* **121**, 446-453 (11 A.D.).
26. Wadiche,J.I., Amara,S.G., & Kavanaugh,M.P. Ion fluxes associated with excitatory amino acid transport. *Neuron* **15**, 721-728 (1995).
27. Zerangue,N. & Kavanaugh,M.P. Flux coupling in a neuronal glutamate transporter. *Nature* **383**, 634-637 (1996).
28. Owe,S.G., Marcaggi,P., & Attwell,D. The ionic stoichiometry of the GLAST glutamate transporter in salamander retinal glia. *J. Physiol* **577**, 591-599 (2006).
29. Tao,Z. *et al.* Mechanism of cation binding to the glutamate transporter EAAC1 probed with mutation of the conserved amino acid residue Thr101. *J Biol Chem* **285**, 17725-17733 (2010).
30. Alekov,A. & Fahlke,C. Channel-like slippage modes in the human anion/proton exchanger CIC-4. *J Gen Physiol* **133**, 485-496 (2009).
31. Gameiro,A., Braams,S., Rauen,T., & Grewer,C. The Discovery of Slowness: Low-Capacity Transport and Slow Anion Channel Gating by the Glutamate Transporter EAAT5. *Biophys. J* **100**, 2623-2632 (2011).
32. Lorenz,C., Pusch,M., & Jentsch,T.J. Heteromultimeric CLC chloride channels with novel properties. *Proc. Natl. Acad. Sci. USA* **93**, 13362-13366 (1996).
33. Melzer,N., Torres-Salazar,D., & Fahlke,Ch. A dynamic switch between inhibitory and excitatory currents in a neuronal glutamate transporter. *Proc. Natl. Acad. Sci. U. S. A* **102**, 19214-19218 (2005).
34. Torres-Salazar,D. & Fahlke,Ch. Neuronal glutamate transporters vary in substrate transport rate but not in unitary anion channel conductance. *J Biol. Chem.* **282**, 34719-34726 (2007).

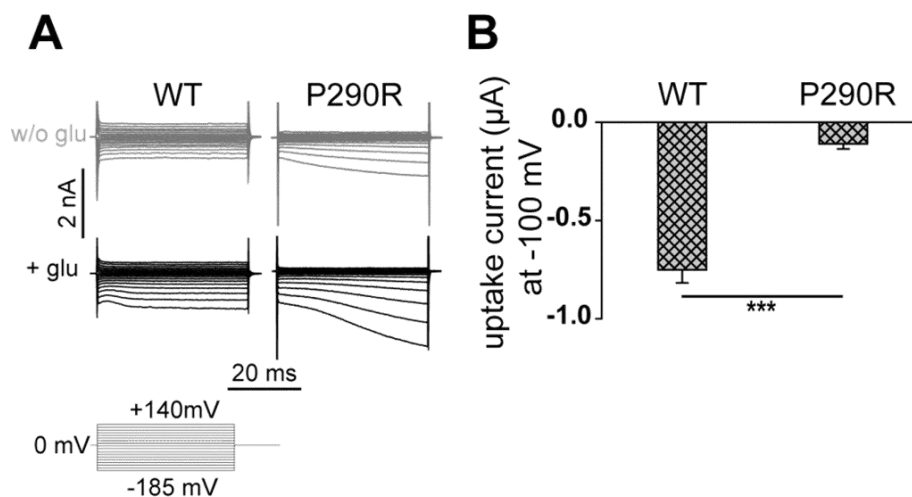
11.9 Supplemental Figures and Information

P259R results in altered residence probabilities for *h*EAAT3 transport states

Modification of the rate constants of reaction 1, 2 12 and 13 produces a shift of the residence probability of EAAT uptake cycle states by P259R (Suppl. Figure 11.7). In the absence of glutamate, mutant transporters reside with higher likelihood in T_o than WT, and sodium-bound states are slightly less occupied, consequently resulting from a weaker sodium binding to P259R EAAT3. Furthermore there is a low probability of the occupation of the state $TiNa1$. In the presence of glutamate, M205C EAAT3 resides mostly in the glutamate-bound outward facing states and to a lesser extent in the inward facing states. M205C-P259R *h*EAAT3 transporters are almost not occupying the inward facing states, except of $TiNa1$, explaining the lower transport capability of mutant EAAT3. Instead of residing in the inward facing states, T_o and to a lesser extent the outward facing sodium- and glutamate-bound states are occupied.

Suppl. Figure 11.5

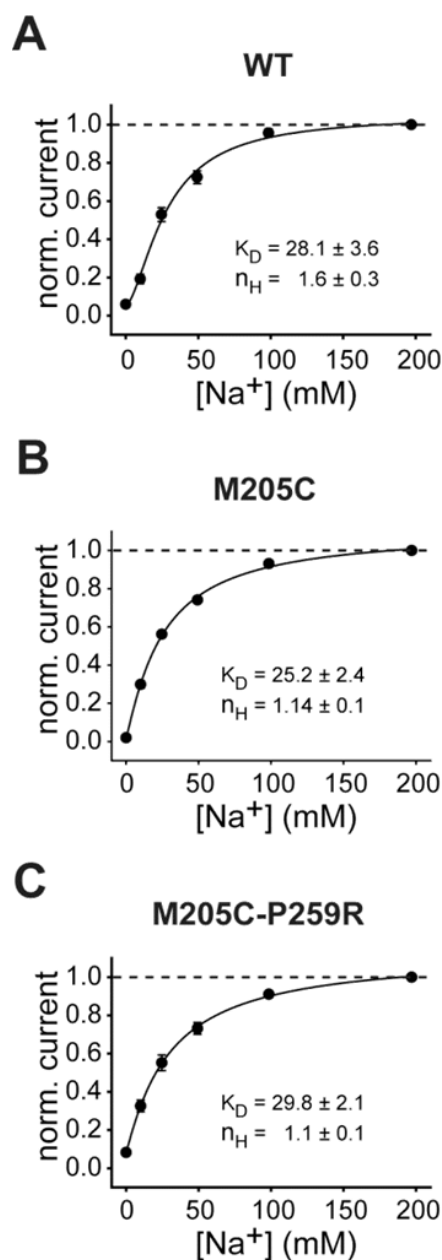
P290R alters EAAT1 glutamate-activated anion currents and uptake currents in mammalian cells and oocytes similar to P259R in EAAT3



Suppl. Figure 11.5: P290R alters EAAT1 glutamate-activated anion currents and uptake currents in mammalian cells and oocytes similar to P259R in EAAT3.

A, representative current recordings from tsA201 cells expressing WT or P290R EAAT1 with standard KNO_3 -based internal solution and a $NaNO_3$ -based external solution before (*light grey, top*) and after application of 1mM glutamate (*black, bottom*). B, averaged uptake currents at -100 mV of oocytes expressing WT or P290R EAAT3. Uptake currents were calculated as difference of current amplitudes with and without glutamate measured in a chloride-free solution. Student's t-test and paired t-test with $p \leq 0.05$ (*) as the level of significance were used ($p \leq 0.01$ (**), $p \leq 0.001$ (***)). The data are given as the means \pm S.E.; $n \geq 8$.

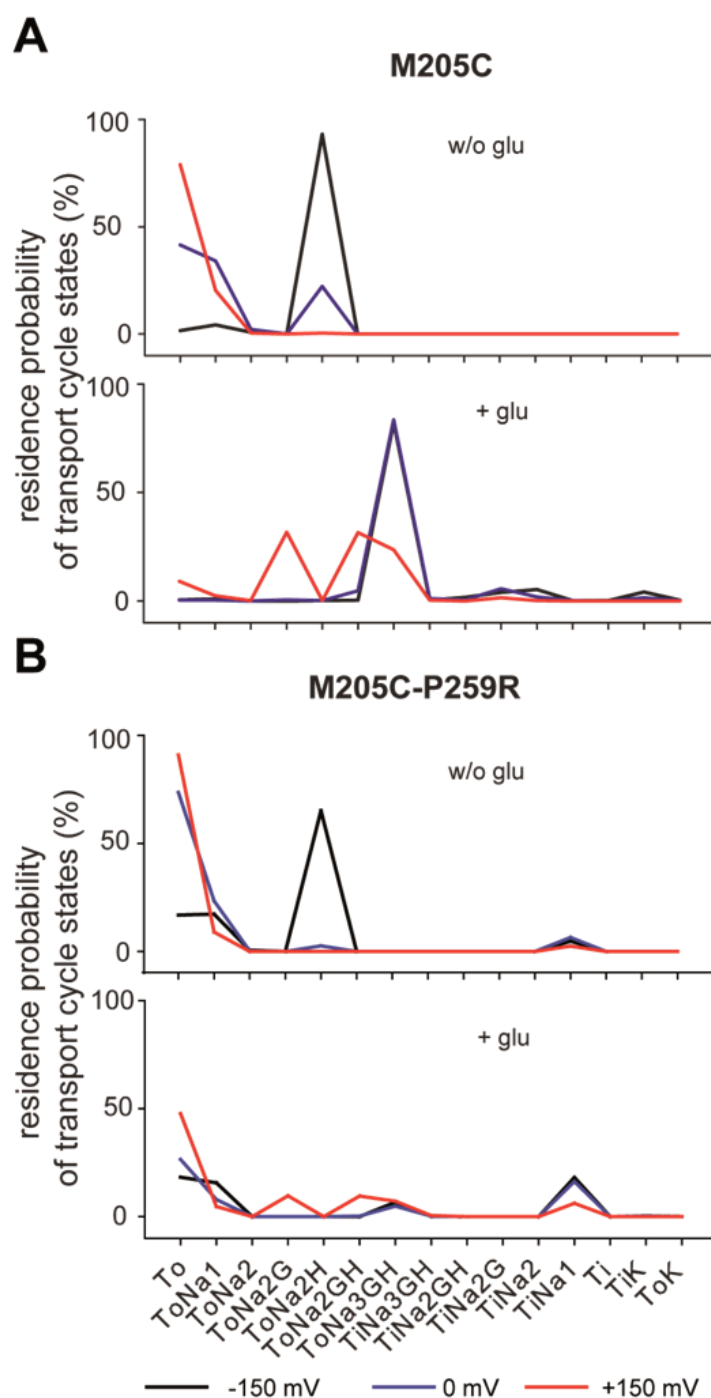
Suppl. Figure 11.6
Sodium dependence of WT, M205C and M205C-P259R EAAT3



Suppl. Figure 11.6: Sodium dependence of WT, M205C and M205C-P259R EAAT3.

A, B and C, dose-response curves of late current amplitudes versus the sodium concentration of WT, M205C or M205C-P259R EAAT3. Apparent dissociation constants (K_D) (in mM) and hill coefficients (n_H) were calculated by fitting the data with the Hill equation. Current amplitudes are normalized to the current in 197 mM sodium. Fluorescence data from at least 7 oocytes are reported as means \pm S.E..

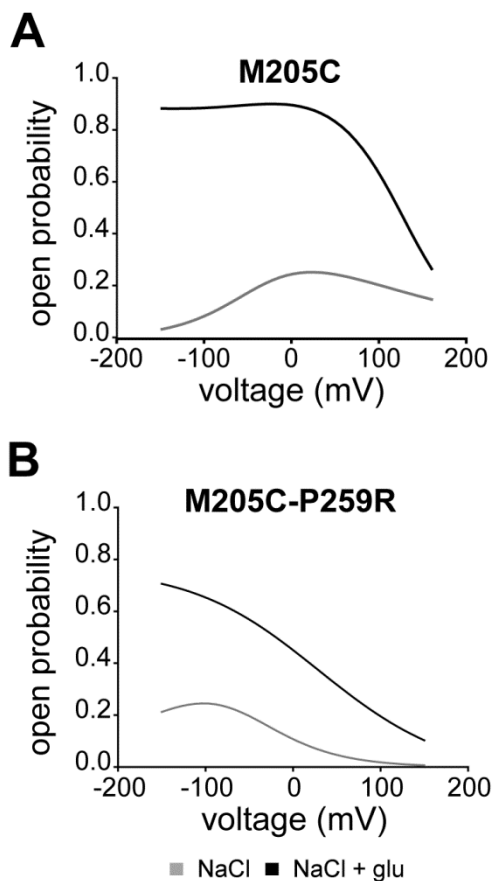
Suppl. Figure 11.7
Simulated conformational changes, uptake and anion currents of M205C and M205C-P259R EAAT3



Suppl. Figure 11.7: Residence probability of each state of EAAT3 transport cycle.

A, B simulated residence probability of each state for M205C (*A*) or M205C-P259R EAAT3 (*B*) without (*top*) or in presence of glutamate (*bottom*) at -150 mV (*black line*), 0 mV (*blue line*) or +150 mV (*red line*).

Suppl. Figure 11.8
Simulated open probabilities of M205C and M205C-P259R EAAT3 anion channels



Suppl. Figure 11.8: Simulated open probabilities of M205C and M205C-P259R EAAT3 anion channels.

A, B simulated open probabilities for M205C (*A*) and M205C-P259R (*B*) EAAT3 in the absence of glutamate (*grey lines*) or in the presence of 1 mM glutamate (*black lines*) at voltages between -150 mV and +150 mV.

12 Abbreviations

Amino acids

A (Ala)	alanine
C (Cys)	cysteine
D (Asp)	aspartic acid
E (Glu)	glutamic acid
F (Phe)	phenylalanine
G (Gly)	glycine
H (His)	histidine
I (Ile)	isoleucine
K (Lys)	lysine
L (Leu)	leucine
M (Met)	methionine
N (Asn)	asparagine
P (Pro)	proline
Q (Gln)	glutamine
R (Arg)	arginine
S (Ser)	serine
T (Thr)	threonine
V (Val)	valine
W (Try)	tryptophan
Y (Tyr)	tyrosine

General abbreviations

AMPA	α -amino-3-hydroxyl-5-methyl-4-isoxazole-propionate
ATP	adenosine triphosphate
BN	blue native
CFP	cyan fluorescence protein

Abbreviations

CNS	central nervous system
DTT	dithiothreitol
EA	episodic ataxia
EAAC1	excitatory amino-acid carrier 1
EAAT	excitatory amino acid transporter
EDTA	ethylene-diamine-tetra-acetic acid
2-FAA	β -2-fluorenyl-aspartylamide
GABA	γ -aminobutyric acid
GFP	green fluorescence protein
GLAST	glutamate aspartate transporter
GLT1	glial glutamate transporter 1
Glt _{Ph}	glutamate transporter in <i>Pyrococcus horikoshii</i>
HEK	human embryonic kidney
HEPES	4-(2-hydroxyethyl)-1-piperazineethanesulfonic acid
HP	hairpin
MDCK	Madin Darby canine kidney
MES	2-(N-morpholino)ethanesulfonic acid
mGluR	metabotropic glutamate receptor
NMDA	N-methyl-D-aspartic acid
PAGE	polyacrylamide gel electrophoresis
PBS	phosphate buffered saline
SDS	sodium dodecylsulfate
SLC	solute carrier
TBOA	threo- β -benzyloxyaspartate
TM	transmembrane domain
tsA201	HEK cell line
VCF	voltage clamp fluorometry
VGLUT	vesicular glutamate transporter
WT	wildtype
YFP	yellow fluorescence protein
ZNS	Zentrales Nervensystem

13 Acknowledgments

I would like to thank Prof. Dr. Christoph Fahlke for the possibility to work in his group and to give me the chance to benefit from his scientific experience. Thanks for providing me such an interesting and sometimes challenging topic. And I like to thank him for the scientific freedom to follow own ideas, his trust, his enthusiasm, his support and the lively discussions with him. I would like to thank in advance Prof. Dr. Gerardy-Schahn and Prof. Dr. Ngezahayo for being my co-referees, for taking the time and effort to read this thesis and take part in my defence. Thanks to the DFG for financial support which enables this work. And I would like to thank all my colleagues who helped me the last years and contribute to the success of this work.

Special thanks go to:

Ariane Leinenweber, for her scientific and emotional support,

David Ewers, for his unhesitating answering all of my questions and his help in many difficult circumstances, Jan-Philipp Machtens, for his help concerning kinetic simulations and for his youthful enthusiasm, Alexi Alekov, for his brilliance and criticism, our glutamate transporter subgroup: David Ewers, Peter Kovermann, Ariane Leinenweber, Jan-Philipp Machtens, Nicole Schneider, Yunping Song and Natalie Winter, Nicole Schneider, for being one of the most pleasant colleagues I can imagine, Matthias Grieschat, for the relaxed atmosphere in our 3 m²-dark-working-box and his special jokes, and Silke Schmidt, for her patience to listen to my scientific problems and for her friendship.

Special thanks go as well to Christin Dähling and our technicians, Toni Becher, Birgit Begemann, Petra Kilian and Silke Schmidt for keeping the lab running like clockwork! Furthermore, I would like to thank all colleagues of the Institute of Neurophysiology for the good teamwork, the lively discussions and the great time!

I would like to thank all people of the animal house of the MHH, helping to keep my frogs healthy and for the uncomplicated surgery scheduling, especially Karl-Heinz Napierski and Paul Zerbe.

I would like to thank Mareike Schumacher, for being the best friend ever, being my soulmate, being my rescue and reason for living.

In love, I thank my grandparents to support me my whole life, in good and in bad times.

14 Curriculum vitae

Personal Information

Linda Sabrina Jasmin Hotzy

born 02.04.1982 in Euskirchen, Germany

Educational and Professional Background

- | | |
|--------------------|---|
| 2011-present | PhD studies at the Naturwissenschaftliche Fakultät,
Gottfried Wilhelm Leibniz Universität Hannover,
conducted at the Zentrum Physiologie,
Institut für Neurophysiologie,
Medizinische Hochschule Hannover |
| 01.12.2007-present | Scientific employee at the Zentrum Physiologie,
Institut für Neurophysiologie,
Medizinische Hochschule Hannover |
| 2001 – 2007 | Biochemistry studies at the Naturwissenschaftliche Fakultät,
Gottfried Wilhelm Leibniz Universität Hannover
degree: Diplom-Biochemikerin |
| 1998 – 2001 | Oberstufengymnasium , Eschwege
degree: Abitur |
| 1992 – 1998 | Gymnasium Friedrich-Wilhelm-Schule, Eschwege
degree: mittlere Reife |

15 Erklärung

Hiermit erkläre ich, dass ich die Dissertation „Fluorometric approaches to analyze the structure-function relationship of Excitatory Amino Acid Transporters (EAATs)“ selbstständig verfasst habe.

Bei der Anfertigung wurden folgende Hilfen Dritter in Anspruch genommen:

Zu den Ergebnissen im Abschnitt „Hetero-oligomerization of neuronal glutamate transporters“ habe ich Messungen an Oocyten beigesteuert.

Jan-Philipp Machtens (Medizinstudent und Doktorand im Institut für Neurophysiologie, Medizinische Hochschule Hannover) hat die mathematische Berechnung des EAAT3 Kinetik-Modells im Abschnitt „Neutralizing aspartate 83 modifies translocation of Excitatory Amino Acid Transporter 3 (EAAT3) glutamate transporters“ vorgenommen.

Nicole Schneider (Doktorandin im Institut für Neurophysiologie, Medizinische Hochschule Hannover) und Dr. Peter Kovermann (Mitarbeiter im Institut für Neurophysiologie, Medizinische Hochschule Hannover) haben die Messungen in Säugetierzellen im Abschnitt „A mutation causing Episodic Ataxia modifies sodium association to EAAT glutamate transporters“ vorgenommen.

Birgit Begemann und Petra Kilian (Technische Assistentinnen im Institut für Neurophysiologie, Medizinische Hochschule Hannover) haben einen Teil der molekularbiologischen Arbeiten übernommen.

Ich habe keine entgeltliche Hilfe von Vermittlungs- bzw. Beratungsdiensten (Promotionsberater oder andere Personen) in Anspruch genommen. Niemand hat von mir unmittelbar oder mittelbar entgeltliche Leistungen für Arbeiten erhalten, die im Zusammenhang mit dem Inhalt der vorgelegten Dissertation stehen.

Ich habe die Dissertation an der folgenden Institution angefertigt: Institut für Neurophysiologie, Medizinische Hochschule Hannover. Die Dissertation wurde bisher nicht für eine Prüfung oder Promotion oder für einen ähnlichen Zweck zur Beurteilung eingereicht. Ich versichere, dass ich die vorstehenden Angaben nach bestem Wissen vollständig und der Wahrheit entsprechend gemacht habe.